11:37:42 OCA PAD INITIATION - PROJECT HEADER INFORMATION 03/01/91

Active

Project #: E-21-664 Cost share #: Rev #: 0
Center # : 10/24-6-R7136-0A0 Center shr #: OCA file #:
Work type : RES
Contract#: STD AGREEMENT DATED 2/14/91 Mod #: Document : AGR
Prime #: Contract entity: GTRC

Subprojects ? : N
Main project #:

Project unit: ELEC ENGR Unit code: 02.010.118
Project director(s):
STUBER G L ELEC ENGR (404)894-2923

Sponsor/division names: BELLSOUTH ENTERPRISES /
Sponsor/division codes: 251 / 004

Award period: 910101 to 911231 (performance) 911231 (reports)

| Sponsor amount | New this change | Total to date |
|---|---|---|
| Contract value | 130,314.00 | 130,314.00 |
| Funded | 130,314.00 | 130,314.00 |
| Cost sharing amount | | 0.00 |

Does subcontracting plan apply ?: N

Title: PERSONAL AND MOBILE COMMUNICATIONS

PROJECT ADMINISTRATION DATA

OCA contact: E. Faith Gleason 894-4820

Sponsor technical contact

MELVIN D. FRERKING
(404)249-4510

BELLSOUTH ENTERPRISES, INC.
8F08
1100 PEACHTREE STREET, N.E.
ATLANTA, GA 30309

Sponsor issuing office

MELVIN D. FRERKING
(404)249-4510

-----SAME-------

Security class (U,C,S,TS) : U ONR resident rep. is ACO (Y/N): N
Defense priority rating : N/A N/A supplemental sheet
Equipment title vests with: Sponsor X GIT
N/A
Administrative comments -
INITIATION.

GEORGIA INSTITUTE OF TECHNOLOGY
OFFICE OF CONTRACT ADMINISTRATION

NOTICE OF PROJECT CLOSEOUT

Closeout Notice Date 01/09/92

Project No. E-21-664 Center No. 10/24-6-R7136-0A0

Project Director STUBER G L School/Lab ELEC ENGR

Sponsor BELLSOUTH ENTERPRISES/

Contract/Grant No. STD AGREEMENT DATED 2/14/91 Contract Entity GTRC

Prime Contract No.

Title PERSONAL AND MOBILE COMMUNICATIONS

Effective Completion Date 911231 (Performance) 911231 (Reports)

| Closeout Actions Required: | Y/N | Date Submitted |
|---|---|---|
| Final Invoice or Copy of Final Invoice | Y | |
| Final Report of Inventions and/or Subcontracts | N | |
| Government Property Inventory & Related Certificate | N | |
| Classified Material Certificate | N | |
| Release and Assignment | N | |
| Other | N | |

Comments

Subproject Under Main Project No.

Continues Project No.

Distribution Required:

| | |
|---|---|
| Project Director | Y |
| Administrative Network Representative | Y |
| GTRI Accounting/Grants and Contracts | Y |
| Procurement/Supply Services | Y |
| Research Property Managment | Y |
| Research Security Services | N |
| Reports Coordinator (OCA) | Y |
| GTRC | Y |
| Project File | Y |
| Other | N |
| | N |

# PERSONAL AND MOBILE COMMUNICATIONS

Final Report for
OCA Project No. E21-664

Prepared for
**BellSouth Enterprises, Inc.**

prepared by

**Gordon L. Stüber**

School of Electrical Engineering
Georgia Institute of Technology
Atlanta, Georgia 30332

Sponsor Technical Contact

**Neale Hightower**

BellSouth Enterprises, Inc.
1100 Peachtree Street, NE
8F08
Atlanta, Georgia 30309

December 1991

# PERSONAL AND MOBILE COMMUNICATIONS

Final Report for
OCA Project No. E21-664

Prepared for
**BellSouth Enterprises, Inc.**

prepared by

**Gordon L. Stüber**

School of Electrical Engineering
Georgia Institute of Technology
Atlanta, Georgia 30332

Sponsor Technical Contact

**Neale Hightower**

BellSouth Enterprises, Inc.
1100 Peachtree Street, NE
8F08
Atlanta, Georgia 30309

December 1991

# Abstract

This report addresses four issues associated with personal and mobile communications. They are as follows; (i) subjective evaluation of the Motorola Narrow AMPS air interface specification, (ii) capacity analysis of DS CDMA for macrocellular applications, (iii) adaptive channel estimation with applications to the IS-54 digital cellular interim standard, and (iv) interference objectives for personal communication networks into microwave radio systems.

# Contents



[1]The work in this section was performed with the assistance of Kahlid Hamied.

[2]The work in this section was performed with the assistance of Chamrœun Kchao.

[3]The work in this section was performed with the assistance of Chamrœun Kchao.

[4]The work in this section was performed with the assistance of Kahlid Hamied.

[5]The work in this section was performed with the assistance of Lih-Bor Yiin and Ming-Ju Ho.

# List of Figures

# List of Tables

# 1 Introduction

This report contains study results on a variety of current issues in personal and mobile communications for North America. It consists of five basic sections as described below.

Section 2 treats a new narrowband analog FDM/FM (NAMPS) standard that has been proposed by Motorola for the North American cellular radio system. This standard has the potential of increasing the capacity of the current analog FDM/FM cellular system by a factor of three. This is primarily achieved by reducing the modulation index so that a carrier spacing of 10 kHz can be used, rather than the 30 kHz carrier spacing that is currently specified by the AMPS standard. The purpose of this part of the study is to evaluate Motorola's NAMPS standard by making subjective comparisons with the current North American AMPS standard. Section 2 is accompanied by an audio cassette tape that contains speech samples for each type of system for a variety of channel conditions.

Section 3 discusses the uplink and downlink performance of a digital cellular radio system that uses direct-sequence code division multiple-access. Approximate expressions are derived for the area averaged bit error probability while accounting for the effects of path loss, log-normal shadowing, multipath-fading, multiple-access interference, and background noise. Three differentially coherent receivers are considered; a multipath rejection receiver, a RAKE receiver with predetection selective diversity combining, and a RAKE receiver with postdetection equal gain combining. The RAKE receivers are shown to improve the performance significantly, except when the channel consists of a single faded path. Error correction coding is also shown to substantially improve the performance, except for slowly fading channels.

In Section 4, the performance of a multiple cell direct-sequence code division multiple-access cellular radio system is evaluated. Approximate expressions are obtained for the area averaged bit error probability and the area averaged outage probability for both the uplink and downlink channels. The analysis accounts for the effects of path loss, multipath-fading, multiple-access interference, and background

noise. Two types of differentially coherent receivers are considered, a multipath rejection receiver, and a RAKE receiver with predetection selective combining. Macroscopic base-station diversity techniques, and uplink and downlink power control are also topics of discussion.

In Section 5, a new non-iterative algorithm is proposed for estimating the sampled impulse response of a multipath-fading InterSymbol Interference (ISI) channel. The algorithm requires no multiplications nor divisions, and only requires a specific training sequence. A channel estimator that uses the algorithm is very easy to implement using any DSP processor. In this report, the channel estimator is applied to receivers that use sequence estimation techniques for combating the effects of ISI. The performance of the proposed algorithm is evaluated through software simulation studies as applied to the North American IS-54 digital cellular standard. These studies show that new algorithm outperforms the LMS algorithm in terms of computational simplicity and speed of convergence, and will result in a significantly lower bit error probability.

Finally, Section 6 is concerned with the various proposals to establish a personal communications network (PCN) in the 1850-1990 MHz band that is currently occupied by private microwave radio systems. These PCN's would use spread-spectrum signaling so as to minimize the interference into the victim microwave radio receivers. The purpose of this study is to determine the level of interference that a victim microwave receiver can tolerate from an overlaying PCN. These interference objectives are obtained by software simulation of the various PCN transmitters and microwave receivers.

# 2 NAMPS Air Interface Specification[6]

## 2.1 Introduction

Recently, Motorola has proposed a new analog FDM/FM air interface specification NAMPS (Narrow Advance Mobile Phone System), for the North American cellular radio system. This new standard has the potential of offering a three-fold increase in capacity, by using a channel spacing of 10 kHz rather than the 30 kHz that is currently being used. This reduction in channel spacing is achieved by using a reduced modulation index, and by changing the method of transmitting supervisory information.

The purpose of this study is to provide a subjective evaluation of the voice quality of the NAMPS standard as compared to the existing AMPS standard. These subjective evaluations are made by transmitting a three second sample of speech over a simulated mobile telephone system. This simulated system includes the complete FM transmitter, complete FM receiver, and an elaborate channel. The channel model accounts for the effects of adjacent channel interference, co-channel interference, multipath Rayleigh fading, and thermal noise. In this study only the downlink, or base-to-mobile channel, is considered.

This section is organized as follows. Subsection 2.2 discusses the transmitters, and Subsection 2.3 discusses the receivers that have been implemented for both the AMPS and NAMPS standards. Subsection 2.4 provides the some details of the channel model. Finally, in Subsection 2.5, the NAMPS standard is compared to the AMPS standard for a variety of channel conditions. Subsection 2.5 is accompanied by an audio cassette tape. This audio demonstration is intended to allow the listener to draw their own conclusions about the speech quality of the NAMPS specification.

[6]The work in this section was performed with the assistance of Kahlid Hamied.

## 2.2 Transmitter Models

This section describes the transmitter models that have been implemented for both the AMPS and NAMPS specifications.

### 2.2.1 AMPS Transmitter

An overview of the transmitter for the AMPS system is shown in Fig. 2.1. As shown, the FM modulator is preceded by an automatic gain control and five voice-processing stages in the following order; a bandpass filter, a 2:1 syllabic compandor, a pre-emphasis filter, a deviation limiter, and a post deviation limiter filter. The transmitter also includes Supervisory Auditory Tones (SAT). Each of these functional blocks is described below.

*Band-Pass Filter:* Transmit-audio filtering requirements are such that the compressor (described in the next section) shall be preceded by a bandpass filter with attenuation that increases at a rate of at least 24 dB/octave below 300 and above 3000 Hz. The bandpass filter is implemented using a lowpass and a highpass filter. A $4^{\text{th}}$ order highpass Chebyshev filter is used with 0.1 p-p dB ripple and a corner frequency of 300 Hz. A $4^{\text{th}}$ order lowpass Chebyshev filter is used with 0.1 dB p-p ripple and a corner frequency of 3000 Hz.

*Compressor:* Syllabic compandors are voice operated devices that are used to improve the telephone channel speech-to-noise ratio. The *compandor* consists of a *com*pressor and exp*andor*. By nature, speech waveforms have a large dynamic range with a high peak factor. The compressor amplifies the weaker speech signals, and reduces the dynamic range of the voice waveform, prior to transmission over a noisy channel.

A 2:1 syllabic compandor is used in the system. The compressor produces a 1 dB change in the output level for every 2 dB change in the input level. Specifically, the input and output of the compressor are related by

$$V_{\text{out}} = 1.33352\sqrt{V_{\text{in}}} \ , \tag{2.1}$$

or

$$V_{\text{out}}(\text{dB}) = \frac{V_{\text{in}}(\text{dB})}{2} + 2.5 \ . \tag{2.2}$$

| Frequency Band | Attenuation Relative to 1000 Hz |
|---|---|
| 3000 - 5900 Hz | $\geq 40\log_{10}(f/3000)$ dB |
| $>$ 5900 and $<$ 6100 Hz | $\geq 35$ dB |
| 6100 - 15000 Hz | $\geq 40\log_{10}(f/3000)$ dB |
| 15000 - 30000 Hz | $\geq 28$ dB |

To set the frequency sensitivity $K_f$ Hz/v of the FM modulator, a 1000 Hz sinusoidal tone is applied to the input of the compressor. The rms voltage of this input tone is set equal to the expected rms speech level at the input to the bandpass filter. The frequency sensitivity of the FM modulator is chosen so that this rms level produces a $\pm 2.9$ kHz peak frequency deviation of the transmitted carrier.

*Pre-emphasis Filter:* The purpose of the pre-emphasis filter is to amplify the high frequencies prior to transmission. This is just a simple zero-pole filter that has a +6 dB/octave response for frequencies between 300 Hz and 3000 Hz. This can be implemented using single zero at 0 Hz and single pole at a frequency higher than 3000 Hz. The pre-emphasis filter that has been implemented has the following transfer function;

$$H(s) = \frac{s + 10\pi}{s + 12000\pi} \quad . \tag{2.3}$$

The zero was chosen at 5 Hz instead of 0 Hz to avoid arithmetic problems in the simulation.

*Deviation Limiter:* The purpose of the deviation limiter is to limit the instantaneous frequency deviation to $\pm 12$ kHz, excluding supervision signals and wideband data signals. This is achieved by clipping the waveform at the output of the pre-emphasis filter at an appropriate level.

*Post-deviation Limiter Filter:* The post deviation limiter filter is a low-pass filter that removes high frequency components that may have been introduced by the deviation limiter. The attenuation characteristic of this filter must exceed the following

The filter is implemented using a $4^{\text{th}}$ order elliptic lowpass filter with 0.3 dB p-p

ripple, a corner frequency of 3000 Hz, and zero at 6 kHz.

*Supervisory Audio Tones:* A supervisory audio tone is added to the output of the post deviation limiter filter prior to modulation. This is a sinusoid at one of the following frequencies;

- 5970 Hz
- 6000 Hz
- 6030 Hz

The amplitude of the tone is adjusted so that, by itself, it will result in a peak frequency deviation of $\pm 2$ kHz. In the audio test, a tone of 6000 Hz is used.

*FM Modulator:* The carrier frequency of the FM modulator must be maintained within $\pm 1.5$ ppm of any assigned channel frequency. Some studies on the sensitivity of the carrier frequency will be performed in Section V. Note that this requirement is 2.5 ppm for the mobile transmitters in the AMPS system. However, we are considering base-to-mobile transmissions.

*Transmit Filter:* A transmit filter may be required to control the bandwidth that is occupied by the transmitted signal. The modulation products outside the region $\pm 20$ kHz from the carrier shall not exceed a level of 26 dB below the unmodulated carrier. Modulation products outside the region $\pm 45$ kHz from the carrier shall not exceed a level of 45 dB below the unmodulated carrier. Modulation products outside the region $\pm 90$ kHz from the carrier shall not exceed a level of a) 60 dB below the unmodulated carrier, or b) 43 plus 10 log 10 (mean output power in Watts) dB below the unmodulated carrier. In our system a transmit filter was not necessary.

### 2.2.2 NAMPS Transmitter

An overview of the transmitter for the NAMPS system is shown in Fig. 2.2. As shown, the transmitter consists of an automatic gain control, a bandpass filter, a 2:1 syllabic compandor, a pre-emphasis filter, a deviation limiter, a post deviation limiter filter, and an FM modulator. The transmitter also includes Digital Supervisory Auditory Tones (DSAT). Each of these functional blocks is described below.

*Band-Pass Filter:* The bandpass filter that is used in the NAMPS transmitter is identical to the one used in the AMPS transmitter.

*Compressor:* The syllabic compandor that is used in the NAMPS transmitter is identical to the one used in the AMPS transmitter. However, the sensitivity of the FM modulator is set so that a peak frequency deviation of $\pm 1.5$ kHz is produced by a 1000 Hz sinusoidal tone having an rms value equal to the expected rms value of the speech waveform at the input to the compressor.

*Pre-emphasis Filter:* The pre-emphasis filter that is used in the NAMPS transmitter is identical to the one used in the AMPS transmitter.

*Deviation Limiter:* The deviation limiter limits the instantaneous frequency deviation to $\pm 5$ kHz. This is achieved by clipping the waveform at the output of the pre-emphasis filter at an appropriate level.

*Post-deviation Limiter Filter:* The post-deviation limiter filter that has been implemented is identical to the one that has been implemented for the AMPS system.

*Digital Supervisory Audio Tones:* Prior to modulation, a Digital Supervisory Audio Tone (DSAT) is added to the baseband signal. The DSAT is one of the following seven digital sequences.

1. 2556CB
2. 255B2B
3. 256A9B
4. 25AD4D
5. 26AB2B
6. 26B2AD
7. 2969AB

The transmission rate is 200 bits/s with a peak frequency deviation of $\pm 700$ Hz.

Motorola has proposed that the DSAT information be transmitted by shaping NRZ data with a $6^{th}$ order Butterworth lowpass filter with a 3 dB point at 90 Hz.

This filter will create severe intersymbol interference in the DSAT information and may cause some detection problems. To solve this problem, we also consider the use of frequency domain raised cosine (RC) pulse shaping with a rolloff factor of 1.0. The theoretical bandwidth occupancy is 200 Hz.

*FM Modulator:* Once again, the carrier frequency of the FM modulator must be maintained within $\pm 0.25$ ppm of any assigned channel frequency. Note that this requirement is 1.0 ppm for the mobile transmitters in the NAMPS system. However, we are considering base-to-mobile transmissions.

*Transmit Filter:* Once again, a transmit filter may be required to control the bandwidth that is occupied by the transmitted signal. The modulation products inside a 300 Hz band centered on any frequency removed from the carrier by 15 kHz shall not exceed a level of 45 dB below the unmodulated carrier. The modulation products inside a 300 Hz band centered on any frequency removed from the carrier by 45 kHz shall not exceed a level of 63 plus 10 log 10 (mean output power in Watts) dB below the unmodulated carrier. In our system, a transmit filter was not required.

## 2.3 Receiver Models

This section describes the receivers models that have been implemented for the AMPS and NAMPS specifications.

### 2.3.1 AMPS Receiver

Fig. 2.3 shows an overview of an AMPS receiver that uses a balanced discriminator demodulator. Likewise, Fig. 2.4 shows an overview for a receiver that uses a Phase Locked Loop (PLL) demodulator. As shown, the FM demodulator is preceded by a receiver filter and followed by two voice processing stages; a de-emphasis filter and an expandor.

*Receiver Filter:* The purpose of the receiver filter is to reject out of band noise and interference. For this purpose a $4^{th}$ order Butterworth bandpass filter with a bandwidth of 30 kHz has been used.

*FM Demodulator:* Two types of FM demodulators have been implemented; a discriminator detector and a PLL. Both of these receivers perform much the same at high signal-to-noise ratios. However, the PLL will provide much better performance at low signal-to-noise ratios. Sometimes, it is suggested that the PLL demodulator be preceded be a bandpass limiter, because the loop gain of the PLL is a function of the amplitude of the input signal. However, the discussion in [1] indicates that a bandpass-limiter is not necessary and will degrade the threshold range of the PLL demodulator. The PLL that has been implemented uses a second-order loop. The loop filter is a first order Butterworth filter with a 3 dB bandwidth of 30 kHz. The VCO frequency sensitivity is 10000 Hz/v.

*Voice Audio Filtering:* Voice audio filtering is used for de-emphasis and to remove the SAT tones. The voice audio filtering that has been implemented has the following three stages:

- Low-Pass: Elliptic, fourth order, 0.3 dB p-p ripple, corner frequency 3000 Hz, zero at 6 kHz.
- High-Pass: Chebyshev, fourth order, 0.1 p-p dB ripple, corner frequency 300 Hz.[7]
- De-emphasis: 2 pole Butterworth bandpass, corner frequency 150 Hz, dampling factor 0.707.

*Expandor:* This is the expandor stage of the 2:1 syllabic compandor. For every 1 dB change in the input level to the 1:2 expandor, the change in the output level is 2 dB. Specifically, the input and output of the expandor are related by

$$V_{\text{out}} = 0.5623 V_{\text{in}}^2 \ , \tag{2.4}$$

or

$$V_{\text{out}}(\text{dB}) = 2V_{\text{in}}(\text{dB}) - 5.0 \ . \tag{2.5}$$

The rms reference input level to the expandor is that corresponding to a 1000 Hz tone from a carrier with a $\pm 2.9$ kHz peak frequency deviation.

[7]This filter may not actually be required for the AMPS recevier.

### 2.3.2 NAMPS Receiver

Fig. 2.5 shows an overview of a NAMPS receiver that uses a balanced discriminator demodulator. Likewise, Fig. 2.6 shows an overview for a NAMPS receiver that uses a PLL demodulator. Again, the FM demodulator is followed by two voice processing stages; a de-emphasis filter and an expandor.

*Receiver Filter:* Again, the purpose of the receiver filter is to reject out of band noise and interference. For this purpose a $4^{th}$ order Butterworth bandpass filter with a bandwidth of 10 kHz has been used.

*FM Demodulator:* Once again, a discriminator detector or a PLL can be used for the FM demodulator. The PLL that has been implemented uses a second-order loop. The loop filter is a first order Butterworth filter with a 3 dB bandwidth of 30 kHz. The frequency sensitivity of the VCO is 10000 Hz/v.

*Voice Audio Filtering:* The voice audio filtering that is used in the NAMPS receiver is identical to the one used in the AMPS recevier. The highpass Chebyshev filter has added importance in the NAMPS receiver, because it is used to reject the sub-audible DSAT information.

*Expandor:* The expandor used in the NAMPS receiver is identical to the one used in the AMPS receiver.

## 2.4 Channel Model

### 2.4.1 Multipath-Fading

Multipath-fading has been simulated by using the method proposed by Jakes [2]. Fig. 2.7 shows a block diagram of the fading simulator.

### 2.4.2 Co-channel Interference, Adjacent Channel Interference, and Noise

It is assumed that the cellular layout is described by a uniform grid of hexagonal cells. The cells are divided into 120° cell sectors.

When cell sectoring is used, it is possible to assign the channel frequencies to the cell sectors in such a way that there is one predominant adjacent-channel

interferer. With a propagation path loss exponent of 4, the worst case Carrier-to-Adjacent channel Interference Ratio (CAIR) for this interferer is approximately 12 dB.

Adjacent channel interference was modeled by assuming one adjacent channel interferer with a CAIR of 12 dB. Adjacent channel interference from other transmitters was neglected. Because of the frequency reuse pattern that is used, adjacent channel interference will arise from adjacent cells. Therefore, all of the signals will be independently faded.

When 120° cell sectoring is used, there are two dominant cochannel interferers. The co-channel interference from each of these co-channel interferers will be different. However, co-channel interference was modeled by assuming the presence of two equal power interfering signals at the same carrier frequency as the desired signal. The desired signal and each of the co-channel interferers will be independently faded. As shown in [5], this is a good approximation.

It is generally accepted that a Carrier-to-Cochannel Interference Ratio (CCIR) of 18 dB is sufficient for operation of the AMPS system. Our tests will determine if the NAMPS specification can also operate at a CCIR of 18 dB. If it can, then a three-fold increase capacity can be achieved.

The receiver will also introduce thermal noise. This has been modeled as additive white Gaussian noise with various Carrier-to-Noise Ratios (CNR's).

## 2.5 Subjective Speech Evaluations

Subjective evaluations have been made by transmitting a 3 second segment of speech over the simulated AMPS and NAMPS mobile radio system described in Subsections ??, ??, and ?? of this section. This has been accomplished for a variety of channel conditions. This section is accompanied by an audio cassette tape that will allow the listener to draw their own conclusions about the quality of the Motorola NAMPS standard. It is important to note that the tests do not account for the effects of acoustic lowpass filtering. This audio cassette tape is very much self explanatory.

### 2.5.1 Audio Tests

The audio cassette tape contains the following tests in the order listed. The reader should play the audio cassette tape at this time.

*1) Speech Sample Used for Demonstration*

*2) Ideal and Noiseless Channel*

The test arrangement is shown in Fig. 2.8.

1. AMPS standard with VCO detector.
2. NAMPS standard with VCO detector, with Motorola DSAT transmit filter.
3. NAMPS standard with VCO detector, with RC DSAT transmit filter.
4. AMPS standard with discriminator detector.
5. NAMPS standard with discriminator detector, with Motorola DSAT transmit filter.
6. NAMPS standard with discriminator detector, with RC DSAT transmit filter.

**The remaining tests for the NAMPS standard are with the RC DSAT transmit filter.**

*3) Rayleigh Fading Channel with Additive White Gaussian Noise*

The test arrangement is shown in Fig. 2.9.

1. AMPS standard with VCO detector. CNR=$\infty$ dB.
2. NAMPS standard with VCO detector. CNR=$\infty$ dB.
3. AMPS standard with discriminator detector. CNR=$\infty$ dB.
4. NAMPS standard with discriminator detector. CNR=$\infty$ dB.
5. AMPS standard with VCO detector. CNR=21 dB.
6. NAMPS standard with VCO detector. CNR=21 dB.

7. AMPS standard with VCO detector. CNR=18 dB.

8. NAMPS standard with VCO detector. CNR=18 dB.

9. AMPS standard with VCO detector. CNR=15 dB.

10. NAMPS standard with VCO detector. CNR=15 dB.

*4) Rayleigh Faded Channel with Adjacent Channel and Co-channel Interference*

The test arrangement is shown in Fig. 2.10.

1. AMPS standard with VCO detector. CACI=12 dB, CCIR=21 dB.

2. NAMPS standard with VCO detector. CACI=12 dB, CCIR=21 dB.

3. AMPS standard with VCO detector. CACI=12 dB, CCIR=18 dB.

4. NAMPS standard with VCO detector. CACI=12 dB, CCIR=18 dB.

5. AMPS standard with VCO detector. CACI=12 dB, CCIR=15 dB.

6. NAMPS standard with VCO detector. CACI=12 dB, CCIR=15 dB.

*5) Transmitter Oscillator Drift*

The test arrangement is similar to the one shown in Fig. 2.10.

1. AMPS standard with VCO detector. CACI=12 dB, CCIR=18 dB, offset = 0 ppm.

2. AMPS standard with VCO detector. CACI=12 dB, CCIR=18 dB, offset = 0.25 ppm.

3. NAMPS standard with VCO detector. CACI=12 dB, CCIR=18 dB, offset = 0 ppm.

4. NAMPS standard with VCO detector. CACI=12 dB, CCIR=18 dB, offset = 0.25 ppm.

*6) Effect of Vehicle Velocity*

The test arrangement is similar to the one shown in Fig. 2.10.

1. AMPS standard with VCO detector. CACI=12 dB, CCIR=18 dB,
velocity = 2 km/hr, interferer velocity = 2 km/hr.

2. NAMPS standard with VCO detector. CACI=12 dB, CCIR=18 dB, velocity = 2 km/hr, interferer velocity = 2 km/hr.

3. AMPS standard with VCO detector. CACI=12 dB, CCIR=18 dB, velocity = 10 km/hr, interferer velocity = 10 km/hr.

4. NAMPS standard with VCO detector. CACI=12 dB, CCIR=18 dB, velocity = 10 km/hr, interferer velocity = 10 km/hr.

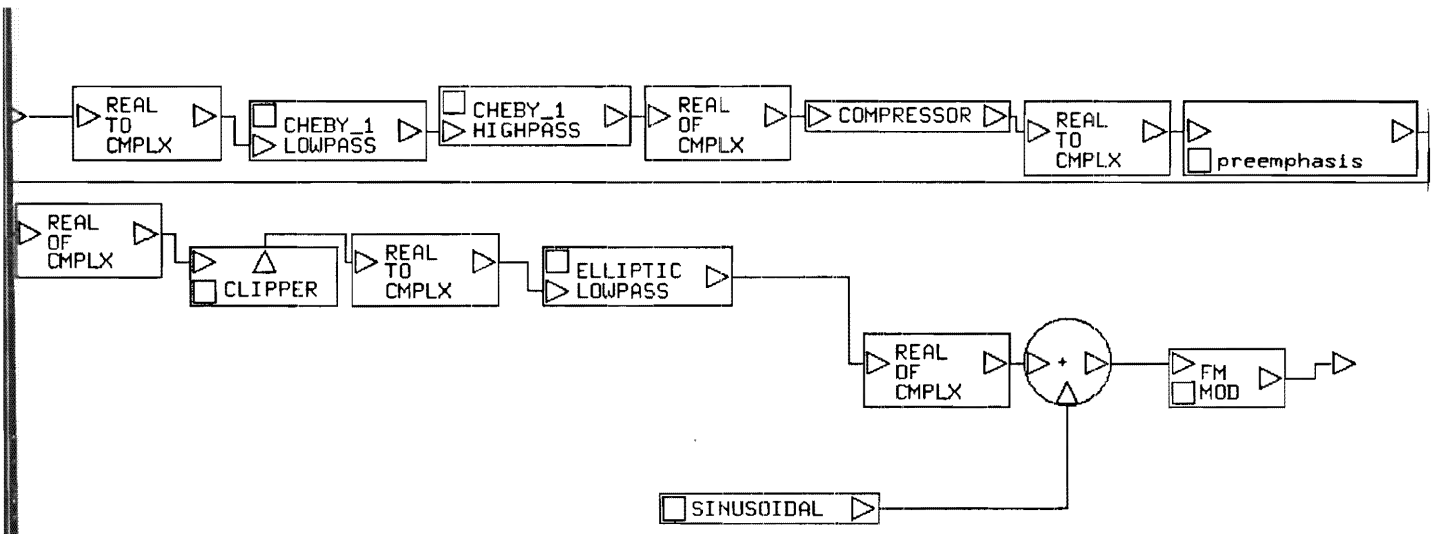


Figure 2.1: AMPS Transmitter.

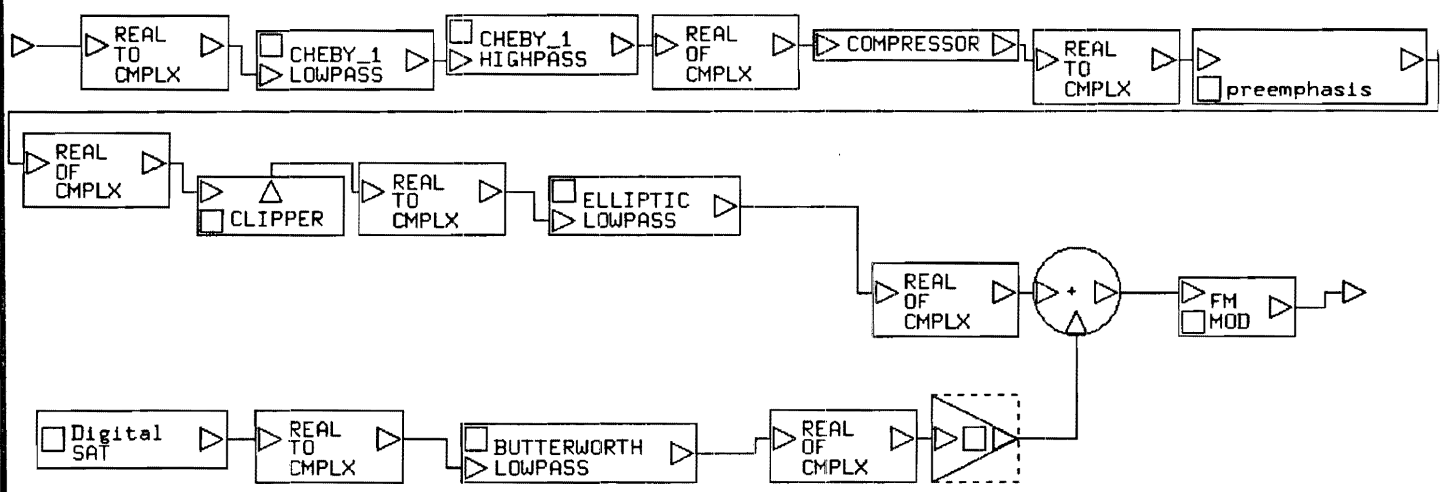


Figure 2.2: NAMPS Transmitter.

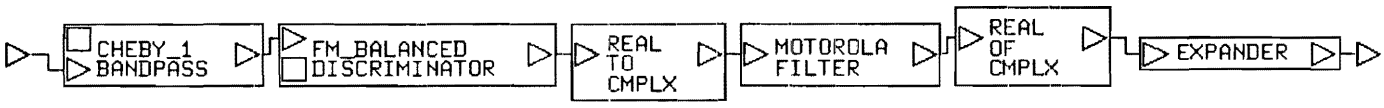


Figure 2.3: AMPS Receiver with Balanced Discriminator.

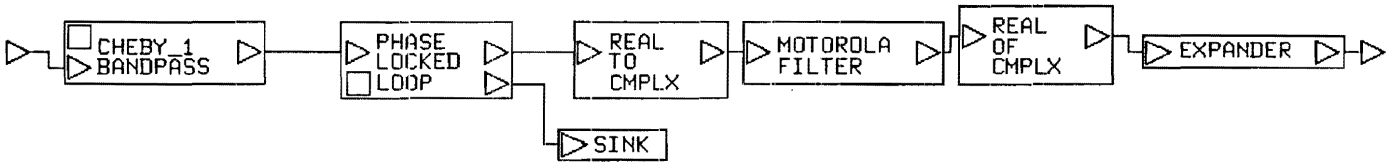


Figure 2.4: AMPS Receiver with Phase Locked Loop.

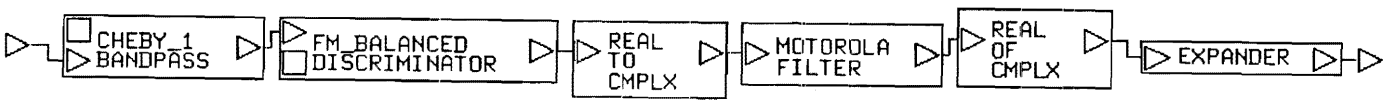


Figure 2.5: NAMPS Receiver with Balanced Discriminator.

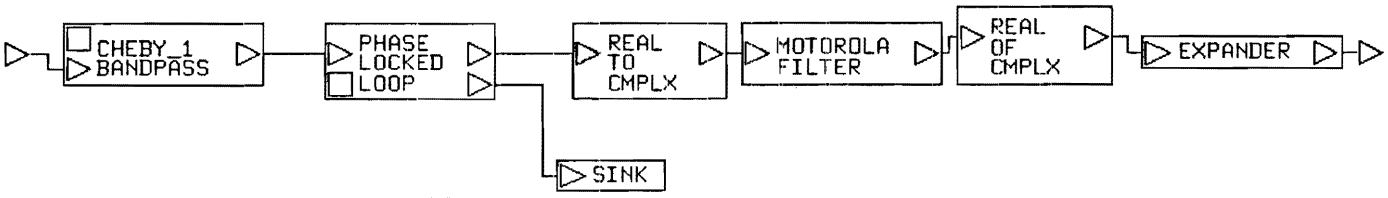


Figure 2.6: NAMPS Receiver with Phase Locked Loop.

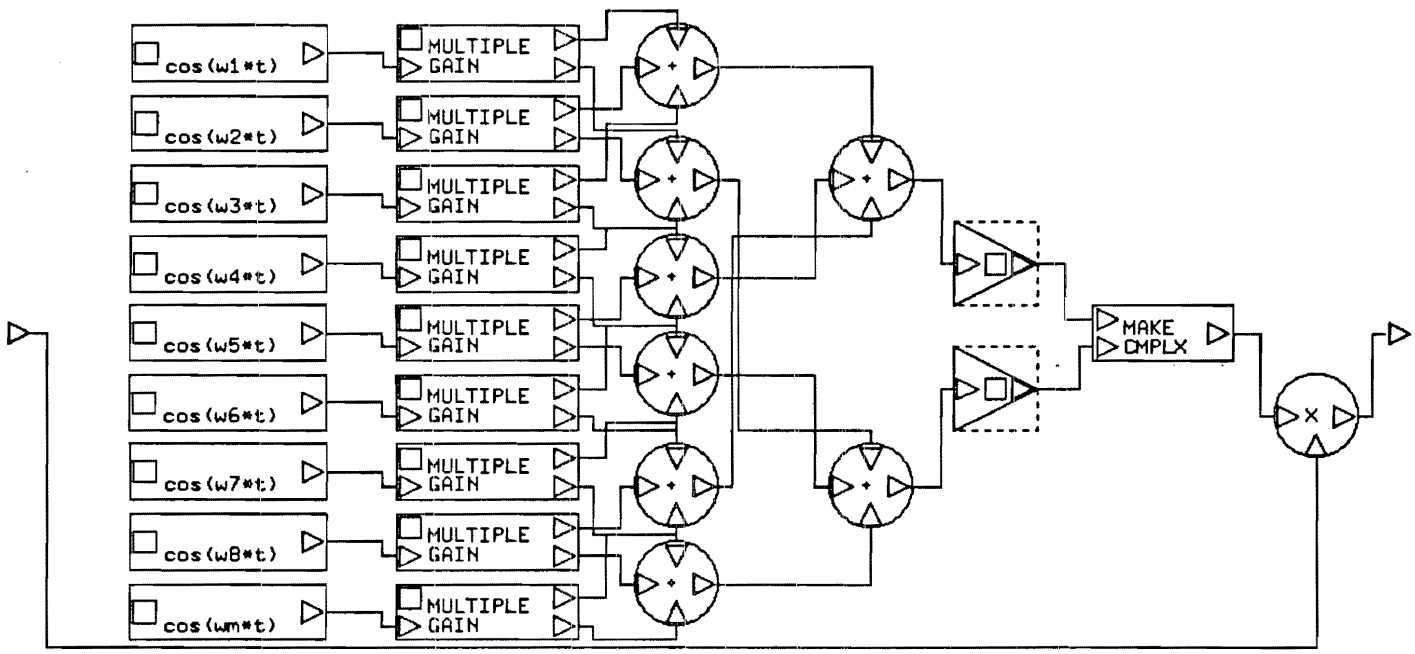


Figure 2.7: Multipath-fading Channel Model.

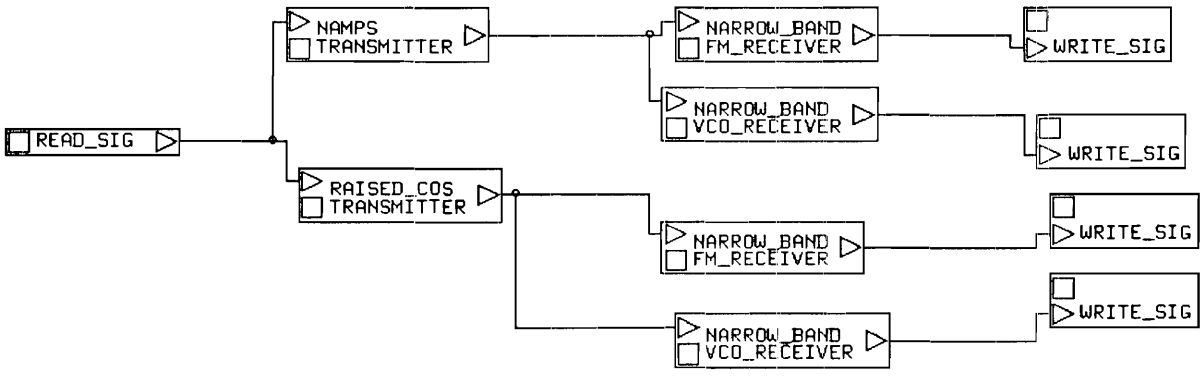


Figure 2.8: Test Arrangement for Ideal and Noiseless Channel.

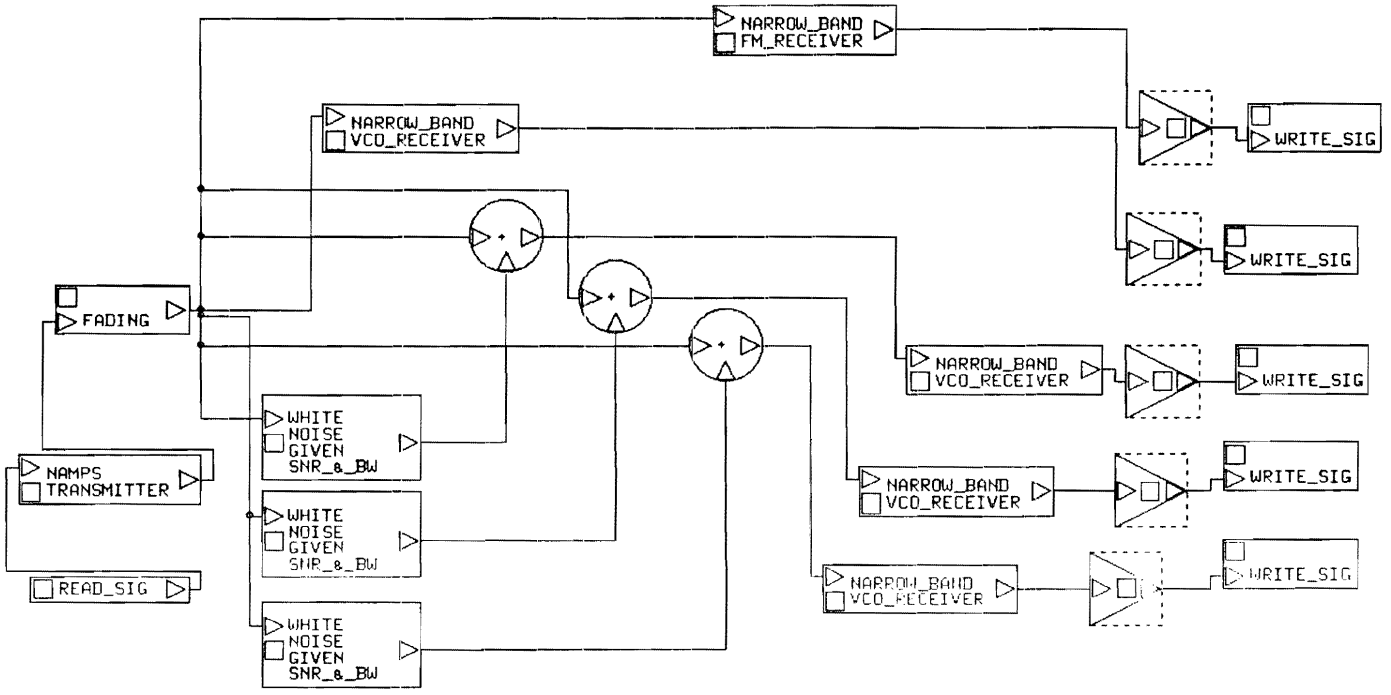


Figure 2.9: Test Arrangement for Rayleigh Faded Channel with Additive White Gaussian Noise.

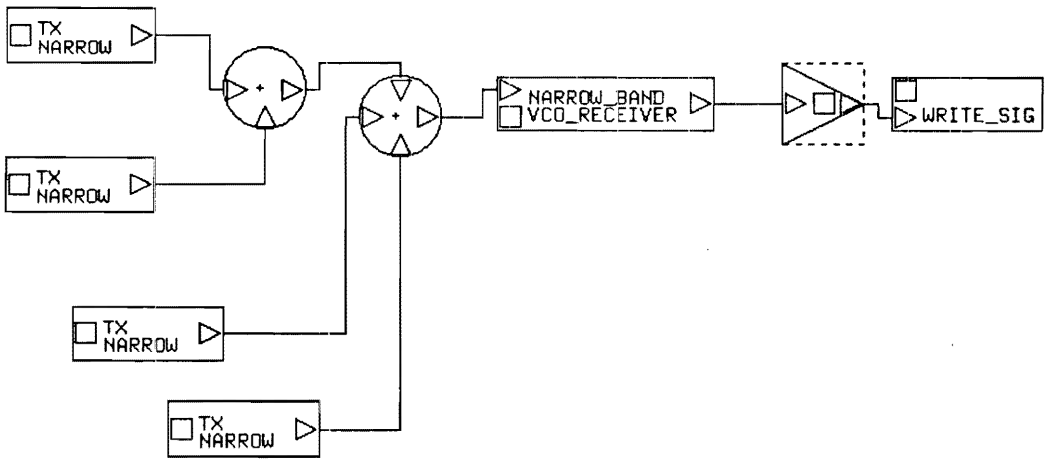


Figure 2.10: Test Arrangement for Rayleigh Faded Channel with Adjacent Channel and Co-channel Interference.

# 3 Single Cell CDMA System[8]

## 3.1 Introduction

Recently, there has been increased interest in the commercial applications of spread-spectrum signaling. Direct-Sequence (DS) Code Division Multiple-Access (CDMA) has been proposed for enhancing the capacity of the North American cellular mobile telephone system [6]. This section evaluates the uplink and downlink performance of a cellular radio system that employs DS CDMA. The analysis accounts for the effects of path loss, log-normal shadowing, multipath-fading, multiple-access interference, and background noise. It is intended to illustrate some of the typical characteristics of a DS CDMA cellular radio system, and demonstrate how the performance depends on certain aspects of the propagation environment. The analysis is restricted to a single isolated cell. Additional results for a multiple cell mobile radio environment are the subject of Section 4.

A very large body of literature exists on the analysis of CDMA cellular systems. Much of this literature, such as the initial work by Cooper and Nettleton [7], considers frequency-hopped CDMA. Here we discuss some of the existing literature on the analysis of DS CDMA cellular systems.

Most analyses of DS CDMA have resulted in Gaussian approximations, and various upper and lower bounds on the bit error probability for additive white Gaussian noise (AWGN) channels [8], [9], [10], [11], [12]. For specular multipath-fading channels, Geraniotis and Pursley have approximated the bit error probability of single user direct-sequence systems that use coherent [13] and noncoherent [14] detection. This analysis has been extended to DS CDMA for a multipath rejection receiver [15]. A few attempts have been made to evaluate the performance of a multipath combining receiver. Lehnert and Pursley [16], [17] have concluded that a multipath combining receiver can overcome the increased effect of multiple-access interference due to multipath, provided that the receiver has perfect knowledge of the amplitudes,

[8]The work in this section was performed with the assistance of Chamrœun Kchao.

delays, and phases of the multiple received signal replicas.

Lam and Steele [18] have evaluated the performance of multipath combining receivers by simulation. For this purpose, they used the frequency-selective, slowly fading, multipath channel model developed by Hashemi [19]. A channel sounding technique was studied that allowed the receiver to lock onto and combine the strongest $M$ signal paths. Despite the use of channel sounding, multipath diversity, and antenna diversity, it was reported that a processing gain of 31 could only support three simultaneous transmissions at a bit error rate less than $10^{-2}$. In contrast, the same system could support twelve simultaneous transmissions on an AWGN channel.

Turin [20] has also estimated the maximum number of allowable users for a DS CDMA system that uses differentially coherent multipath combining receivers. For an AWGN channel, it was reported that the maximum number of allowable users is about 10 – 20% percent of the processing gain for a bit error rate of $10^{-5}$ – $10^{-3}$. However, for an urban multipath-fading channel without power control, this figure drops to 1–5% even with ideal multipath combining receivers. Xiang [21] also observed the same effect. If the channels consist of a single faded link then DS CDMA may be unusable, a conclusion also reached by Gardner and Orr [22]. Power control will only partially recover the reduction in capacity due to multipath-fading, because power control cannot compensate for rapid signal fluctuations caused by multipath-fading [20]. Finally, Rappaport and Milstein [23], [24] have examined the effect of path loss and user distribution on the performance of a DS CDMA cellular system. They showed that reuse efficiency can range from a high of 0.68 for a fourth law path loss exponent to a low of 0.42 for a square law path loss exponent.

This section differs from existing literature in several respects. It differs from Rappaport and Milstein [23], [24] by concentrating on the effects of multipath-fading rather than path loss. It differs from Turin [20] by using a different method of analysis, a more extensive treatment of power control, and a discussion of both the uplink and downlink performance. Finally, it differs from Xiang [21] by using a different channel model. Xiang models the channel as a random number of discrete Nakagami faded multipaths. We model the channel as consisting of a continuum of multipaths that

results in a fixed number of resolvable Rayleigh faded paths.

The remainder of this section is organized as follows. Subsection 3.2 discusses the system and channel model. The uplink performance is evaluated in Subsection 3.3 for three differentially coherent receivers; a multipath rejection receiver, a RAKE receiver with predetection selective diversity combining, and a RAKE receiver with postdetection equal gain combining. Power control and error correction coding are also considered. Subsection 3.4 discusses the downlink performance for a multipath rejection receiver and a RAKE receiver with predetection selective diversity combining.

## 3.2 System and Channel Model

The system consists of a single isolated circular cell of radius $R$ with a centrally located base-station. There are $K$ mobile transceivers that are using direct-sequence CDMA to establish a full-duplex channel with the base-station. The mobile transceivers are assumed to be uniformly distributed throughout the cell area.

Propagation at UHF/VHF frequencies used in cellular mobile radio systems is largely influenced by path loss, shadowing, and multipath-fading. Each of these phenomenon is caused by a different underlying physical principle, and each should be accounted for when evaluating the performance of a cellular system.

### 3.2.1 Multipath-Fading

Mobile radio channels are effectively modeled as a continuum of multipath components. The equivalent low-pass channel has the time-variant impulse response [23]

$$c(\tau;t) = \alpha(\tau;t)\exp\{-j2\pi f_c\tau\} \quad , \tag{3.1}$$

where $f_c$ is the carrier frequency. A widely used model for multipath-fading channels is the Wide Sense Stationary Uncorrelated Scattering (WSSUS) model, where the low-pass impulse response $c(\tau;t)$ is a complex Gaussian random process having a complex autocorrelation

$$\frac{1}{2}\mathrm{E}[c^*(\tau_1;t)c(\tau_2;t+\Delta t)] = Q(\tau_1,\Delta t)\delta(\tau_1-\tau_2) \quad . \tag{3.2}$$

The function $Q(\tau) \equiv Q(\tau, 0)$ is called the Multipath Intensity Profile (MIP), and gives the average power output of the channel as a function of the time delay $\tau$. The MIP can assume various forms, but quite often a mobile radio channel is well characterized by the exponential MIP [24]

$$Q(\tau) = \psi \exp\{-\tau/T_m\} \quad , \qquad 0 \leq \tau \leq T_{\max} \quad . \tag{3.3}$$

This same model was the outcome of the European COST207 multipath propagation study and was subsequently included in the specifications for the GSM system [25]. In our analysis it is assumed that all channels have the same MIP, but in reality every channel will have a distinct MIP.

The low-pass impulse response of the channel is commonly modeled as a tapped delay line with a tap spacing equal to $T_c$ [26], [27], [28], [29], i.e.,

$$c(\tau; t) = \sum_{n=-\infty}^{\infty} c_n(t)\delta(\tau - nT_c) \quad , \tag{3.4}$$

where the $\{c_n(t)\}$ are the tap gains. For a continuum of multipath components, the $c_n(t)$ are complex Gaussian random processes. For a WSSUS channel the $c_n(t)$ are uncorrelated and, hence, independent. If the $c_n(t)$ have zero-mean, then the magnitudes $|c_n(t)|$ are Rayleigh distributed at any time $t$. Since the total multipath spread is $T_{\max}$, the tapped delay line can be truncated at $L = \lfloor T_{\max}/T_c \rfloor + 1$ taps, where $\lfloor x \rfloor$ is the largest integer contained in $x$. For a slowly varying channel $c_n(t) = c_n$ for the duration of several data bits.

Assuming the above tapped delay line model, the instantaneous received bit energy-to-background noise ratio is

$$\lambda = \sum_{n=0}^{L_i-1} \lambda_n \quad , \tag{3.5}$$

where $\lambda_n = |c_n|^2\lambda$ and $\lambda \triangleq \frac{E_b}{N_o}$ is the received bit energy-to-background noise ratio in the absence of multipath-fading. If the $|c_n|$ are Rayleigh distributed, then the $\lambda_n$ have the exponential Probability Distribution Function (PDF)

$$\mathrm{f}_{\lambda_n}(\lambda_n) = \frac{1}{\Lambda_n} \exp\left\{-\frac{\lambda_n}{\Lambda_n}\right\} \quad , \tag{3.6}$$

where

$$\Lambda_n = \mathrm{E}[|c_n|^2]\lambda \quad . \tag{3.7}$$

The $\Lambda_n$ are related to the MIP. From (3.3), the average power output of the channel at delay $nT_c$ is

$$Q(nT_c) = \psi \exp\{-n/\varepsilon\} \quad , \tag{3.8}$$

where $\varepsilon = T_m/T_c$ is the delay spread relative to a chip duration. Following the development in [29], suppose that $Q(nT_c + \tau) \approx Q(nT_c)$ for $0 \leq \tau \leq T_c$, meaning that the channel impulse response is stationary for delay intervals of length $T_c$. Then the average received bit energy-to-background noise ratio associated with the $n^{\text{th}}$ path is

$$\Lambda_n = T_c Q(nT_c)\lambda \quad . \tag{3.9}$$

Taking the expectation of both sides of (3.5), and using (3.8) and (3.9) gives

$$\Lambda = \sum_{n=0}^{L-1} \Lambda_n = \lambda T_c \psi \frac{1 - \exp\{-L/\varepsilon\}}{1 - \exp\{-1/\varepsilon\}} \quad , \tag{3.10}$$

where $\Lambda$ is interpreted as the total average received bit energy-to-background noise ratio. It follows that

$$\Lambda_n = \frac{(1 - \exp\{-1/\varepsilon\})\exp\{-n/\varepsilon\}}{1 - \exp\{-L/\varepsilon\}}\Lambda \quad . \tag{3.11}$$

When obtaining numerical results it will be assumed, somewhat arbitrarily, that $\varepsilon = L - 1/2$.

### 3.2.2 Multiple-access Interference

For direct-sequence CDMA, the self interference and multiple-access interference at the front end of the receiver matched to the desired signal can be modeled as additional broadband Gaussian noise. For a nonfaded channel, a rigorous comparison of this Gaussian approximation with exact error probabilities has been undertaken for deterministic sequences [7], [9], and random sequences [8], [10], under the assumption of coherent detection. Similar results have also been obtained for differentially coherent detection [30]. These results show that the Gaussian approximation becomes very

optimistic with decreasing $K$, and increasing $\Lambda$. For multipath-fading channels, a rigorous comparison of a Gaussian approximation with more accurate approximations has also been made [11], [12], [13]. These results show that a Gaussian approximation is satisfactory, even for small $K$ and large $\Lambda$, giving only slightly optimistic results.

### 3.2.3 Shadowing

Shadowing is caused by terrain features such as buildings and hills. Hilly terrain causes diffraction loss, while buildings cause scattering losses. The effect is a very slow change in the *local* mean value $\Lambda$. Shadowing is often modeled as being log-normal, meaning that $\Lambda^d = 10\log_{10}\Lambda$ is normally distributed [31], [24], [32], [33], [34].[9] Defining $\overline{\Lambda}^d \triangleq \mathrm{E}[\Lambda^d]$, the conditional PDF of $\Lambda^d$ is

$$\mathrm{f}_{\Lambda^d|\overline{\Lambda}^d}(\Lambda^d|\overline{\Lambda}^d) = \frac{1}{\sqrt{2\pi}\sigma}\exp\left\{-\frac{1}{2\sigma^2}(\Lambda^d - \overline{\Lambda}^d)^2\right\} \quad . \tag{3.12}$$

Typically, $\sigma$ ranges from 6 to 12 dB. For our purpose $\sigma = 8$ dB will be used. If shadowing is neglected, then $\mathrm{f}_{\Lambda^d|\overline{\Lambda}^d}(\Lambda^d|\overline{\Lambda}^d) = \delta(\Lambda^d - \overline{\Lambda}^d)$.

### 3.2.4 Path Loss

A multitude of path loss prediction models exist for UHF/VHF land mobile radio in flat, urban, suburban, open, and hilly terrains [24], [32], [31]. Most of these models are empirical with a few exceptions. The simplest theoretical model, and the one used in this paper, assumes that the value of $\overline{\Lambda}$ in (3.12) is

$$\overline{\Lambda} = \begin{cases} \left(\frac{k}{\beta}\right)^{\alpha} , & r < \beta \\ \left(\frac{k}{r}\right)^{\alpha} , & r \geq \beta \end{cases} , \tag{3.13}$$

where $r$ is the distance between the transmitter and receiver, and $k$ is a constant of proportionality. The path loss exponent $\alpha$ ranges from 2 in free space to 4 in a dense urban area. The parameter $\beta$ is included because $\lim_{r\to 0} r^{-\alpha} = \infty$.

For a uniformly located mobile in a circular cell of radius $R$, the PDF of the mobile location, in cylindrical co-ordinates is $p(r,\theta) = r/(\pi R^2)$, $0 \leq r \leq R$, and $0 \leq$

[9] The superscript $d$ implies units of decibels.

$\theta \leq 2\pi$ . By using a univariate transformation, the PDF of $\overline{\Lambda}$ in (3.13) is

$$f_{\overline{\Lambda}}(\overline{\Lambda}) = \frac{\beta^2}{R^2}\delta\left(\overline{\Lambda} - \left(\frac{k}{\beta}\right)^{\alpha}\right) + \frac{2k^2}{\alpha R^2}\overline{\Lambda}^{-\frac{\alpha+2}{\alpha}} \quad , \quad \left(\frac{k}{R}\right)^{\alpha} \leq \overline{\Lambda} \leq \left(\frac{k}{\beta}\right)^{\alpha} \quad . \tag{3.14}$$

It is convenient to make the following definitions:

- $\Lambda_f \triangleq \left(\frac{k}{R}\right)^{\alpha}$, the total average received bit energy-to-background noise ratio at distance $R$, which occurs when a mobile is on the cell fringe.
- $\zeta \triangleq \beta/R$.

Using these definitions the PDF of $\overline{\Lambda}$ becomes

$$f_{\overline{\Lambda}}(\overline{\Lambda}) = \zeta^2\delta\left(\overline{\Lambda} - \frac{\Lambda_f}{\zeta^{\alpha}}\right) + \frac{2}{\alpha}\Lambda_f^{\frac{2}{\alpha}}\overline{\Lambda}^{-\frac{\alpha+2}{\alpha}} \quad , \quad \Lambda_f \leq \overline{\Lambda} \leq \frac{\Lambda_f}{\zeta^{\alpha}} \quad . \tag{3.15}$$

When obtaining numerical results, it will be assumed that $\zeta = 0.1$ and $\alpha = 4$.

## 3.3 Uplink Performance Analysis

### 3.3.1 Multipath Rejection Receiver

Consider a multipath rejection receiver that processes the signal received over the zero path, and rejects the signal received over all other paths.[10] In a mobile radio environment, the probability of multipaths with significant power will decrease with increasing delay relative to the dominant path. Hence, the self interference due to multipath can be minimized by using spreading codes that have small autocorrelation sidelobes in the time intervals during which delayed signals with significant power are expected. For large delays, the stringent requirements on the autocorrelation function can be relaxed. The spreading codes still must have small cross-correlation sidelobes over all delays, because the uplink transmissions are asynchronous. It is easy to find reasonably large sets of sequences that satisfy these properties. For example, a set of $2^m + 1$ Gold sequences can be generated of length $2^m - 1$. These sequences have autocorrelation values from the set $\{2^m - 1, -1, t_m - 2, -t_m\}$, and crosscorrelation

[10]Here we assume the exponential MIP in (3.3) so that the zero path is the dominant path.

values from the set $\{-1, t_m - 2, -t_m\}$, where

$$t_m = \begin{cases} 2^{(m+1)/2} + 1, & m \text{ odd} \\ 2^{(m+2)/2} + 1, & m \text{ even} \end{cases} . \tag{3.16}$$

Of these $2^m + 1$ sequences, $2^{m-n+1} + 1$ will have their first autocorrelation sidelobe ($t_m - 2$ or $t_m$) at least $n$ chip durations from the main lobe. Consequently, these $2^{m-n+1} + 1$ sequences will introduce negligible self interference if they are used on a channel having $n$ or fewer paths.

In the subsequent analysis, the self interference due to multipath will be neglected, under the assumption that appropriate codes are used. This is a very important assumption, because a significant performance degradation will result from a poor choice of spreading codes, e.g., completely random sequences. Then by treating the multiple-access interference as additional Gaussian noise, the instantaneous received bit energy-to-*total* noise ratio associated with transmitter $\hat{j}$ is

$$\begin{aligned} R_{\hat{j}} &= \frac{|c_0^{\hat{j}}|^2 E_b}{N_o + \eta^{-1} \sum_{(i,n)\in U} |c_n^i|^2 E_b} \\ &= \frac{\lambda_0^{\hat{j}}}{1 + \eta^{-1} \sum_{(i,n)\in U} \lambda_n^i} , \end{aligned} \tag{3.17}$$

where $U = \{(i,n) : 1 \le i \le K, 0 \le n \le L-1, \text{ and } i \ne \hat{j}\}$, $\eta$ is the processing gain, and $\lambda_n^j \triangleq |c_n^j|^2 \frac{E_b}{N_o}$. For a (nonfaded) AWGN channel,

$$R_{\hat{j}} = \frac{\Lambda^{\hat{j}}}{1 + \eta^{-1} \sum_{\substack{i=1 \\ i\ne j}} \Lambda^i} . \tag{3.18}$$

To compute the bit error probability, first define the mean vector

$$\overline{\mathbf{\Lambda}} = (\overline{\Lambda}_0^1, \ldots, \overline{\Lambda}_0^K; \overline{\Lambda}_1^1, \ldots, \overline{\Lambda}_1^K; \ldots; \overline{\Lambda}_L^1, \ldots, \overline{\Lambda}_L^K) , \tag{3.19}$$

and the *local* mean vector

$$\mathbf{\Lambda} = (\Lambda_0^1, \ldots, \Lambda_0^K; \Lambda_1^1, \ldots, \Lambda_1^K; \ldots; \Lambda_L^1, \ldots, \Lambda_L^K) . \tag{3.20}$$

The joint PDF of $\overline{\mathbf{\Lambda}}$, denoted by $p_1(\overline{\mathbf{\Lambda}})$, and the joint conditional PDF of $\mathbf{\Lambda}$, denoted by $p_2(\mathbf{\Lambda}|\overline{\mathbf{\Lambda}})$, can be obtained by using (3.11), (3.12), and (3.15). The bit error probability associated with transmitter $\hat{j}$, as a function of $\mathbf{\Lambda}$, is

$$P_{\hat{j}}(\mathbf{\Lambda}) = \int_0^\infty G(r_{\hat{j}}) \mathrm{f}_{R_j|\mathbf{\Lambda}}(r_{\hat{j}}|\mathbf{\Lambda}) dr_{\hat{j}} , \tag{3.21}$$

where $G(r_{\hat{j}})$ is the bit error probability as a function of the instantaneous bit energy-to-total noise ratio, and $\mathrm{f}_{R_{\hat{j}}|\mathbf{\Lambda}}(r_{\hat{j}}|\mathbf{\Lambda})$ is the conditional PDF of $R_{\hat{j}}$ . For illustration purposes, DPSK signaling is considered where

$$G(r_{\hat{j}}) = \frac{1}{2}\exp\{-r_{\hat{j}}\} \quad . \tag{3.22}$$

Other types of modulation and detection can be analyzed by defining the appropriate function $G(r_{\hat{j}})$ at this point. Averaging (3.21) over the joint PDF of $\overline{\mathbf{\Lambda}}$ and the joint conditional PDF $p_2(\mathbf{\Lambda}|\overline{\mathbf{\Lambda}})$ will account for the random mobile locations and shadowing, and gives the area averaged bit error probability[11]

$$P = \int_{\Lambda_f}^{\Lambda_f/\zeta^\alpha} \int_0^\infty P_{\hat{j}}(\mathbf{\Lambda}) p_2(\mathbf{\Lambda}|\overline{\mathbf{\Lambda}}) p_1(\overline{\mathbf{\Lambda}}) d\mathbf{\Lambda} d\overline{\mathbf{\Lambda}} \quad . \tag{3.23}$$

In order to evaluate (3.21), $\mathrm{f}_{R_{\hat{j}}|\mathbf{\Lambda}}(r_{\hat{j}}|\mathbf{\Lambda})$ is required. For a (nonfaded) AWGN channel this is simply

$$\mathrm{f}_{R_{\hat{j}}|\mathbf{\Lambda}}(r_{\hat{j}}|\mathbf{\Lambda}) = \delta\left(r_{\hat{j}} - \frac{\Lambda^{\hat{j}}}{1+\eta^{-1}\sum_{\substack{i=1\\ i\neq\hat{j}}} \Lambda^i}\right) \quad . \tag{3.24}$$

For the multipath-fading channel model defined in Section II-A

$$\mathrm{f}_{R_{\hat{j}}|\mathbf{\Lambda}}(r_{\hat{j}}|\mathbf{\Lambda}) = \frac{1}{\Lambda_0^{\hat{j}}}\exp\left\{-\frac{r_{\hat{j}}}{\Lambda_0^{\hat{j}}}\right\} \sum_{(i,n)\in U} \mathcal{N}_{i,n} \left( \frac{\left(\frac{r_{\hat{j}}}{\Lambda_0^{\hat{j}}}\frac{\Lambda_n^i}{\eta} + 1 + \frac{\Lambda_n^i}{\eta}\right)}{\left(\frac{r_{\hat{j}}}{\Lambda_0^{\hat{j}}}\frac{\Lambda_n^i}{\eta} + 1\right)^2} \right) \quad , \tag{3.25}$$

where

$$\mathcal{N}_{i,n} = \prod_{(j,k)\in U\setminus(i,n)} \frac{\Lambda_n^i}{\Lambda_n^i - \Lambda_k^j} \quad , \tag{3.26}$$

and $U \setminus (i,n) = \{(j,k) \in U : (j,k) \neq (i,n)\}$.

Using (3.21), (3.22), and (3.25) gives

$$P_{\hat{j}}(\mathbf{\Lambda}) = \frac{1}{2}\sum_{(i,n)\in U} \mathcal{N}_{i,n}\left\{1 - \frac{\eta\Lambda_0^{\hat{j}}}{\Lambda_n^i}\exp\left\{\frac{\eta\Lambda_0^{\hat{j}}}{\Lambda_n^i} + \frac{\eta}{\Lambda_n^i}\right\} E_1\left(\frac{\eta\Lambda_0^{\hat{j}}}{\Lambda_n^i} + \frac{\eta}{\Lambda_n^i}\right)\right\} \quad , \tag{3.27}$$

where $E_n(\,\cdot\,)$ is the exponential integral of order $n$.

*1) Power Control:* Power control is a technique that is essential for the uplink of cellular systems employing DS CDMA. Here, we assume that the mobiles can adjust

[11]Note that the area averaged bit error probability is the same for every transmitter and, therefore, the dependency on $\hat{j}$ is removed.

their transmitted power to compensate for the effects of path loss and shadowing only. Power control is not used to compensate for the rapid signal fluctuations introduced by multipath-fading.

It is assumed that the total transmitted power from all $K$ mobiles in a cell is the same, regardless of whether or not power control is used. With power control, the total transmitted power is divided among the mobiles so that same signal power is received at the base-station for every mobile. In this case $\Lambda$ and $\Lambda_f$ are related by

$$\Lambda = \frac{KR^\alpha}{\sum_{i=1}^{K} d(r_i)} \Lambda_f \quad , \tag{3.28}$$

where

$$d(r_i) = \begin{cases} 1 & , \quad r_i < \beta \\ (r_i)^\alpha & , \quad r_i \geq \beta \end{cases} \quad . \tag{3.29}$$

Suppose that ideal power control is used so that $\Lambda_n^j = \Lambda_n$, $1 \leq j \leq K$. Since all channels have the same MIP, the $\lambda_n^j$, $1 \leq j \leq K$ are independent and identically distributed, i.e.,

$$\mathrm{f}_{\lambda_n^j}(\lambda_n) = \frac{1}{\Lambda_n} \exp\left\{-\frac{\lambda_n}{\Lambda_n}\right\} \quad , \qquad 1 \leq j \leq K \quad . \tag{3.30}$$

It follows that the PDF of $R_j$ in (3.17) is

$$\mathrm{f}_{R_j}(r_j) = \left\{\prod_{n=0}^{L-1} \left(\frac{\eta}{\Lambda_n}\right)^{K-1}\right\} \sum_{n=0}^{L-1} \sum_{k=0}^{K-2} \frac{1}{k!} \mathcal{D}_n^k \frac{1}{\Lambda_0} \exp\left\{-\frac{r_j}{\Lambda_n}\right\} \left\{\frac{\frac{r_j}{\Lambda_0} + \frac{\eta}{\Lambda_n} + K - 1 - k}{\left(\frac{r_j}{\Lambda_0} + \frac{\eta}{\Lambda_n}\right)^{K-k}}\right\} \quad , \tag{3.31}$$

where

$$\mathcal{D}_n^k = \frac{d^k}{ds^k} \left\{\prod_{\substack{i=0 \\ i \neq n}}^{L-1} \left(\frac{1}{s + \frac{\eta}{\Lambda_i}}\right)^{K-1}\right\} \Big|_{s=-\frac{\eta}{\Lambda_n}} \quad . \tag{3.32}$$

Since $\mathbf{\Lambda}$ is not random when power control is being used, substituting (3.31) and (3.22) into (3.21) gives the area averaged bit error probability

$$\begin{aligned} P \;=\; & \frac{1}{2} \left\{\prod_{n=0}^{L-1} \left(\frac{\eta}{\Lambda_n}\right)^{K-1}\right\} \sum_{n=0}^{L-1} \sum_{k=0}^{K-2} \frac{1}{k!} \mathcal{D}_n^k \left(\frac{\Lambda_n}{\eta}\right)^{K-1-k} \\ & \times \left\{1 - \frac{\eta\Lambda_0}{\Lambda_n} \exp\left\{\frac{\eta\Lambda_0}{\Lambda_n} + \frac{\eta}{\Lambda_n}\right\} E_{K-1-k}\left(\frac{\eta\Lambda_0}{\Lambda_n} + \frac{\eta}{\Lambda_n}\right)\right\} \quad . \end{aligned} \tag{3.33}$$

Fig. 3.1 plots the bit error probability with power control, as given by Eq. (3.33) for a multipath-fading channel, and by Eqs. (3.21)-(3.23), and (3.24) for a nonfaded

channel. The performance degradation due to multipath-fading is significant. Fig. 3.2 further illustrates the deleterious effect of multipath. In fact, an increase in the number of channel paths has an effect similar to an increase in the number of simultaneous transmissions. Fig. 3.3 shows the bit error probability without power control, obtained from Eqs. (3.23) and (3.27), and demonstrates the necessity of using power control to maintain an acceptable performance. The failure to use power control will result in a large reduction in capacity. Fig. 3.4 further illustrates this point by showing the bit error probability with and without power control for an interference limited environment (no background noise).

### 3.3.2 RAKE Receivers with Power Control

The bit error rate performance can be improved by using multipath diversity techniques. In this section, we evaluate the performance of two different $\mathcal{L}$-tap RAKE receivers; one uses predetection selective diversity combining, and the other uses post-detection equal gain diversity combining.

The instantaneous bit energy-to-*total* noise ratio that is received over path $t$ from transmitter $\hat{j}$ is

$$R_{\hat{j},t} = \frac{\lambda_t^{\hat{j}}}{1 + \eta^{-1} \sum_{(i,n)\in U} \lambda_n^i} \quad . \tag{3.34}$$

The instantaneous processed bit energy-to-*total* noise ratio with predetection selective diversity combining is

$$R_{\hat{j}}^s = \max\{R_{\hat{j},t} : 0 \le t \le \mathcal{L} - 1\} \quad , \tag{3.35}$$

Likewise, the total instantaneous processed bit energy-to-*total* noise ratio with post-detection equal gain combining is

$$R_{\hat{j}}^c = \sum_{t=0}^{\mathcal{L}-1} R_{\hat{j},t} \quad . \tag{3.36}$$

*1) Predetection Selective Combining:* It can be shown that the PDF of $R_{\hat{j}}^s$ is

$$\begin{aligned} \mathrm{f}_{R_{\hat{j}}^s}(r_{\hat{j}}^s) \;=\; & \prod_{n=0}^{L-1} \left(\frac{\eta}{\Lambda_n}\right)^{K-1} \sum_{t=1}^{\mathcal{L}} \sum_{j_1,\ldots,j_t} (-1)^{t+1} \sum_{n=0}^{L-1} \sum_{k=0}^{K-2} \left(\frac{\hat{\mathcal{D}}_n^k}{k!}\right) \\ & \times \; \mathcal{B}_t \exp[-r_{\hat{j}}^s \mathcal{B}_t] \left(\frac{r_{\hat{j}}^s \mathcal{B}_t + \frac{\eta}{\Lambda_n} + K - 1 - k}{\left(r_{\hat{j}}^s \mathcal{B}_t + \frac{\eta}{\Lambda_n}\right)^{K-k}}\right) \end{aligned} \tag{3.37}$$

where

$$\hat{\mathcal{D}}_n^k = \frac{\mathrm{d}^k}{\mathrm{d}s^k}\left\{\prod_{\substack{i=0\\ i\neq n}}^{L-1}\left(\frac{1}{s+\frac{\eta}{\Lambda_i}}\right)^{K-1}\right\}\Bigg|_{s=-\frac{\eta}{\Lambda_n}} , \tag{3.38}$$

$$\mathcal{B}_t = \frac{1}{\Lambda_{j_1}^{\hat{j}}} + \cdots + \frac{1}{\Lambda_{j_t}^{\hat{j}}} , \tag{3.39}$$

and $\sum_{j_1,\ldots,j_t}$ is summed over the $t$-element subsets of $\{0,1,2,\ldots,\mathcal{L}-1\}$.

Substituting (3.38) and (3.22) into (3.21) gives the area averaged bit error probability

$$\begin{aligned} P &= \frac{1}{2}\prod_{n=0}^{L-1}\left(\frac{\eta}{\Lambda_n}\right)^{K-1}\sum_{t=1}^{\mathcal{L}}\sum_{j_1,\ldots,j_t}(-1)^{t+1}\sum_{n=0}^{L-1}\sum_{k=0}^{K-2}\left(\frac{\hat{\mathcal{D}}_n^k}{k!}\right)\left(\frac{\Lambda_n}{\eta}\right)^{K-1-k} \\ &\quad\times\left\{1-\frac{\eta}{\mathcal{B}_t\Lambda_n}\exp\left\{\frac{\eta}{\mathcal{B}_t\Lambda_n}+\frac{\eta}{\Lambda_n}\right\}E_{K-1-k}\left(\frac{\eta}{\mathcal{B}_t\Lambda_n}+\frac{\eta}{\Lambda_n}\right)\right\} . \end{aligned} \tag{3.40}$$

*2) Postdetection Equal Gain Combining:* It can be shown that the PDF of $R_{\hat{j}}^c$ is

$$\begin{aligned} \mathrm{f}_{R_{\hat{j}}^c}(r_{\hat{j}}^c) &= \prod_{n=0}^{L-1}\left(\frac{\eta}{\Lambda_n}\right)^{K-1}\sum_{t=0}^{\mathcal{L}-1}\sum_{n=0}^{L-1}\sum_{k=0}^{K-2}\left(\frac{\hat{\mathcal{D}}_n^k}{k!}\right)\left(\frac{\mathcal{C}_t}{\Lambda_t^{\hat{j}}}\right) \\ &\quad\times\quad \exp\left\{-\frac{r_{\hat{j}}^c}{\Lambda_t^{\hat{j}}}\right\}\left(\frac{\frac{r_{\hat{j}}^c}{\Lambda_t^{\hat{j}}}+\frac{\eta}{\Lambda_n}+K-1-k}{\left(\frac{r_{\hat{j}}^c}{\Lambda_t^{\hat{j}}}+\frac{\eta}{\Lambda_n}\right)^{K-k}}\right) \end{aligned} \tag{3.41}$$

where,

$$\mathcal{C}_t = \prod_{\substack{i=0\\ i\neq t}}^{\mathcal{L}-1}\frac{\Lambda_t^{\hat{j}}}{\Lambda_t^{\hat{j}}-\Lambda_i^{\hat{j}}} . \tag{3.42}$$

For differential detection and postdetection equal gain combining, the bit error probability as a function of the total instantaneous processed bit energy-to-*total* noise ratio is [23]

$$G(r_{\hat{j}}^c) = \frac{1}{2^{2\mathcal{L}-1}}\exp\{-r_{\hat{j}}^c\}\sum_{t=0}^{\mathcal{L}-1}b_t(r_{\hat{j}}^c)^t , \tag{3.43}$$

where

$$b_k = \frac{1}{k!}\sum_{\ell=0}^{\mathcal{L}-1-k}\binom{2\mathcal{L}-1}{\ell} . \tag{3.44}$$

Substituting (3.42) and (3.43) into (3.21), gives the area averaged bit error probability

$$
\begin{aligned}
P \;=\; & \frac{1}{2^{2\mathcal{L}-1}} \prod_{n=0}^{L-1} \left(\frac{\eta}{\Lambda_n}\right)^{K-1} \sum_{t=0}^{\mathcal{L}-1} \frac{\mathcal{C}_t}{\Lambda_t} \sum_{n=0}^{L-1} \sum_{k=0}^{K-2} \left(\frac{\hat{\mathcal{D}}_n^k}{k!}\right) \left(\frac{\Lambda_n}{\eta}\right)^{K-1-k} \\
& \times \sum_{t'=0}^{\mathcal{L}-1} b_{t'} \left(\frac{\eta\Lambda_t}{\Lambda_n}\right)^{t'+1} \sum_{\ell=0}^{t'} \binom{t'}{\ell} (-1)^{t'-\ell} \\
& \times \left\{ \frac{1}{\left(\frac{\eta}{\Lambda_n} + \frac{\eta\Lambda_t}{\Lambda_n}\right)} + \left( \frac{\ell+1-K+k}{\left(\frac{\eta}{\Lambda_n} + \frac{\eta\Lambda_t}{\Lambda_n}\right)} + \frac{\Lambda_n(K-1+k)}{\eta} \right) \right. \\
& \qquad \left. \times \left( \frac{\exp\left[\frac{\eta}{\Lambda_n} + \frac{\eta\Lambda_t}{\Lambda_n}\right]}{\left(\frac{\eta}{\Lambda_n} + \frac{\eta\Lambda_t}{\Lambda_n}\right)^{\ell+1-K+k}} \right) \Gamma\left(\ell+1-K+k, \frac{\eta}{\Lambda_n} + \frac{\eta\Lambda_t}{\Lambda_n}\right) \right\} \quad ,
\end{aligned}
\tag{3.45}
$$

where $\Gamma(\cdot,\cdot)$ is the incomplete gamma function defined by

$$
\Gamma(\alpha, x) = \int_x^\infty e^{-t} t^{\alpha-1} dt \quad . \tag{3.46}
$$

Fig. 3.5 plots the bit error probability for an $\mathcal{L}$-tap RAKE receiver with predetection selective diversity combining. Fig. 3.6 compares the performance of predetection selective diversity combining and postdetection equal gain combining. As expected, with differential detection, postdetection equal gain combining performs somewhat better. These results show that a RAKE receiver can provide a significant improvement in performance provided that the channel has the right amount of dispersion. However, if the channel either consists of a single faded path or is very dispersive, then the performance can be quite poor.

### 3.3.3 Error Correction Coding

It is well known that the performance of a digital communication system can usually be improved by using error correction coding. However, for mobile communications, fading induced channel memory can degrade the coded performance. Traditionally, this is remedied by using enough interleaving to destroy the channel memory. Unfortunately, a large interleaving delay is unacceptable for voice communication. Even a moderate interleaving delay is undesirable, because it makes echo cancellation necessary.

In a radio mobile environment, the fading rate depends on vehicle speed. At high vehicle speeds, the fading rate is fast enough so that a small amount of interleav-

ing will effectively destroy the channel memory. However, at low vehicle speeds, the delay requirements imposed by voice transmission will preclude the use of interleaving, so the channel will have memory. The effect of vehicle speed on the performance of error correction codes is illustrated here by considering $t$ error correcting BCH $(n, k)$ codes. Two extreme cases are considered; slow fading, where the bit energy-to-*total* noise ratio is random but constant over the duration of an entire codeword, and fast fading, where the channel is memoryless.

*1) Fast Fading:* With fast fading, the probability of decoded bit error is approximately

$$P \approx \frac{1}{n} \sum_{i=e+1}^{n} i \binom{n}{i} P_u^i (1 - P_u)^{n-i} \quad , \tag{3.47}$$

where $P_u$ is the code symbol error probability. To obtain $P_u$, we simply use the previous expressions for the uncoded bit error probability and replace $\Lambda$ with $r\Lambda$, where $r = k/n$ is the code rate.

*2) Slow Fading:* With slow fading, the decoded bit error probability is approximately

$$P \approx \int_0^\infty \left\{ \frac{1}{n} \sum_{i=e+1}^{n} i \binom{n}{i} G(r_j)^i (1 - G(r_j))^{n-i} \right\} \mathrm{f}_{R_j^{s,c}}(r_j^{s,c} | \mathbf{\Lambda}) dr_j^{s,c} \quad , \tag{3.48}$$

For selective diversity this results in

$$\begin{aligned} P \approx\ & \frac{1}{2n} \left\{ \prod_{\ell=0}^{L-1} \left( \frac{\eta}{\Lambda_\ell} \right)^{K-1} \right\} \sum_{e=\tau+1}^{n} e \binom{n}{e} \sum_{e'=0}^{n-e} \binom{n-e}{e'} (-1)^{e'} \\ & \times \sum_{t=1}^{\mathcal{L}} \sum_{j_1,\ldots,j_t} (-1)^{t+1} \sum_{\ell=0}^{L-1} \sum_{k=0}^{K-2} \left( \frac{\hat{\mathcal{D}}_\ell^k}{k!} \right) \left( \frac{\Lambda_\ell}{\eta} \right)^{K-1-k} \\ & \times \left\{ 1 - \frac{\eta(e+e')}{\mathcal{B}_t \Lambda_\ell} \exp\left\{ \frac{\eta(e+e')}{\mathcal{B}_t \Lambda_\ell} + \frac{\eta}{r\Lambda_\ell} \right\} E_{K-1-k}\left( \frac{\eta(e+e')}{\mathcal{B}_t \Lambda_\ell} + \frac{\eta}{r\Lambda_\ell} \right) \right\} \quad . \end{aligned} \tag{3.49}$$

Since both coding and processing gain result in bandwidth expansion, comparisons must be made on the basis of equal bandwidth. When coding is used, the processing gain is $\eta = r\eta^*$, where $r$ is the code rate, and $\eta^*$ is the processing gain for an uncoded system.

Fig. 3.7 shows the performance of BCH (15,$k$) codes for a 4-tap RAKE receiver with predetection selective diversity combining. Results are shown for both fast fading and slow fading. Observe that when the channel is memoryless (fast fading),

the performance is improved significantly as the code rate decreases. Hence, coding is more effective than processing gain. However, when the channel has memory (slow fading), coding actually results in a higher bit error probability. In this case, processing gain is more effective than coding.

## 3.4 Downlink Performance Analysis

For the downlink of a cellular radio system, all signals experience identical fading when transmitted to a particular receiver. That is, $\lambda_n^j = \lambda_n$, $1 \leq j \leq K$. As a result, (3.34) reduces to

$$R_{\hat{j}} = \frac{\lambda_t^{\hat{j}}}{1 + \eta^{-1}(K-1)\sum_{n=0}^{L-1}\lambda_n} \quad . \tag{3.50}$$

Define the local mean vector

$$\mathbf{\Lambda} \triangleq (\Lambda_0, \ldots, \Lambda_L) \quad . \tag{3.51}$$

Suppose that $\Lambda_p \neq \Lambda_k$ for $p \neq k$, as is the case for an exponential MIP. Then the conditional PDF of $R_j^s$ for a RAKE receiver with predetection selective diversity combining is

$$\begin{aligned} \mathrm{f}_{R_j^s|\mathbf{\Lambda}}(r_j^s) &= \sum_{t=1}^{\mathcal{L}} \sum_{j_1,\ldots,j_t} (-1)^{t+1} \sum_{n=0}^{L-1} \mathcal{N}_n \mathcal{B}_t \exp\left\{-r_j^s \mathcal{B}_t\right\} \\ &\quad \times \left( \frac{\left(r_j^s \mathcal{B}_t (K-1)\frac{\Lambda_n}{\eta} + 1 + (K-1)\frac{\Lambda_n}{\eta}\right)}{\left(r_j^s \mathcal{B}_t (K-1)\frac{\Lambda_n}{\eta} + 1\right)^2} \right) \quad . \end{aligned} \tag{3.52}$$

where

$$\mathcal{N}_n = \prod_{\substack{k=0 \\ k\neq n}}^{L-1} \frac{\Lambda_n}{\Lambda_n - \Lambda_k} \quad , \tag{3.53}$$

and $\mathcal{B}_t$ is defined in (3.39). Using (3.52), (3.21), and (3.22) gives

$$\begin{aligned} P_j^s(\mathbf{\Lambda}) &= \frac{1}{2} \sum_{t=1}^{\mathcal{L}} \sum_{j_1,\ldots,j_t} (-1)^{t+1} \sum_{n=0}^{L-1} \mathcal{N}_n \\ &\quad \times \left\{ 1 - \frac{\eta}{\mathcal{B}_t (K-1)\Lambda_n} \exp\left\{ \frac{\eta}{\mathcal{B}_t (K-1)\Lambda_n} + \frac{\eta}{(K-1)\Lambda_n} \right\} \right. \\ &\quad \left. \times E_1\left( \frac{\eta}{\mathcal{B}_t (K-1)\Lambda_n} + \frac{\eta}{(K-1)\Lambda_n} \right) \right\} \quad . \end{aligned} \tag{3.54}$$

The performance of a multipath rejection receiver can be easily obtained by setting $\mathcal{L} = 1$ in (3.54), leading to

$$P_{\hat{j}}(\mathbf{\Lambda}) = \frac{1}{2}\sum_{n=0}^{L-1}\mathcal{N}_n\left\{1 - \frac{\eta\Lambda_0}{(K-1)\Lambda_n}\exp\left\{\frac{\eta\Lambda_0}{(K-1)\Lambda_n} + \frac{\eta}{(K-1)\Lambda_n}\right\}\right.$$
$$\left.\times E_1\left(\frac{\eta\Lambda_0}{(K-1)\Lambda_n} + \frac{\eta}{(K-1)\Lambda_n}\right)\right\} . \tag{3.55}$$

Corresponding expressions can be obtained for the bit error probability with equal gain combining, but they are omitted here for brevity. In all cases, the area averaged bit error probability is given by (3.23).

Fig. 3.8 plots the bit error probability as given by (3.55) for a multipath-fading channel, and by Eqs. (3.21)-(3.23), and (3.24) for a nonfaded channel. Similar to the uplink, the performance degradation due to multipath-fading is significant. Fig. 3.9 plots the bit error probability for a multipath rejection receiver and an $\mathcal{L}$-tap RAKE receiver with predetection selective diversity combining. This figure shows that multipath diversity can offer a significant improvement in the performance, but the degree of improvement diminishes rapidly with the number of simultaneous transmissions. Once again, if the channel either consists of a single faded path or is very dispersive, then the performance can be quite poor.

Finally, Fig. 3.10 illustrates the effect of log-normal shadowing on the downlink performance. It is seen that in the region of moderate $\Lambda_f$, shadowing will cause an increase in the area averaged bit error probability. However, for an interference limited environment (large $\Lambda_f$), shadowing does not have much effect.

## 3.5 Concluding Remarks

This section has analyzed the performance of three differentially coherent spread spectrum receivers in a cellular radio environment; a multipath rejection receiver, a RAKE receiver with predetection selective diversity combining, and a RAKE receiver with postdetection equal gain combining. It was shown that multipath-fading can have a severe effect on the performance of a multipath-rejection receiver, especially when the channel is highly dispersive. A RAKE receiver was shown to improve the performance

significantly for a moderately dispersive channel. However, if the channel consists of a single faded path, a RAKE receiver cannot provide a performance improvement. In this case, antenna diversity may be required to guarantee an acceptable level of performance. It was also shown that error correction coding can provide a significant improvement in performance, provided that the channel fading rate is fast enough. However, for slowly varying channels it may not be desirable to use coding.

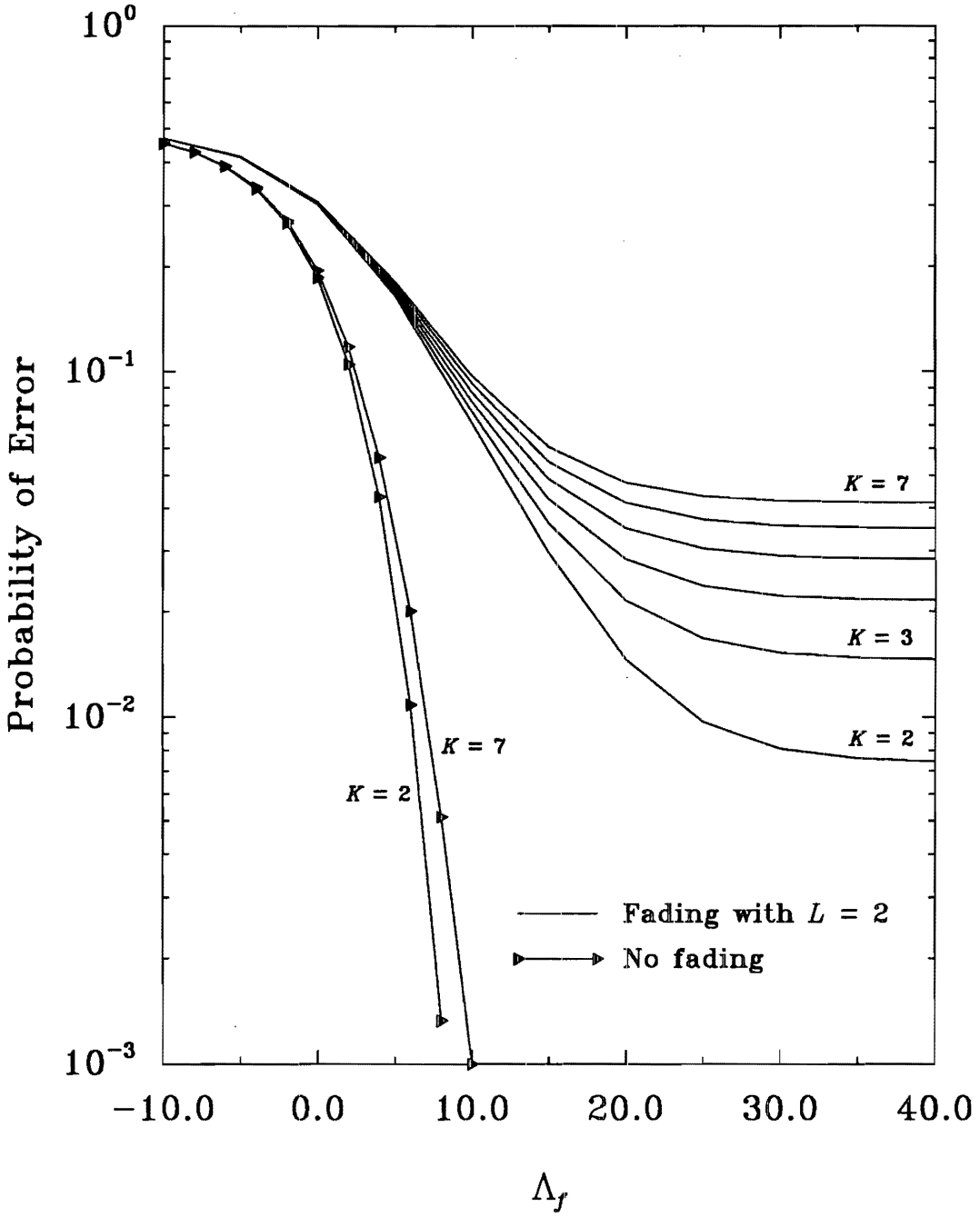


Figure 3.1: Uplink bit error probability against $\Lambda_f$ with power control and a multipath rejection receiver, for varying numbers of simultaneous transmissions; $L = 2, \eta = 100$

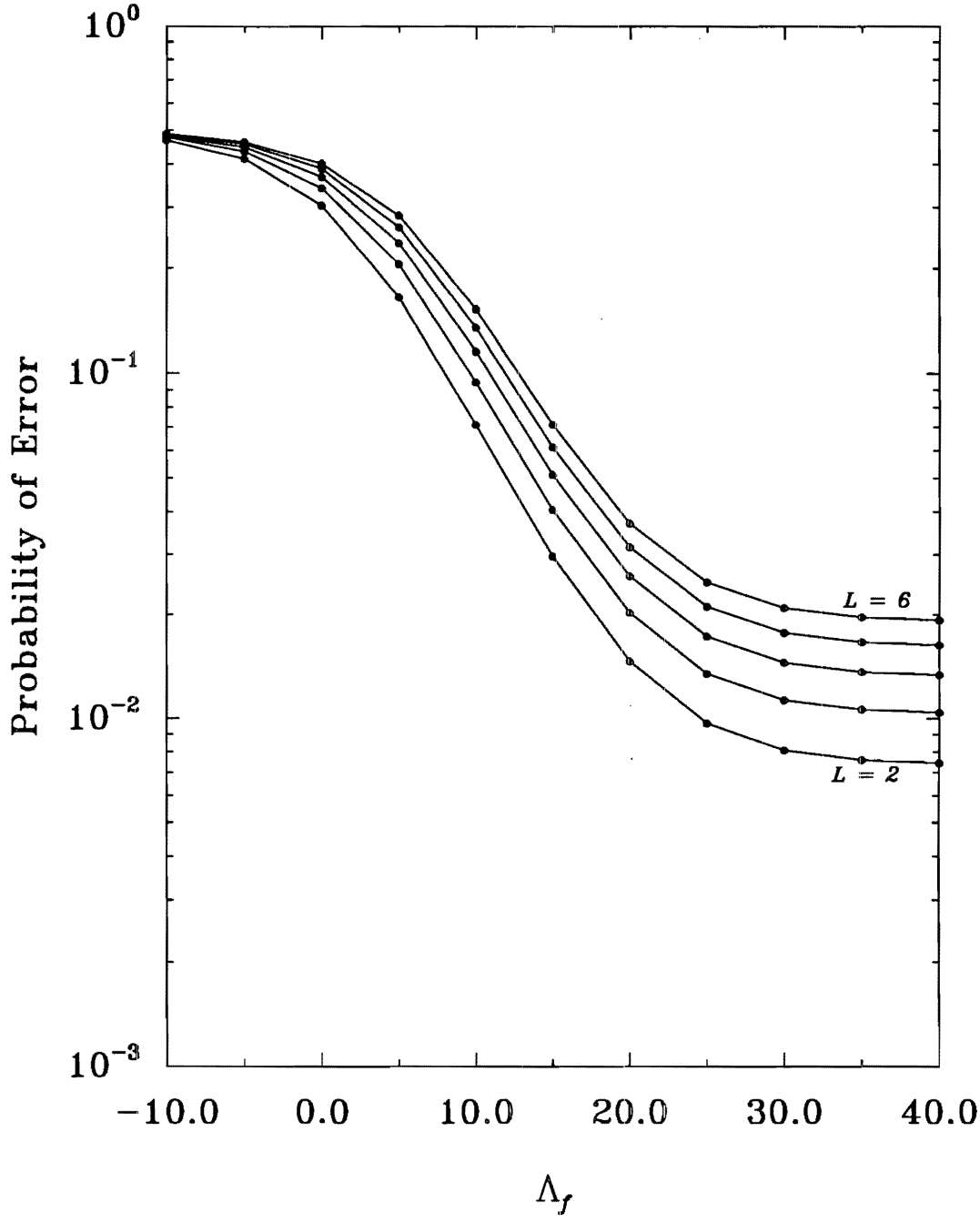


Figure 3.2: Degradation in uplink bit error probability with a multipath rejection receiver due to increased multiple-access interference from multipath, for varying numbers of channel paths; $K = 2, \eta = 100$

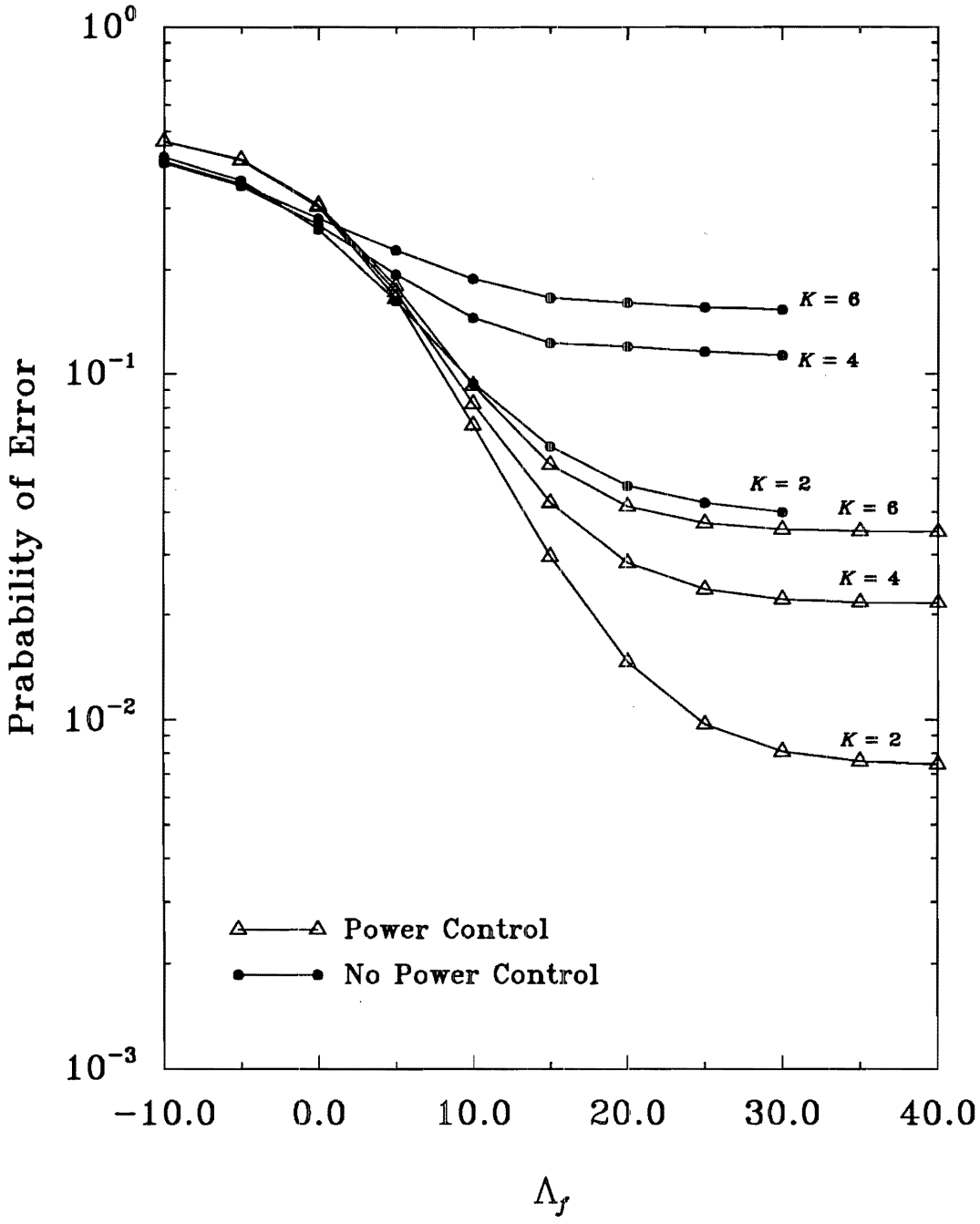


Figure 3.3: Uplink bit error probability with a multipath rejection receiver, and with and without power control, for varying numbers of simultaneous transmissions; $L = 2, \eta = 100$

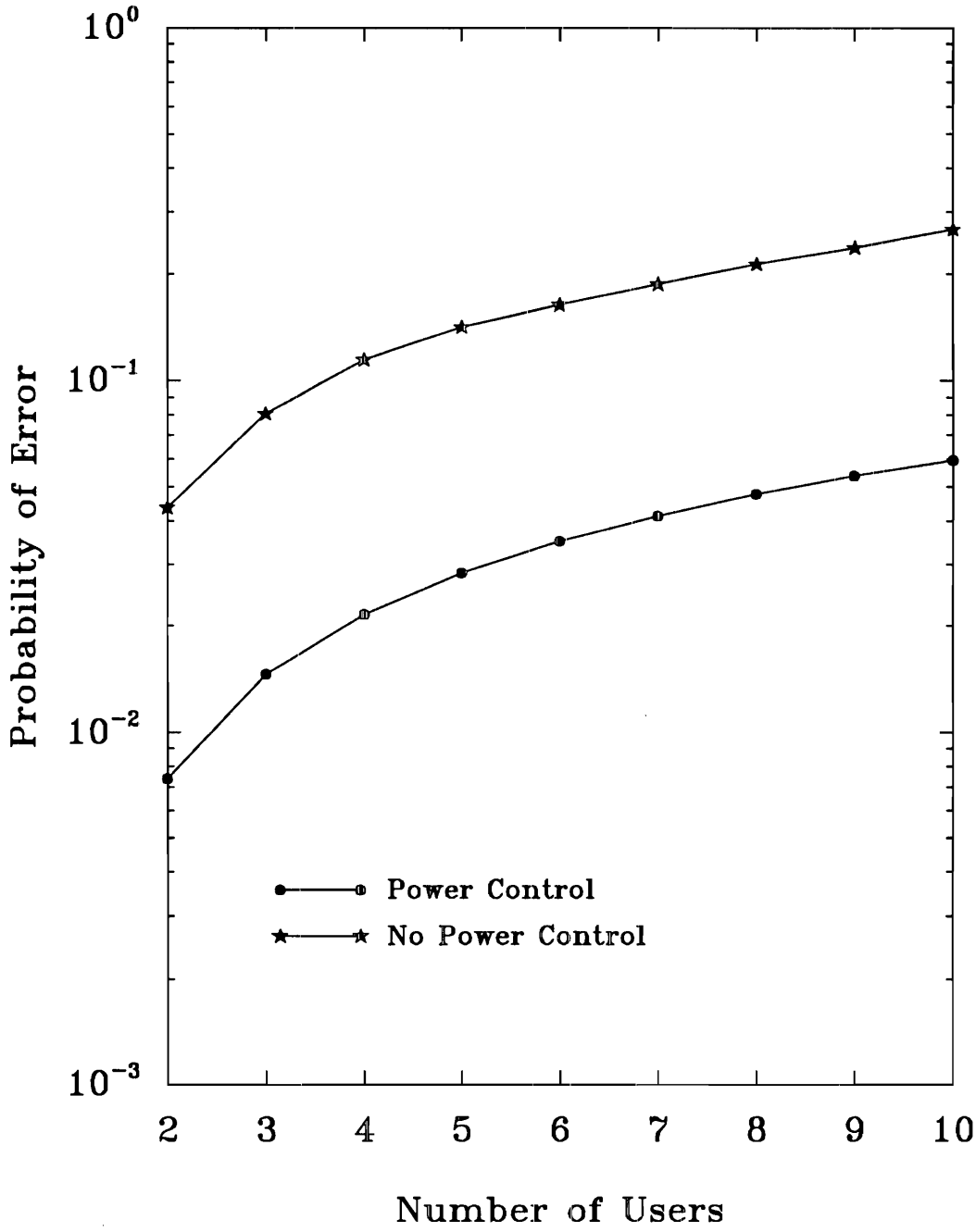


Figure 3.4: Uplink bit error probability with a multipath rejection receiver, and with and without uplink power control, for an interference limited environment (negligible background noise); $\Lambda_f = \infty$, $L = 2, \eta = 100$

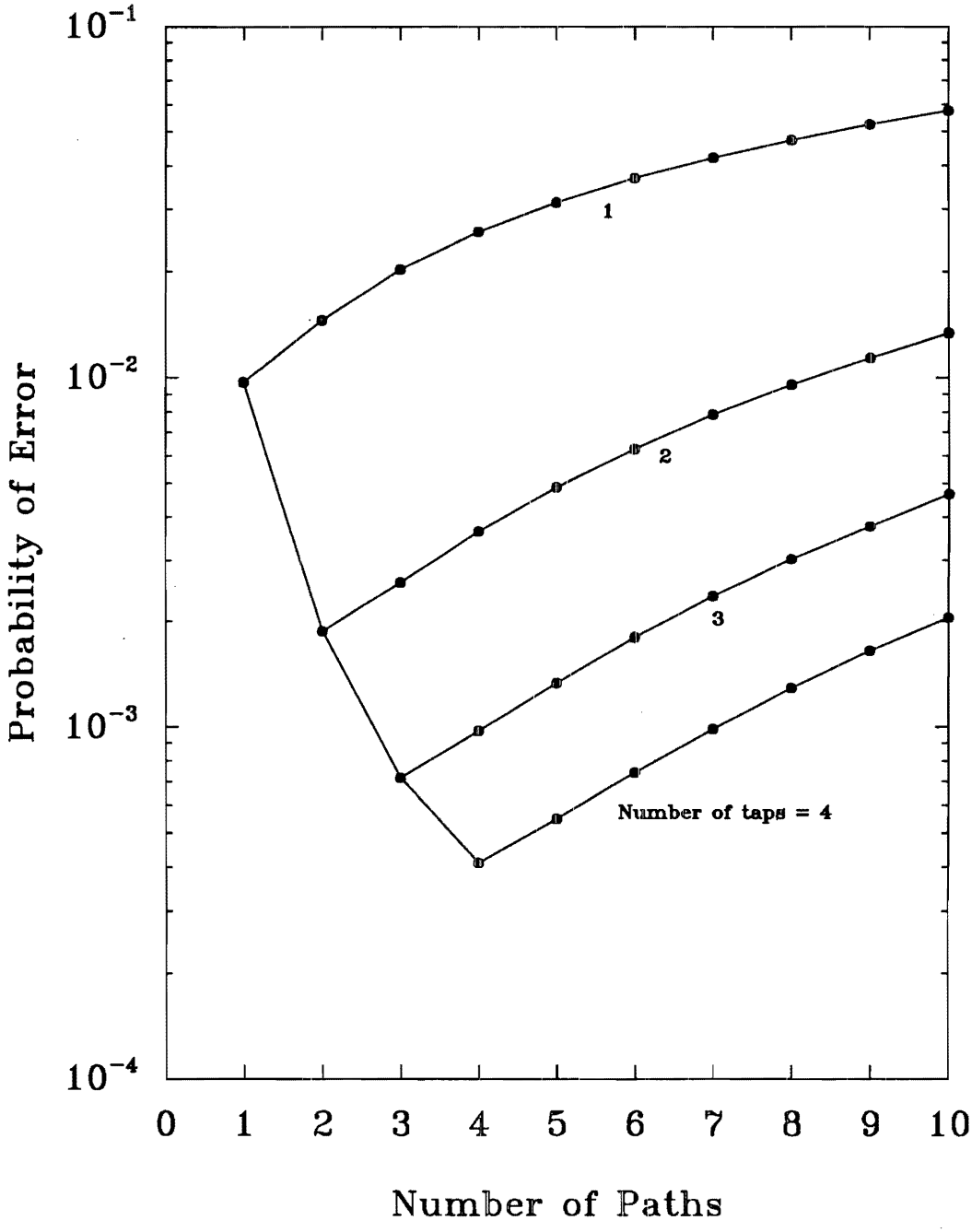


Figure 3.5: Uplink bit error probability with an $\mathcal{L}$-tap selective combining RAKE receiver and power control, for varying numbers of RAKE taps in an interference limited environment; $\Lambda_f = \infty$, $K = 3, \eta = 100$

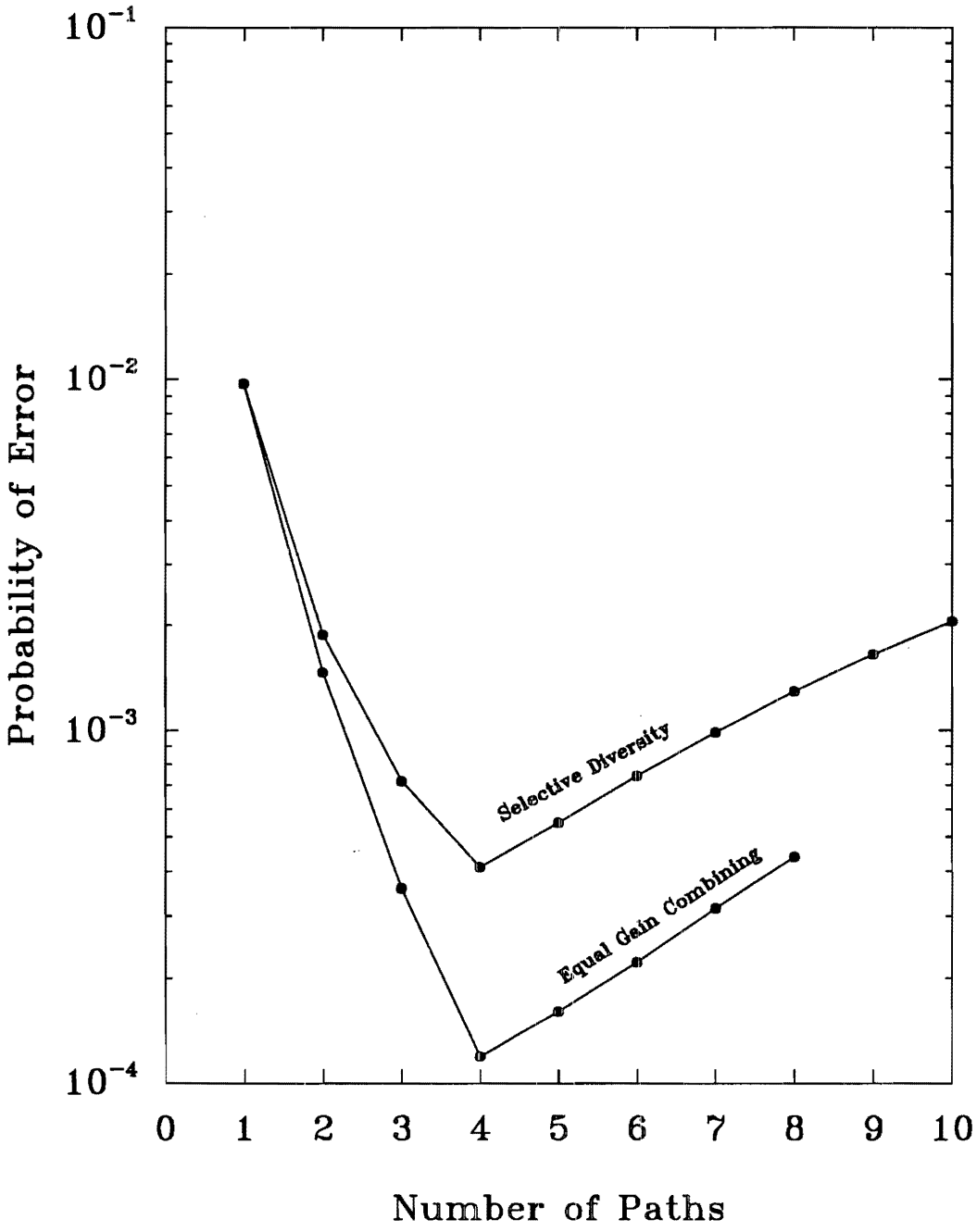


Figure 3.6: Comparison of selective and equal gain combining for a 4-tap RAKE receiver with power control, in an interference limited environment; $\Lambda_f = \infty$, $K = 3, \eta = 100$

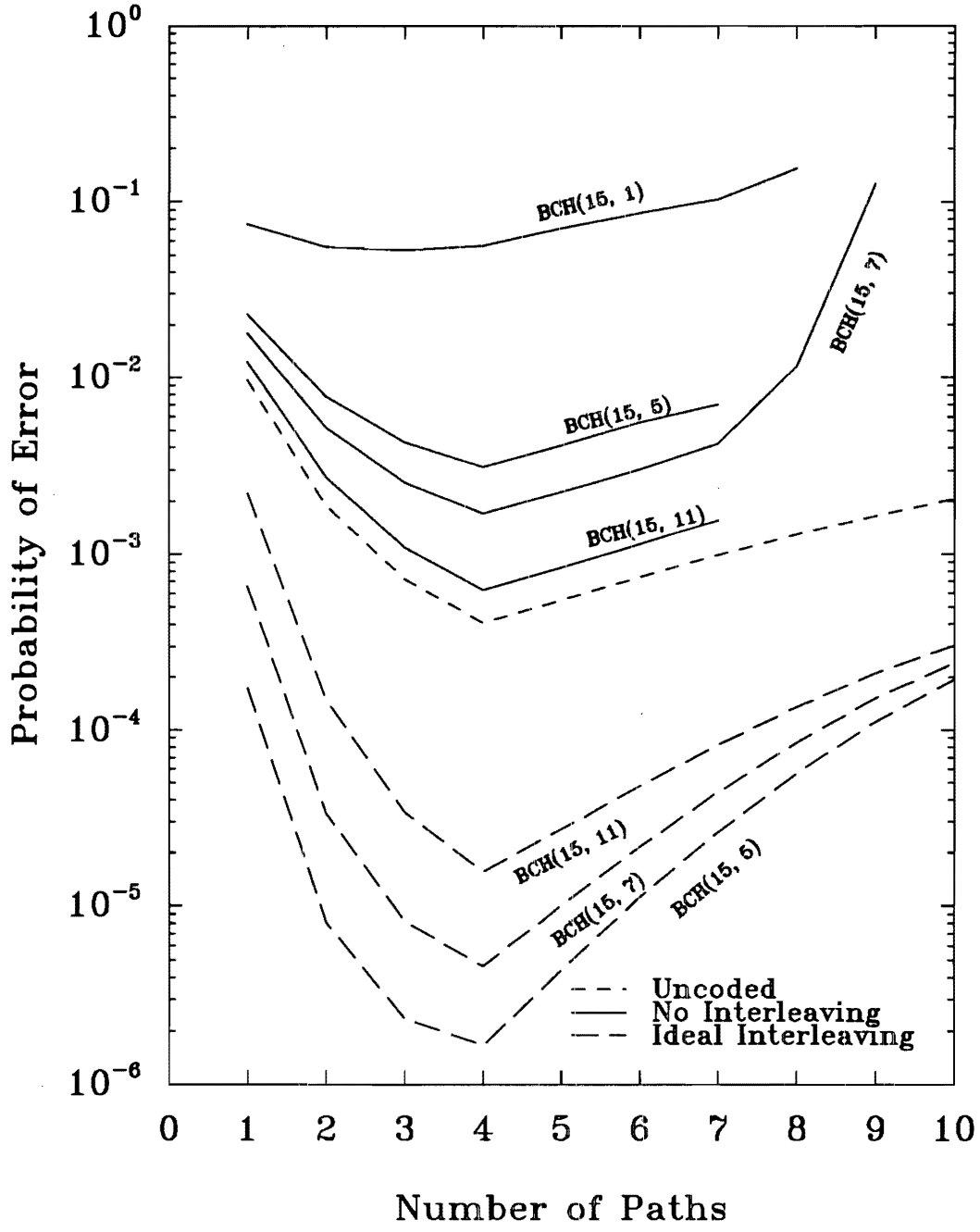


Figure 3.7: Bit error probability for a 4-tap RAKE receiver with selective combining and BCH (15,$k$) error correcting codes, in an interference limited environment; $K = 3$, $\eta = 100$

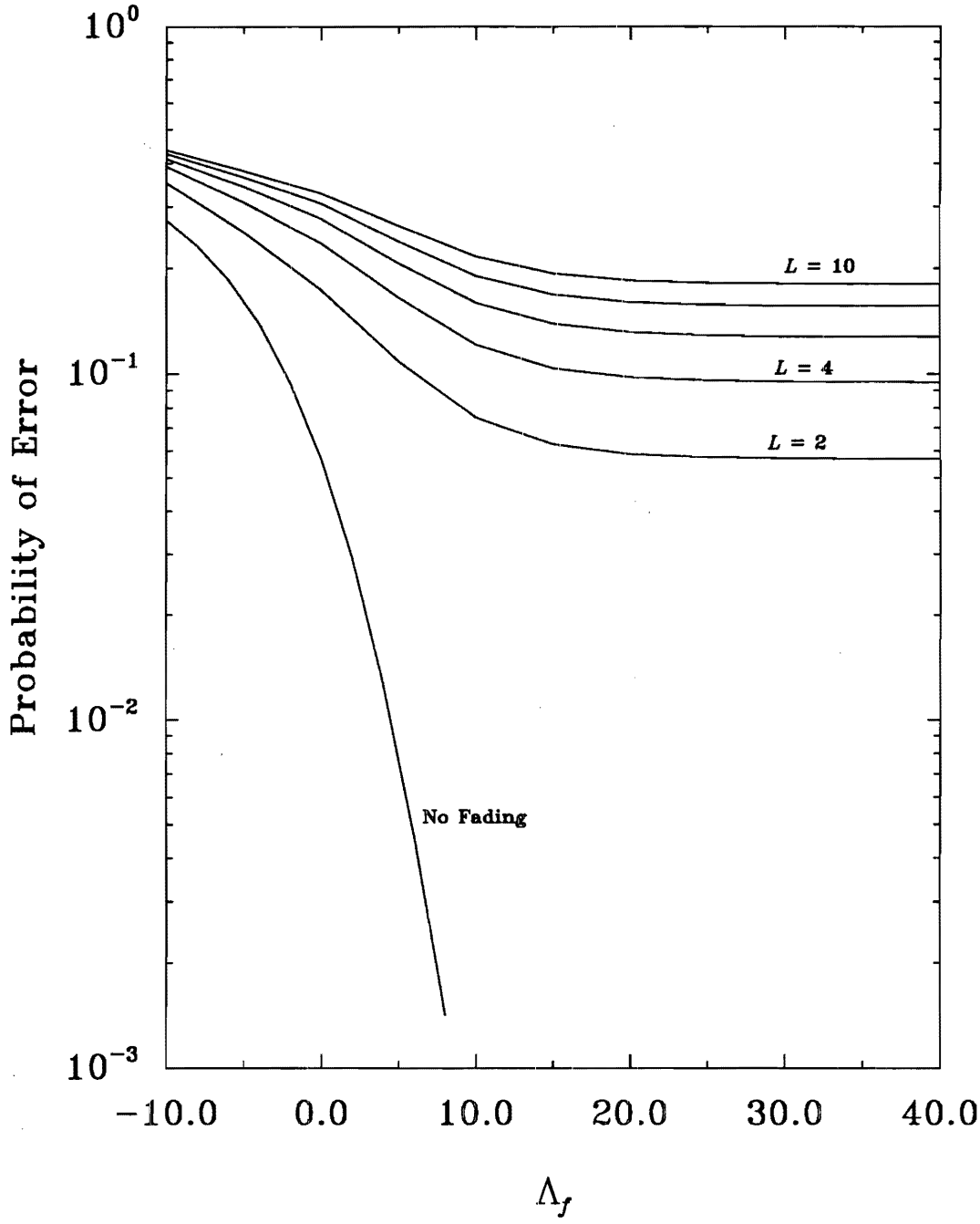


Figure 3.8: Downlink bit error probability against $\Lambda_f$ with a multipath rejection receiver, for varying numbers of channel paths; $K = 10, \eta = 100$

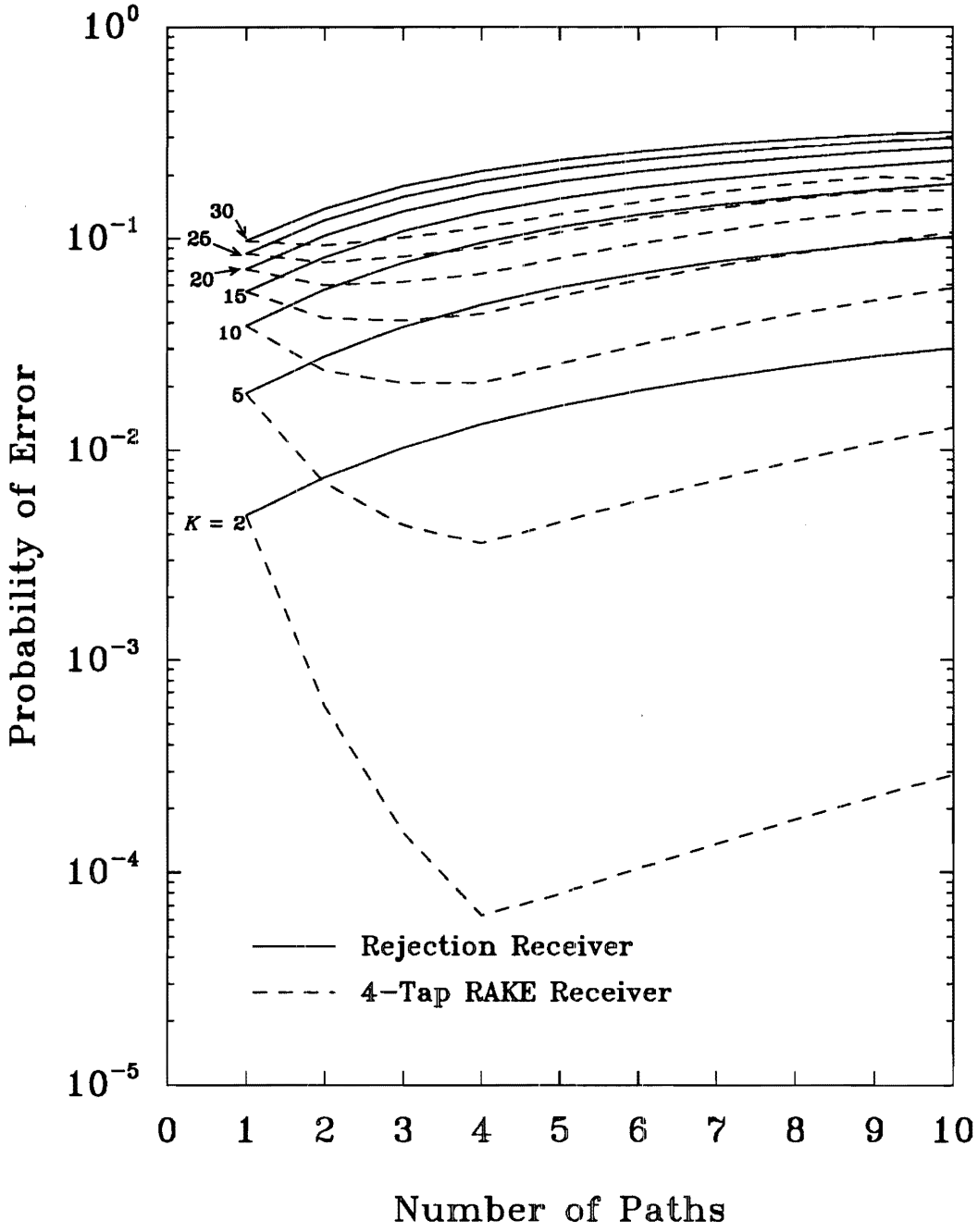


Figure 3.9: Downlink bit error probability with a multipath rejection receiver and an 4-tap RAKE receiver with selective combining, for varying numbers of simultaneous transmissions in an interference limited environment; $\Lambda_f = \infty$, $\eta = 100$

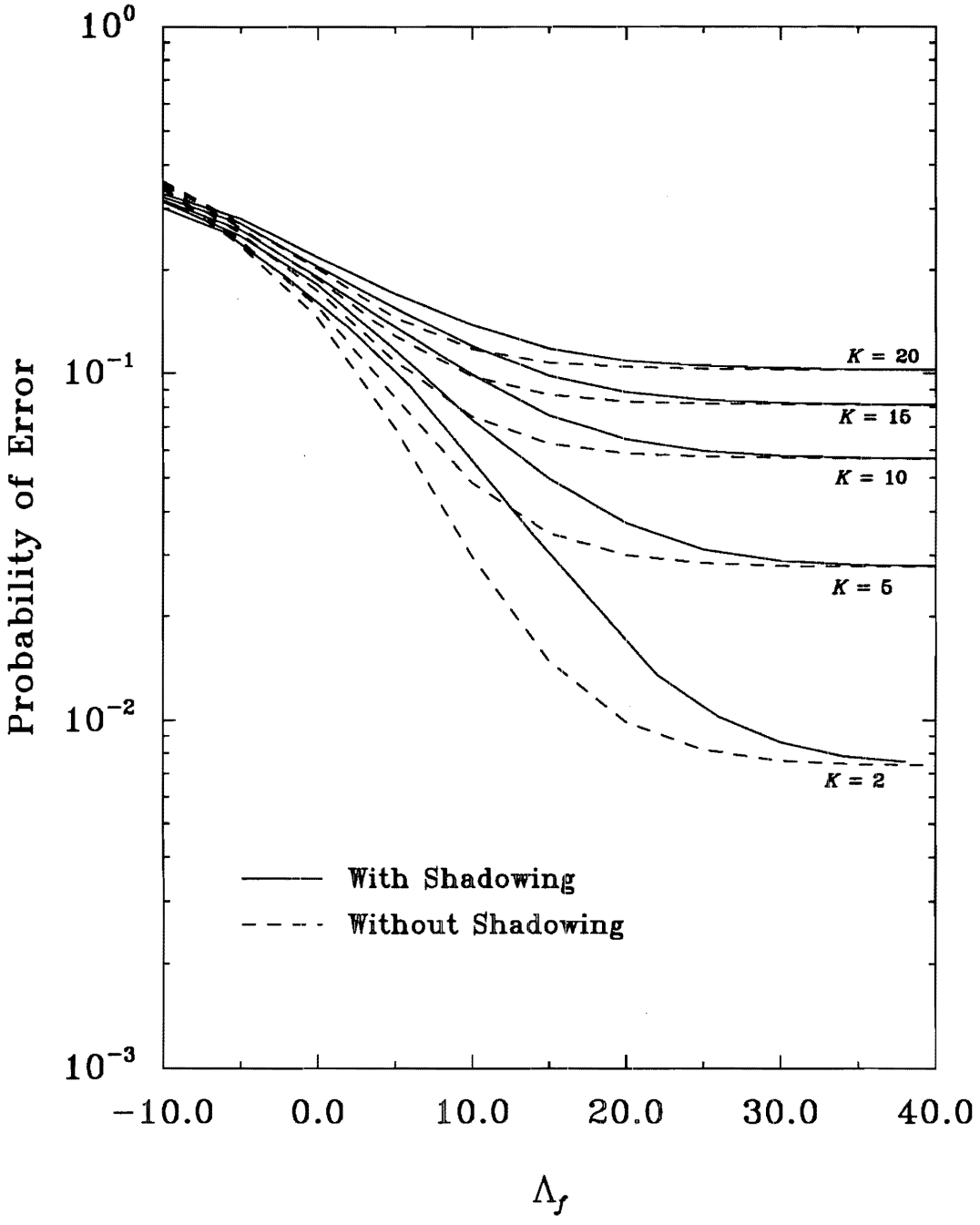


Figure 3.10: Increase in downlink bit error probability due to log-normal shadowing with a multipath rejection receiver, for varying numbers of simultaneous transmissions; $L = 2$, $\eta = 100$, $\sigma = 8$ dB

# 4 Multiple Cell CDMA System[12]

## 4.1 Introduction

The previous section considered the performance of a single cell Direct-Sequence Code Division Multiple-Access (DS CDMA) mobile radio system. This section complements the previous section by considering the performance of a DS CDMA system in a multiple cell mobile radio environment. It is not intended to provide a rigorous analysis of the specific DS CDMA cellular system proposed by Qualcomm [37]. Rather, it is intended to illustrate some of the generic properties and characteristics of a multiple cell DS CDMA mobile radio system.

A number of papers have appeared in the recent literature that evaluate multiple cell DS CDMA land mobile radio systems, and a few are mentioned here. Lee [38] has provided an overview of cellular DS CDMA. Gilhousen *et. al.* [37] have provided a capacity analysis of a DS CDMA system that accounts for the effects of path loss and log-normal shadowing, but does not explicitly consider the effects of multipath-fading. Pickholtz *et. al.* [39] have considered the use of DS CDMA for sharing a frequency band with narrow-band users. Rappaport and Milstein [23, 24] have examined the effect of path loss and user distribution on the performance of a DS CDMA cellular system. Vojčić *et. al.* [40] have compared the capacity of TDMA and DS CDMA for microcellular radio channels characterized by multipath-fading. Finally, Simpson and Holtzman [41], and Ariyavisitakul and Chang [42], have studied the effect of adaptive power control and interleaving on the performance of a coded DS CDMA cellular system.

Parts of this section consider some of the same issues addressed in the above literature, but with a different approach and emphasis. In this section, the basic approach is to evaluate the area averaged error probability, and to evaluate the error probability as a function of the distance from the base-station. A Gaussian approximation is used for the multiple-access interference that accounts for the variation in

[12]The work in this section was performed with the assistance of Chamrœun Kchao.

multiple-access interference due to multipath-fading. By using this approach, we consider some of the more common issues such as the use of RAKE receivers and uplink (mobile-to-base) power control, but also treat some peculiar features of a multiple cell DS CDMA system. One such feature is macroscopic base-station diversity, where the uplink transmissions can be received simultaneously by several base-stations [43]. Usually, the base-stations that are closest to a mobile are the most effective for this purpose. Sometimes the more distant base-stations are more effective, depending on the severity of shadowing and the locations of the interfering mobiles. In this section, two macroscopic diversity combining techniques are considered; majority logic combining and selective diversity combining.

It is well known that power control is essential for the uplink of a DS CDMA cellular system. For a multiple cell DS CDMA system, it is also possible that power control can improve the downlink (base-to-mobile) performance. The reason is the corner effect, where a mobile in a cell corner is equidistant from three base-stations and will experience an increase in multiple-access interference. Nettleton and Alavi [44, 45], and Lee [38], have shown that downlink power control can be quite effective for channels without multipath-fading. This section will determine if a similar claim can be made for multipath-fading channels.

In DS CDMA cellular systems, every cell uses the same carrier frequency, or set of carrier frequencies. This limits the reduction in multiple-access interference that can be gained from propagation path loss. Cell sectoring is effective for reducing multiple-access interference. It is common practice to use 120° cell sectors. For either the uplink or downlink, 120° cell sectoring reduces the multiple-access interference by roughly a factor of three. On the downlink, only one-third of the mobiles are in each cell sector (on average). On the uplink, the number of interfering mobiles is reduced by a factor of 3 (on average). Multiple-access interference can also be reduced by using voice activity detection, where a source does not transmit during the inactive voice periods [46]. This section assumes the use of 120° cell sectoring and provides some results on voice activity detection.

The remainder of the section is organized as follows. Subsection 4.2 presents

the system and channel model. General expressions are derived for the area averaged bit error probability and area averaged outage probability, in Subsection 4.3. Subsection 4.4 discusses the uplink performance and addresses the issues of power control and macroscopic base-station diversity. Section 4.5 considers the downlink performance and discusses the use of downlink power control. Finally, Section 4.6 provides some concluding remarks.

## 4.2 System and Channel Model

The cellular layout is described by a uniform planar grid of hexagonal cells of radius $R$.[13] Each cell contains a centrally located base-station. The cells are divided into 120° sectors, where each sector employs the same carrier frequency. The mobiles are uniformly distributed throughout the system area with a density of $K$ mobiles per cell. Since cell sectoring is used the number of mobiles in sector $c$, denoted by $K_c$, is a random variable.[14] The effects of voice activity detection are modeled by assuming that each transmitter is independently active with probability $p$, so that the number of active transmitters in each sector has a $(K_c, p)$ binomial distribution.

The channel model accounts for the effects of path loss, multipath-fading, multiple-access interference, and background noise. Details of the channel model are available in [47], and only a summary is presented here.

### 4.2.1 Multipath-Fading

Mobile radio channels are effectively modeled as a continuum of multipath components, and the low-pass impulse response of the channel $c(\tau; t)$ is commonly modeled as a tapped delay line with a tap spacing equal to the pseudo-noise chip rate $T_c$ [28, 29, 30, 31], i.e.,

$$c(\tau; t) = \sum_{n=-\infty}^{\infty} c_n(t)\delta(\tau - nT_c) \quad , \tag{4.1}$$

[13] $R$ is the distance from the center to a corner of a cell.

[14] Since the same carrier frequency is used for every sector of every cell, references will be made to sectors rather than cells.

where the tap gains $\{c_n(t)\}$ are complex Gaussian random processes. For a wide sense stationary channel with uncorrelated scattering the $c_n(t)$ are uncorrelated and, because they are Gaussian, independent. For a total multipath spread $T_{\max}$, the tapped delay line can be truncated at $L = \lfloor T_{\max}/T_c \rfloor + 1$ taps, where $\lfloor x \rfloor$ is the largest integer contained in $x$. For a slowly varying channel, $c_n(t) = c_n$ for the duration of several tens of data bits.

Assuming the above tapped delay line model, the total *instantaneous* received bit energy-to-background noise ratio is

$$\lambda = \sum_{n=0}^{L-1} \lambda_n \quad , \tag{4.2}$$

where $\lambda_n = |c_n|^2\theta$ and $\theta \triangleq \frac{E_b}{N_o}$ is the received bit energy-to-background noise ratio in the absence of multipath-fading. If the $|c_n|$ are Rayleigh distributed, then the $\lambda_n$ are exponentially distributed with mean value $\Lambda_n = \mathrm{E}[|c_n|^2]\theta$. The $\Lambda_n$ are related to the Multipath Intensity Profile (MIP) of the channel, $Q(\tau)$. Following the development in [29], suppose that $Q(nT_c + \tau) \approx Q(nT_c)$ for $0 \leq \tau \leq T_c$, meaning that the channel impulse response is stationary for delay intervals of length $T_c$. Then

$$\Lambda_n = T_c Q(nT_c)\theta \quad , \quad 0 \leq n \leq L-1 \quad . \tag{4.3}$$

The channel MIP can assume various forms, but a mobile radio channel is well characterized by the exponential MIP

$$Q(nT_c) = \psi \exp\{-n/\varepsilon\} \quad , \quad 0 \leq n \leq L-1 \quad , \tag{4.4}$$

where $\psi$ is a constant that specifies the total average received signal power, and $\varepsilon$ is a measure of the delay spread of the channel relative to a chip duration. This model has been included in the specifications for the GSM-System [25]. Our analysis will assume that all channels have the same MIP, but in reality all channels will have a unique MIP. Taking the expectation of both sides of (4.2), and using (4.3) and (4.4) gives

$$\Lambda = \sum_{n=0}^{L-1} \Lambda_n = \theta T_c \psi \frac{1 - \exp\{-L/\varepsilon\}}{1 - \exp\{-1/\varepsilon\}} \quad , \tag{4.5}$$

where $\Lambda$ is interpreted as the total *average* received bit energy-to-background noise ratio. It follows from (4.3), (4.4), and (4.5) that

$$\Lambda_n = \frac{(1-\exp\{-1/\varepsilon\})\exp\{-n/\varepsilon\}}{1-\exp\{-L/\varepsilon\}}\Lambda \quad , \quad 0 \le n \le L-1 \quad . \tag{4.6}$$

When obtaining numerical results it will be assumed, somewhat arbitrarily, that $\varepsilon = L - \frac{1}{2}$.

### 4.2.2 Path Loss

A multitude of path loss prediction models exist for UHF/VHF land mobile radio [24, 32, 31]. A simple theoretical model assumes that

$$\Lambda = \begin{cases} \zeta^{-\alpha}\Lambda_f \ , & 0 \le \hat{r} \le \zeta \\ \hat{r}^{-\alpha}\Lambda_f \ , & \zeta \le \hat{r} \le 1 \end{cases} \ , \tag{4.7}$$

where

$\hat{r}$ $\triangleq$ normalized distance between the receiver and transmitter ($\hat{r} = 1$ when the actual distance is equal to $R$).

$\Lambda_f$ $\triangleq$ the value of $\Lambda$ when $\hat{r} = 1$.

$\alpha$ $\triangleq$ propagation path loss exponent.

The parameter $\zeta$ is included, because $\lim_{\hat{r}\to 0}\hat{r}^{-\alpha}\Lambda_f = \infty$. The path loss exponent ranges from $\alpha = 2$ in free space to $\alpha = 4$ in a dense urban area. When obtaining numerical results, it will be assumed that $\zeta = 0.1$ and $\alpha = 4$.[15]

### 4.2.3 Self Interference and Multiple-Access Interference

As mentioned in [35], it is desirable to find reasonably large sets of spreading sequences that have small autocorrelation sidelobes in the time intervals during which delayed signals with significant power are expected. This will minimize the self-interference

[15]The numerical results will not be applicable to a microcellular environment, where $2 \lesssim \alpha \lesssim 3$ is more realistic [21], [22].

due to multipath. The spreading sequences must have small cross-correlation sidelobes over all delays, because the uplink transmissions are asynchronous. A subset of the Gold sequences can be constructed having these desirable correlation properties. In particular, there are $2^m + 1$ Gold sequences of length $2^m - 1$ that have autocorrelation values from the set $\{2^m - 1, -1, t_m - 2, -t_m\}$, and crosscorrelation values from the set $\{-1, t_m - 2, -t_m\}$, where

$$t_m = \begin{cases} 2^{(m+1)/2} + 1, & m \text{ odd} \\ 2^{(m+2)/2} + 1, & m \text{ even} \end{cases} . \tag{4.8}$$

Of these $2^m + 1$ sequences, $2^{m-n+1} + 1$ of them will have their first autocorrelation sidelobe ($t_m - 2$ or $-t_m$) at least $n$ chip durations from the main lobe. Consequently, this subset of sequences will introduce negligible self-interference if used on a channel having $n$ or fewer significant paths.[16]

The spreading sequences are usually deterministic and periodic, as in the above example. Nevertheless, the analysis of DS CDMA is often simplified by assuming that the spreading sequences are completely random. With this approach, the multiple-access interference at the front end of the receiver matched to the desired signal is modeled as additional broadband Gaussian noise [48, 13, 14, 15, 12]. The presence or absence of chip and phase alignment of the co-users can be accounted for by scaling the processing gain [12]. The effect of using deterministic rather than random spreading sequences can also be accounted for by scaling the processing gain, but in a more complicated fashion [48].

Two Gaussian approximations are considered in this section. We do not compare the Gaussian approximations with more accurate approximations, but the results in [13, 14, 15] tend to suggest that a Gaussian approximation is quite accurate.

## 4.3 General Performance Analysis

Let $\lambda_n^{i(c)}$ be the instantaneous received bit energy-to-background noise ratio that is associated with path $n$ and transmitter $i$ located in sector $c$. If the self interference due

[16]References to a channel path refer to a channel tap in the tapped delay line channel model.

to multipath is neglected, and the multiple-access interference is treated as additional broadband Gaussian noise, then the instantaneous received bit energy-to-*total* noise ratio that is associated with transmitter $\hat{\jmath}$ and path $t$ is [46][17]

$$R_{\hat{\jmath},t} = \frac{\lambda_t^{\hat{\jmath}(0)}}{1 + \eta^{-1} \sum_{c,i,n \in U} \lambda_n^{i(c)}} \quad , \tag{4.9}$$

where $\eta$ is the processing gain. In the denominator of (4.9), the "1" accounts for the background noise, while the summation accounts for the multiple-access interference from all other co-users sharing the same bandwidth. The set $U$ in (4.9) is defined as

$$U \triangleq \bigcup_{c \in \mathcal{A}} U_c \tag{4.10}$$

where

$$U_c = \{(c,i,n) : k_{ci} = 1,\ 1 \le i \le K_c,\ 0 \le n \le L-1, \text{ and } (c,i) \ne (0,\hat{\jmath})\} \quad , \tag{4.11}$$

and $k_{ci} = 1$ if transmitter $i$ in sector $c$ is active, and $k_{ci} = 0$ otherwise. The set $\mathcal{A}$ in (4.10) differs for the uplink and downlink. For the uplink, multiple-access interference is caused by mobiles that are located in the shaded sectors of Fig. 4.1, where only the adjacent cells are shown. For the downlink, multiple-access interference is caused by base-stations transmitting to mobiles that are located in the shaded regions of Fig. 4.2, where again, only the adjacent cells are shown. In either case, $\mathcal{A}$ is the appropriate set of shaded sectors.

The instantaneous *processed* bit energy-to-total noise ratio depends on the type of receiver that is used. For a multipath rejection receiver this is[18]

$$R_{\hat{\jmath}}^r = R_{\hat{\jmath},0} \quad . \tag{4.12}$$

Likewise, if an $\mathcal{L}$-tap RAKE receiver is used with predetection selective diversity combining, then

$$R_{\hat{\jmath}}^s = \max\{R_{\hat{\jmath},t} : 0 \le t \le \mathcal{L}-1\} \quad . \tag{4.13}$$

[17]Unless otherwise indicated, it is always assumed that the reference mobile is located in sector 0.

[18]Here we assume the exponential MIP in (4.4) so that the zero path is the dominant path.

In the sequel, the bit error probability of a multipath rejection receiver can be obtained by simply setting $\mathcal{L} = 1$ in the various expressions that will be derived. Similar to the development in [35], it is also possible to use a RAKE receiver with postdetection equal gain combining. Although this type of diversity combining provides slightly better performance, it will not be considered here for the sake of brevity.

To compute the bit error probability and outage probability, define the mean vector

$$\mathbf{\Lambda} \triangleq (\Lambda_0^{1(0)}, \ldots, \Lambda_{L-1}^{1(0)}; \ldots; \Lambda_0^{K_0(0)}, \ldots, \Lambda_{L-1}^{K_0(0)}; \ldots; \Lambda_0^{i(c)}, \ldots, \Lambda_{L-1}^{i(c)}; \ldots \ ) \ , \qquad (4.14)$$

where $\Lambda_n^{i(c)} = \mathrm{E}[\lambda_n^{i(c)}]$. The vector $\mathbf{\Lambda}$ is random because the mobile locations are random, and the joint Probability Density Function (PDF) of $\mathbf{\Lambda}$ is denoted by $\mathrm{f}(\mathbf{\Lambda})$. The elements of $\mathbf{\Lambda}$ are related by (4.6). In order to account for the random user voice activity, let the binary vector

$$\mathbf{K}_\ell = (k_{01}, k_{02}, \ldots, k_{0K_0}, k_{11}, k_{12}, \ldots, k_{1K_1}, \ldots, k_{c1}, k_{c2}, \ldots, k_{cK_c}, \ldots \ ) \qquad (4.15)$$

represent the $\ell^{\text{th}}$ activity pattern. Again, $k_{ci} = 1$ if transmitter $i$ in sector $c$ is active, and $k_{ci} = 0$ otherwise. It is always assumed that the reference transmitter is active, i.e., $k_{0\hat{\jmath}} = 1$. Assuming that all mobiles are independently active with probability $p$, the probability of the $\ell^{\text{th}}$ activity vector is

$$\mathrm{p}(\mathbf{K}_\ell) = \prod_{\substack{c \in A \\ (c,j) \neq (0,j)}} \prod_{j=1}^{K_c} p^{k_{cj}} (1-p)^{1-k_{cj}} \ . \qquad (4.16)$$

The bit error probability associated with transmitter $\hat{\jmath}$, as a function of $\mathbf{\Lambda}$ and $\mathbf{K}_\ell$, is

$$P_{\hat{\jmath}}(\mathbf{\Lambda}, \mathbf{K}_\ell) = \int_0^\infty G(r_{\hat{\jmath}}^s) \mathrm{f}_{R_{\hat{\jmath}}^s|\mathbf{\Lambda}}(r_{\hat{\jmath}}^s|\mathbf{\Lambda}) dr_{\hat{\jmath}}^s \ , \qquad (4.17)$$

where $G(r_{\hat{\jmath}}^s)$ is the bit error probability as a function of the instantaneous processed bit energy-to-total noise ratio, and $\mathrm{f}_{R_{\hat{\jmath}}^s|\mathbf{\Lambda}}(r_{\hat{\jmath}}^s|\mathbf{\Lambda})$ is the conditional PDF of $R_{\hat{\jmath}}^s$. The conditional PDF $\mathrm{f}_{R_{\hat{\jmath}}^s|\mathbf{\Lambda}}(r_{\hat{\jmath}}^s|\mathbf{\Lambda})$ assumes various forms that will be derived throughout the remainder of the paper. The function $G(r_{\hat{\jmath}}^s)$ depends on the type of detection and diversity combining being used. If either a differentially coherent multipath rejection receiver, or a differentially coherent RAKE receiver with predetection selective

combining is used, then [25]

$$G(r_j^s) = \frac{1}{2}\exp\{-r_j^s\} \quad . \tag{4.18}$$

Note that (4.18) implies that differential detection is performed on the signal after despreading, rather than on the chip sequence. Other types of receivers, e.g. coherent receivers, can be analyzed by defining the appropriate function $G(r_j)$ at this point.

The area averaged bit error probability is obtained by averaging over the density of $\mathbf{\Lambda}$ to account for the random mobile locations, and the distribution of $\mathbf{K}_\ell$ to account for the random user voice activity. This leads to

$$P = \int_0^\infty \left\{ \sum_\ell \mathrm{p}(\mathbf{K}_\ell) P_j(\mathbf{\Lambda}, \mathbf{K}_\ell) \right\} \mathrm{f}(\mathbf{\Lambda}) d\mathbf{\Lambda} \quad . \tag{4.19}$$

When obtaining numerical results, the averaging over $\mathbf{\Lambda}$ can be accomplished by generating a large number of uniformly distributed mobile locations. For each set of mobile locations, a large number of activity vectors are generated, and $P_j(\mathbf{\Lambda}, \mathbf{K}_\ell)$ is calculated for each activity vector. Finally, an empirical average of the $P_j(\mathbf{\Lambda}, \mathbf{K}_\ell)$'s is formed.

Sometimes it is desirable to compute the area averaged outage probability, which is defined as the area averaged probability that $P_j(\mathbf{\Lambda}, \mathbf{K}_\ell)$ will exceed a constant $P^*$. This is given by

$$O(P^*) = \int_0^\infty \left\{ \sum_\ell \mathrm{p}(\mathbf{K}_\ell) u\left(P_j(\mathbf{\Lambda}, \mathbb{K}_\ell) - P^*\right) \right\} \mathrm{f}(\mathbf{\Lambda}) d\mathbf{\Lambda} \quad , \tag{4.20}$$

where $u(\,\cdot\,)$ is the unit step function.

Error correction coding can also be used to improve the performance, as discussed in [41, 47, 42]. Error correction coding is not considered in this section, again for brevity, but it is easy to include in our formulation using the approach in [47]. We simply note that the effectiveness of error correction coding depends upon how well the combination of adaptive power control and delay constrained interleaving can create a memoryless coding channel, under conditions of varying Doppler spread. This issue has been partially addressed in [41, 42], but it is not completely resolved.

## 4.4 Uplink Performance Analysis

### 4.4.1 Uplink Performance Without Power Control

For the uplink channel, the channel tap gains $c_n^{i(c)}$ are uncorrelated for all $c$, $n$, and $i$. Furthermore, if power control is not used, then the $\Lambda_n^{i(c)}$ will be distinct $\forall\ c, i,$ and $n$.[19] After some algebraic details [49], the conditional density of $R_j^s$ in (4.13) is

$$\mathrm{f}_{R_j^s|\mathbf{\Lambda}}(r_j^s|\mathbf{\Lambda}) = \sum_{t=1}^{\mathcal{L}} \sum_{\vartheta_1,\ldots,\vartheta_t} (-1)^{t+1} \sum_{(c,i,n)\in U} \mathcal{N}_{c,i,n}\mathcal{B}_t \exp\left\{-r_j^s\mathcal{B}_t\right\} \left( \frac{\left(r_j^s\mathcal{B}_t\frac{\Lambda_n^{i(c)}}{\eta} + 1 + \frac{\Lambda_n^{i(c)}}{\eta}\right)}{\left(r_j^s\mathcal{B}_t\frac{\Lambda_n^{i(c)}}{\eta} + 1\right)^2} \right) , \tag{4.21}$$

where

$$\mathcal{N}_{c,i,n} = \prod_{(m,k,l)\in U\setminus\{(c,i,n)\}} \frac{\Lambda_n^{i(c)}}{\Lambda_n^{i(c)} - \Lambda_l^{k(m)}} , \tag{4.22}$$

$$\mathcal{B}_t = \frac{1}{\Lambda_{\vartheta_1}^{j(0)}} + \cdots + \frac{1}{\Lambda_{\vartheta_t}^{j(0)}} , \tag{4.23}$$

and $\sum_{\vartheta_1,\ldots,\vartheta_t}$ is the summation over the distinct $t$-element subsets of $\{0,1,2,\ldots,\mathcal{L}-1\}$.

Using (4.21) and (4.18) in (4.17) gives

$$\begin{aligned} P_j^s(\mathbf{\Lambda},\mathbf{K}_\ell) &= \frac{1}{2}\sum_{t=1}^{\mathcal{L}} \sum_{\vartheta_1,\ldots,\vartheta_t} (-1)^{t+1} \sum_{(c,i,n)\in U} \mathcal{N}_{c,i,n} \\ &\times \left\{1 - \frac{\eta}{\mathcal{B}_t\Lambda_n^{i(c)}} \exp\left\{\frac{\eta}{\mathcal{B}_t\Lambda_n^{i(c)}} + \frac{\eta}{\Lambda_n^{i(c)}}\right\} E_1\left(\frac{\eta}{\mathcal{B}_t\Lambda_n^{i(c)}} + \frac{\eta}{\Lambda_n^{i(c)}}\right)\right\} , \end{aligned} \tag{4.24}$$

where $E_n(x) = \int_1^\infty e^{-xt}t^{-n}dt$ is the exponential integral of order $n$.

Sometimes the above expressions exhibit numerical instability when $|U|$, the cardinality of $U$, is very large (there are many cells, mobiles, and/or channel paths). Numerical instability was observed to occur when $\sum_c K_c L \gtrsim 400$. Under this condition, the conditional PDF in (4.21) will not numerically integrate to unity. Fortunately, when $|U|$ is large the central limit theorem can be invoked and a Gaussian approximation can be used. The mean and variance of the random variable $\chi = \eta^{-1}\sum_{c,i,n\in U}\lambda_n^{i(c)}$ in (4.9) are

$$\mu = \eta^{-1} \sum_{c,i,n\in U} \Lambda_n^{i(c)} , \tag{4.25}$$

[19] This is certainly true for all $c$ and $i$, but it also assumes distinct values of $\Lambda_n$ in (4.3). This latter assumption is made throughout this section, but does not result in any loss of generality.

and

$$\sigma^2 = \eta^{-2} \sum_{c,i,n \in U} [\Lambda_n^{i(c)}]^2 \quad , \tag{4.26}$$

respectively. The random variable $\chi$ is approximated as being Gaussian. Note from (4.9) and (4.13) that the accuracy of the Gaussian approximation depends $|U|$, but does not depend on the diversity order $\mathcal{L}$. Because the multiple-access interference $\chi$ cannot assume a negative value, a further approximation is used. In particular, only the positive portion of the Gaussian PDF is used and is normalized by the factor $Q(-\mu/\sigma)$ to form a valid PDF. This further approximation is reasonably accurate when $Q(-\mu/\sigma)$ is close to unity. The condition under which this occurs can be roughly stated as follows. Suppose that the path loss is neglected so that the $\Lambda_n^{i(c)}$ are equal. In this case $\mu/\sigma = \sqrt{|U|}$. Even when the total number of interfering mobiles is quite small, $Q(-\mu/\sigma) \approx 1$, e.g. when $|U| = 6$, $\mu/\sigma = 2.45$ and $Q(-\mu/\sigma) = 0.993$. From this argument, it follows that the conditional PDF in (4.21) has the approximate form [47]

$$\begin{aligned} \mathrm{f}_{R_j^s|\mathbf{\Lambda}}(r_j^s|\mathbf{\Lambda}) \;\approx\; & \sum_{t=1}^{\mathcal{L}} \sum_{\vartheta_1,\ldots,\vartheta_t} (-1)^{t+1} \frac{\mathcal{B}_t \sigma}{\sqrt{2\pi} Q(-\mu/\sigma)} \left[ \exp\left\{ -\frac{\mu^2}{2\sigma^2} - \mathcal{B}_t r_j^s \right\} \right. \\ & + \sqrt{2\pi} \left( \frac{1 + \mu - \mathcal{B}_t \sigma^2 r_j^s}{\sigma} \right) \exp\left\{ -(1+\mu)\mathcal{B}_t r_j^s + \frac{\mathcal{B}_t^2 \sigma^2}{2} (r_j^s)^2 \right\} \\ & \left. \times \; \mathrm{Q}\left( \frac{\mathcal{B}_t \sigma^2 r_j^s - \mu}{\sigma} \right) \right] \quad . \end{aligned} \tag{4.27}$$

Using (27) and (4.18) in (4.17) gives

$$\begin{aligned} P_j^s(\mathbf{\Lambda}, \mathbf{K}_\ell) \;=\; & \frac{1}{2} \sum_{t=1}^{\mathcal{L}} \sum_{\vartheta_1,\ldots,\vartheta_t} (-1)^{t+1} \frac{\mathcal{B}_t}{Q(-\mu/\sigma)} \left[ \frac{\exp\left\{ -\frac{\mu^2}{2\sigma^2} \right\}}{\sqrt{2\pi}(1 + \mathcal{B}_t)} \sigma \right. \\ & + \int_0^\infty \left( 1 + \mu - \mathcal{B}_t \sigma^2 r_j^s \right) \exp\left\{ -\left( (1+\mu)\mathcal{B}_t + 1 \right) r_j^s + \frac{\mathcal{B}_t^2 \sigma^2}{2} (r_j^s)^2 \right\} \\ & \left. \times \; \mathrm{Q}\left( \frac{\mathcal{B}_t \sigma^2 r_j^s - \mu}{\sigma} \right) dr_j^s \right] \quad . \end{aligned} \tag{4.28}$$

### 4.4.2 Uplink Performance with Average Power Control

Suppose that the emitted power levels from all mobiles are adjusted so that the base-stations receive the same total average signal power from each mobile in a cell sector.

Since the average received interference from mobiles in other cells is a constant, the ratio of the *average received total bit energy* to the *average received total noise ratio* will also be the same for every mobile in a cell sector. This power control technique is similar in some ways to the intracell power balancing scheme proposed by Nettleton and Alavi [43]. Let $\Lambda^{(c)}$ be the total average received bit energy-to-background noise ratio at base-station $c$ from any mobile in sector $c$. The total average *transmitted* bit energy-to-background noise ratio from all mobiles in sector $c$ is

$$\Psi_c = \Lambda^{(c)} \sum_{i=1}^{K_c} \mathrm{d}(\hat{r}_{(c)}^{i(c)}) \quad , \tag{4.29}$$

where

$$\mathrm{d}(\hat{r}) = \begin{cases} 1 \ , & 0 \le \hat{r} \le \zeta \\ (\hat{r}R)^{\alpha} \ , & \zeta \le \hat{r} \le 1 \end{cases} \quad , \tag{4.30}$$

and $\hat{r}_{(c)}^{i(c)}$ is the normalized distance between the sector $c$ base-station, and mobile $i$ in sector $c$. In order to make a fair comparison to the case when power control is not used, $\Psi_c$ is related to $\Lambda_f$ by $\Psi_c = K_c R^{\alpha} \Lambda_f$. Then by using (4.29)

$$\Lambda^{(c)} = \frac{K_c R^{\alpha}}{\sum_{i=1}^{K_c} \mathrm{d}(\hat{r}_{(c)}^{i(c)})} \Lambda_f \quad , \tag{4.31}$$

Finally, the total average received bit energy-to-background noise ratio, at the sector 0 base-station, from mobile $i$ in sector $c$ is

$$\Lambda^{i(c)} = \Lambda^{(c)} \frac{\mathrm{d}(\hat{r}_{(c)}^{i(c)})}{\mathrm{d}(\hat{r}_{(0)}^{i(c)})} \quad , \tag{4.32}$$

and $\hat{r}_{(0)}^{i(c)}$ is the normalized distance between the sector 0 base-station and mobile $i$ in cell $c$.

*1) Error Probability:* Once again, the channel tap gains $c_n^{i(c)}$ are uncorrelated for all $i$, $c$, and $n$. With perfect average power control $\Lambda_n^{i(0)}$ is the same for all mobiles in sector 0, and is simply denoted by $\Lambda_n^{(0)}$. However, the $\Lambda_n^{i(c)}$'s with $c \neq 0$ are all distinct. As in Section IV-1, it is possible to derive the exact conditional density $\mathrm{f}_{R_j^s|\mathbf{\Lambda}}(r_j^s|\mathbf{\Lambda})$ and the corresponding expression for $P_j^s(\mathbf{\Lambda}, \mathbb{K}_\ell)$. We refer the interested reader to [47] for these expressions. Unfortunately, the exact expression for $P_j^s(\mathbf{\Lambda}, \mathbf{K}_\ell)$ exhibits

numerical instability even when $|U|$ is relatively small, in this case when $|U| \gtrsim 36$. As before, a Gaussian approximation can be used to remedy this problem, provided that $|U|$ is large enough. In this case, the mean and variance of the Gaussian random variable $\chi = \eta^{-1} \sum_{c,i,n \in U} \lambda_n^{i(c)}$ in (4.9) are

$$\mu = \eta^{-1} \sum_{i=1}^{K_0} k_{0i} \Lambda_n^{(0)} + \eta^{-1} \sum_{c,i,n \in V} \Lambda_n^{i(c)} \quad , \tag{4.33}$$

and

$$\sigma^2 = \eta^{-2} \sum_{i=1}^{K_0} k_{0i} [\Lambda_n^{(0)}]^2 + \eta^{-2} \sum_{c,i,n \in V} [\Lambda_n^{i(c)}]^2 \quad , \tag{4.34}$$

respectively. The set $V$ in (4.33) and (4.34) is defined as

$$V \triangleq \bigcup_{\substack{c \in \mathcal{A} \\ c \neq 0}} V_c \quad , \tag{4.35}$$

where

$$V_c = \{(c,i,n) : k_{ci} = 1, 1 \leq i \leq K_c, 0 \leq n \leq L-1\} \quad , \tag{4.36}$$

and $\mathcal{A}$ is the set of shaded sectors in Fig. 4.1.

The values of $\Lambda^{i(c)}$ obtained from (4.32) are used with (4.6) to obtain $\mu$ and $\sigma$, which are in turn used in (4.29) to approximate the error probability $P_j^s(\mathbf{\Lambda}, \mathbf{K}_\ell)$. Finally, the area averaged bit error probability and area averaged outage probability are obtained from (4.19) and (4.20), respectively.

### 4.4.3 Macroscopic Base-Station Diversity

Suppose that the signal from each mobile is received and processed by the three closest base-stations, thereby providing macroscopic diversity.[20] The system area is effectively partitioned into a uniform triangular grid as shown in Fig. 4.3, such that the base-stations on the vertices of each triangle are used to process the signals from all mobiles located within each triangle. For example, in Fig. 4.3 the signal from the reference mobile is processed by base-stations 0, 2, and 3.

[20] If shadowing is neglected, then the three closest base-stations will always be the most effective.

Let $P_{\hat{j}}(\mathbf{\Lambda}^d, \mathbf{K}_\ell)$, $d = 0, 1, 2$, be the bit error probabilities corresponding to the base-stations that are processing the signal from mobile $\hat{j}$, and let $\mathbf{\Lambda}^d$ be the mean vector $\mathbf{\Lambda}$ corresponding to base-station $d$.

*1) Majority Logic Combining:* Since each of the base-stations provides an independent estimate of an information bit, a majority logic decision can be made. In this case, the value of $P_{\hat{j}}(\mathbf{\Lambda}, \mathbf{K}_\ell)$ used in (4.19) and (4.20) is

$$\begin{aligned} P_{\hat{j}}(\mathbf{\Lambda}, \mathbf{K}_\ell) &= P_{\hat{j}}(\mathbf{\Lambda}^0, \mathbb{K}_\ell) P_{\hat{j}}(\mathbf{\Lambda}^1, \mathbf{K}_\ell) P_{\hat{j}}(\mathbf{\Lambda}^2, \mathbf{K}_\ell) \\ &\quad + \left[1 - P_{\hat{j}}(\mathbf{\Lambda}^0, \mathbb{K}_\ell)\right] P_{\hat{j}}(\mathbf{\Lambda}^1, \mathbf{K}_\ell) P_{\hat{j}}(\mathbf{\Lambda}^2, \mathbf{K}_\ell) \\ &\quad + P_{\hat{j}}(\mathbf{\Lambda}^0, \mathbf{K}_\ell) \left[1 - P_{\hat{j}}(\mathbf{\Lambda}^1, \mathbf{K}_\ell)\right] P_{\hat{j}}(\mathbf{\Lambda}^2, \mathbf{K}_\ell) \\ &\quad + P_{\hat{j}}(\mathbf{\Lambda}^0, \mathbf{K}_\ell) P_{\hat{j}}(\mathbf{\Lambda}^1, \mathbf{K}_\ell) \left[1 - P_{\hat{j}}(\mathbf{\Lambda}^2, \mathbf{K}_\ell)\right] \quad . \end{aligned} \tag{4.37}$$

*2) Selective Combining:* An alternative to majority logic combining is selective combining, where a selection is made in favour the base-station that provides the smallest bit error probability $P_{\hat{j}}(\mathbf{\Lambda}^d, \mathbf{K}_\ell)$. The resulting bit error probability used in (4.19) and (4.20) is

$$P_{\hat{j}}(\mathbf{\Lambda}, \mathbf{K}_\ell) = \min\left\{P_{\hat{j}}(\mathbf{\Lambda}^0, \mathbf{K}_\ell), P_{\hat{j}}(\mathbf{\Lambda}^1, \mathbf{K}_\ell), P_{\hat{j}}(\mathbf{\Lambda}^2, \mathbb{K}_\ell)\right\} \quad . \tag{4.38}$$

### 4.4.4 Numerical Results

All numerical results assume a processing gain of $\eta = 1000$. Only the multiple-access interference from the reference cell and the first tier of surrounding cells is included in the calculations. The multiple-access interference from the higher tiers of cells is neglected, since it has relatively little impact on the performance [48].

Fig. 4.4 plots the area averaged bit error probability with base-station diversity, but without uplink power control. The exact conditional conditional PDF in (4.21) and the corresponding error probability in (4.24) were used. A significant improvement is achieved by using selective diversity. This improvement will probably diminish for large $K$, but will be restored if shadowing is present. Majority logic combining is seen to improve the performance slightly at large $\Lambda_f$, but it is actually worse at small $\Lambda_f$. The reason this performance degradation is that the bit error probabilities on the diversity branches are not equal.

Fig. 4.5 plots the area averaged bit error probability against the number of mobiles per cell for $\Lambda_f \to \infty$.[21] Results are shown with and without base-station diversity, and with and without average power control. As shown in Fig. 4.5, (4.24) and (4.28) are the same for large $K$, but differ significantly for small $K$.

Fig. 4.6 plots the area averaged bit error probability against the number of channel paths, using (4.28). Even a small amount of multipath diversity improves the performance significantly, provided that the channel has the right amount of dispersion. However, if the channel either consists of a single faded path or is very dispersive, then the performance can be severely degraded because the lack of diversity or the increased multiple-access interference, respectively.

Figs. 4.8 and 4.9 plot the bit error probability and outage probability as a function of the distance from the base-station, using (4.28). It is seen that uplink average power control keeps the error probability and outage probability almost constant regardless of the distance from the base-station.

Finally, Fig. 4.10 shows the effect of using voice activity detection. Results are shown with the exact conditional PDF $f_{R_j^s|\mathbf{A}}(r_j^s|\mathbf{A})$ and its Gaussian approximation. The instantaneous bit error probability depends, in a rather complicated way, on the number and location of active mobiles. Despite of this fact, it is verified that a voice activity factor of $p$ simply increases the capacity by a factor of $1/p$ even for small $K$.

### 4.4.5 Estimate of Uplink Channel Capacity

In order to estimate the uplink capacity we must make a variety of simplifying assumptions. First, it is assumed that the channel is characterized by a rectangular power delay profile instead of the more realistic exponential power delay profile. This assumption has opposite effects on the estimate of channel capacity. It makes the capacity estimate somewhat pessimistic because the multiple-access interference will be higher. At the same time it makes the capacity estimate optimistic, because a RAKE receiver will gain a greater diversity advantage.

[21]The condition $\Lambda_f \to \infty$ means that the background noise is negligible when compared to the multiple-access interference.

Since uplink power control is used, the ratio of the average received total bit energy to the average received total noise ratio is the same for every mobile in a cell sector. We then make the assumption that the average received total noise has a constant variance. In actual fact, the variance will not be constant due to multipath-fading, and this assumption will make the capacity estimate pessimistic. We also make the assumptions that adjacent cells increase the level of multiple-access interference by a factor of 1.5, cell sectoring increases the capacity by a factor of 3, and voice activity gating increase the capacity by a factor of 2. Finally, we assume that the uplink transmissions are chip and phase asynchronous and, therefore, the effective processing gain in (4.9) is increased by a factor of 3 [10]. As a result of these assumptions, the ratio of the average received total bit energy to the average received total noise ratio on each diversity branch is approximately

$$\bar{\gamma} = \frac{3\eta}{1.5(K/6-1)L} \quad , \tag{4.39}$$

where $K$ is the number of mobiles per cell.

With the above assumptions, a value of $1.9 \times 10^{-4}$ should be observed for $L = 2$ and a 2-Tap RAKE receiver in Fig. 4.7, which is almost exactly what we observe. At $L = 10$ we should observe a value of $4.0 \times 10^{-3}$. The observed value is approximately $2.0 \times 10^{-3}$ which is smaller only by about a factor of 2. So our assumptions are reasonable.

The error probability depends on the type of diversity combining and detection being used. We assume that a RAKE receiver is used with either differentially coherent detection or coherent detection. The base-station uses spatial diversity with $n_A$ antennas, so that the number of diversity branches is $n_A \times \mathcal{L}$, where $\mathcal{L}$ is the number of taps on each RAKE receiver. The RAKE receiver uses either selective combining or maximal ratio combining. With maximal ratio combining, the bit error probability is [23]

$$P_b = \left(\frac{1-\mu}{2}\right) \sum_{k=0}^{\mathcal{L}-1} \binom{\mathcal{L}-1+k}{k} \left(\frac{1+\mu}{2}\right)^k \quad , \tag{4.40}$$

where

$$\mu = \begin{cases} \sqrt{\frac{\bar{\gamma}}{1+\bar{\gamma}}} & \text{coherent} \\ \frac{\bar{\gamma}}{1+\bar{\gamma}} & \text{differentially coherent} \end{cases} . \tag{4.41}$$

With selective combining and coherent detection

$$P_b = \frac{\mathcal{L}}{2} \sum_{k=0}^{\mathcal{L}-1} \frac{\binom{\mathcal{L}-1}{k}(-1)^k}{1+k} \left[ 1 - \sqrt{\frac{\bar{\gamma}}{1+k+\bar{\gamma}}} \right] . \tag{4.42}$$

With selective combining and differentially coherent detection

$$P_b = \frac{\mathcal{L}}{2} \sum_{k=0}^{\mathcal{L}-1} \frac{\binom{\mathcal{L}-1}{k}(-1)^k}{1+k+\bar{\gamma}} . \tag{4.43}$$

We make the final assumption that the bit error probability is constant throughout a cell, which is justified from Fig. 4.8.

By using the above expressions, we have computed the number of mobiles per cell that will result in an error probability of $10^{-3}$. A processing gain of 1000 was assumed, corresponding to a baseband data rate of 12.5 kb/s. This data rate is chosen so that comparisons can be made to the IS-54 TDMA system with a raw data rate of 12.8 kb/s per channel. Results in [48] suggest that the total capacity in a given bandwidth allocation is not sensitive to the choice of processing gain. In Table 4.1, these capacities are compared to a TDMA system with 178 channels/cell. This number is determined as follows. There are 416 available carrier frequencies which are divided amongst 7 cells. Each carrier provides 3 channels, so there are 178 channels/cell. Each channel a data rate of 12.8 kb/s. Hence, the baseband data rates of the CDMA and TDMA systems are roughly the same, and any difference can easily by accounted for by scaling the capacity estimates.

Observe from Table 4.1 that the capacity with equal gain combining is roughly 4 times the capacity with selective combining. Also, the capacity with coherent detection is 2 times the capacity with differentially coherent detection. As long as antenna diversity is used with a RAKE receiver, i.e, $\mathcal{L} \geq 2$, CDMA provides a larger capacity than TDMA. Antenna diversity is necessary to prevent the unacceptably large error probability (and corresponding poor capacity) that will result for channels with a single faded path. This is evident from Table 4.1 and also Figs. 4.6 and

| Channel Paths $L$ | Antennas $n_A$ | RAKE Taps $\mathcal{L}$ | Selective Combining | | Maximal Ratio Combining | |
|---|---|---|---|---|---|---|
| | | | Coherent | Diff. Coherent | Coherent | Diff. Coherent |
| 1 | 1 | 3 | 0.30 | 0.17 | 0.30 | 0.17 |
| 2 | 1 | 3 | 1.89 | 1.15 | 2.65 | 1.32 |
| 3 | 1 | 3 | 2.81 | 1.84 | 5.00 | 2.39 |
| 1 | 2 | 1 | 3.75 | 2.27 | 5.27 | 2.60 |
| 2 | 2 | 1 | 1.89 | 1.15 | 2.65 | 1.32 |
| 3 | 2 | 1 | 1.27 | 0.78 | 1.78 | 0.89 |
| 4 | 2 | 1 | 0.96 | 0.59 | 1.34 | 0.68 |
| 2 | 2 | 2 | 6.25 | 2.74 | 13.34 | 6.14 |
| 3 | 2 | 2 | 4.18 | 1.84 | 8.91 | 4.10 |
| 4 | 2 | 2 | 3.14 | 1.39 | 6.68 | 3.09 |
| 3 | 2 | 3 | 6.30 | 4.43 | 17.49 | 7.51 |
| 4 | 2 | 3 | 4.74 | 3.33 | 13.13 | 5.65 |

Table 4.1: Uplink Capacity Estimates (Capacity CDMA/Capacity TDMA)

4.7. Finally, the benefits of using base-station diversity have not been included in Table 4.1.

## 4.5 Downlink Performance Analysis

### 4.5.1 Downlink Performance Without Power Control

For the downlink channel, $c_n^{i(c)}$ is uncorrelated with $c_{\hat{n}}^{i(\hat{c})}$, for $(c,n) \neq (\hat{c},\hat{n})$. However, all signals received from the same base-station will have propagated over the same channel. Therefore, for fixed $(c,n)$, the $c_n^{i(c)}$ are all equal. Without power control $\Lambda_n^{i(c)}$ is the same for all mobiles in sector $c$, and is denoted by $\Lambda_n^{(c)}$. But the $\Lambda_n^{(c)}$ are all distinct with respect to $c$ and $n$. After some algebraic details [47], the conditional PDF of $R_j^s$ in (4.13) is

$$\mathrm{f}_{R_j^s|\mathbf{\Lambda}}(r_j^s|\mathbf{\Lambda}) = \sum_{t=1}^{\mathcal{L}} \sum_{\vartheta_1,\ldots,\vartheta_t} (-1)^{t+1} \sum_{c\in\mathcal{A}} \sum_{n=0}^{L-1} \hat{\mathcal{N}}_{c,n} \mathcal{B}_t \exp\left\{-r_j^s \mathcal{B}_t\right\} \left( \frac{\left( r_j^s \mathcal{B}_t \frac{\hat{\Lambda}_n^{(c)}}{\eta} + 1 + \frac{\hat{\Lambda}_n^{(c)}}{\eta} \right)}{\left( r_j^s \mathcal{B}_t \frac{\hat{\Lambda}_n^{(c)}}{\eta} + 1 \right)^2} \right), \tag{4.44}$$

where

$$\hat{\mathcal{N}}_{c,n} = \prod_{\substack{i\in\mathcal{A} \\ (i,k)\neq(c,n)}} \prod_{k=0}^{L-1} \frac{\hat{\Lambda}_n^{(c)}}{\hat{\Lambda}_n^{(c)} - \hat{\Lambda}_k^{(i)}} \quad , \tag{4.45}$$

$$\hat{\Lambda}_n^{(c)} = \begin{cases} (K_0 - 1)\Lambda_n^{(c)} & , \quad c = 0 \\ K_c \Lambda_n^{(c)} & , \quad c \neq 0 \end{cases} \quad . \tag{4.46}$$

By using (4.44) and (4.18), (4.17) becomes

$$\begin{aligned} P_j^s(\mathbf{\Lambda}, \mathbf{K}_\ell) &= \frac{1}{2} \sum_{t=1}^{\mathcal{L}} \sum_{\vartheta_1,\ldots,\vartheta_t} (-1)^{t+1} \sum_{c\in\mathcal{A}} \sum_{n=0}^{L-1} \hat{\mathcal{N}}_{c,n} \\ &\times \left\{ 1 - \frac{\eta}{\mathcal{B}_t \hat{\Lambda}_n^{(c)}} \exp\left\{ \frac{\eta}{\mathcal{B}_t \hat{\Lambda}_n^{(c)}} + \frac{\eta}{\hat{\Lambda}_n^{(c)}} \right\} E_1 \left( \frac{\eta}{\mathcal{B}_t \hat{\Lambda}_n^{(c)}} + \frac{\eta}{\hat{\Lambda}_n^{(c)}} \right) \right\} \quad . \end{aligned} \tag{4.47}$$

Finally, Eqs. (4.19) and (4.20) give the area average bit error probability and the area averaged outage probability, respectively.

### 4.5.2 Downlink Performance with Average Power Control

One approach for implementing downlink power control is to maintain the same ratio of the *average received bit energy* to the *average received total noise* for every mobile in a cell sector. This is similar in some ways to the intracell power balancing scheme proposed by Alavi and Nettleton [44]. Here, we call it intrasector power balancing.

*1) Intrasector Power Balancing:* Let $\Psi(i,c)$ be the total average *transmitted* bit energy-to-background noise ratio corresponding to a total average *received* bit energy-to-background noise ratio of $\Lambda(i,c)$ at mobile $i$ in sector $c$. The sum of the total transmitted average bit energy-to-background noise ratios for sector $c$ is

$$\Psi_c = \sum_{i=1}^{K_c} \Psi(i,c) \quad , \tag{4.48}$$

To make a fair comparison to the case when power control is not used, $\Psi_c$ and $\Lambda_f$ are related by $\Psi_c = K_c R^\alpha \Lambda_f$. Let $\hat{r}_{(b)}^{i(c)}$ be the normalized distance between the sector $b$ base-station and mobile $i$ in sector $c$. The sum of the total average received bit energy-to-background noise ratios from all base-stations, at mobile $i$ in sector $c$, is

$$\sum_{b\in\mathcal{A}} \frac{\Psi_b}{\mathrm{d}(\hat{r}_{(b)}^{i(c)})} \tag{4.49}$$

where d( · ) has been defined in (4.30). Assume that the signal from transmitter $i$ of the sector $c$ base-station is intended for mobile $i$ in sector $c$. Then the average received bit energy-to-average received total noise ratio, at mobile $i$ in sector $c$, is

$$S^{i(c)} = \frac{\frac{\Psi(i,c)}{\mathrm{d}(\hat{r}_{(c)}^{i(c)})}}{\eta^{-1}\left(\sum_{b\in\mathcal{A}} \frac{\Psi_b}{\mathrm{d}(\hat{r}_{(b)}^{i(c)})} - \frac{\Psi(i,c)}{\mathrm{d}(\hat{r}_{(c)}^{i(c)})}\right) + 1} \quad . \tag{4.50}$$

Rearranging this expression gives

$$\Psi(i,c) = \frac{S^{i(c)}}{1+\eta^{-1}S^{i(c)}}\mathrm{d}(\hat{r}_{(c)}^{i(c)})\left(\eta^{-1}\sum_{b\in\mathcal{A}}\frac{\Psi_b}{\mathrm{d}(\hat{r}_{(b)}^{i(c)})}+1\right) \quad . \tag{4.51}$$

However, from (4.48)

$$\Psi_c = \sum_{i=1}^{K_c}\frac{S^{i(c)}}{1+\eta^{-1}S^{i(c)}}\mathrm{d}(\hat{r}_{(c)}^{i(c)})\left(\eta^{-1}\sum_{b\in\mathcal{A}}\frac{\Psi_b}{\mathrm{d}(\hat{r}_{(b)}^{i(c)})}+1\right) \quad . \tag{4.52}$$

With intrasector power balancing, the power transmitted to each mobile in a sector is adjusted so that $S^{i(c)} = S^{(c)}$, $i = 1, \ldots, K_c$. Therefore, (4.52) gives

$$S^{(c)} = \frac{\Psi_c}{\sum_{i=1}^{K_c}\mathrm{d}(\hat{r}_{(c)}^{i(c)})\left(\eta^{-1}\sum_{b\in\mathcal{A}}\frac{\Psi_b}{\mathrm{d}(\hat{r}_{(b)}^{i(c)})}+1\right)-\eta^{-1}\Psi_c} \quad . \tag{4.53}$$

By using (4.53) with $\Psi_\ell = K_\ell R^\alpha \Lambda_f$, the $S^{(c)}$ for all $c$ can be obtained. After doing so, the $\Psi(i,c)$ for all $c$ and $1 \le i \le K_c$ can be generated from (4.51). Finally, if the bit error probability of mobile $\hat{\jmath}$ in sector 0 is of interest, then

$$\Lambda^{i(c)} = \frac{\Psi(i,c)}{\mathrm{d}(\hat{r}_{(c)}^{\hat{\jmath}(0)})} \quad . \tag{4.54}$$

*2) Error Probability:* Once again, for the downlink with power control, $c_n^{i(c)}$ is uncorrelated with $c_{\hat{n}}^{\hat{i}(\hat{c})}$, for $(c,n) \neq (\hat{c},\hat{n})$, and $c_n^{i(c)} = c_n^{i(c)}$, $\forall\, i, \hat{\imath}$. However, with power control $\Lambda_n^{i(c)} \neq \Lambda_{\hat{n}}^{\hat{i}(\hat{c})}$ whenever $(c,i,n) \neq (\hat{c},\hat{\imath},\hat{n})$. It follows that the conditional PDF of $R_j^s$ in (4.13) is [47]

$$\mathrm{f}_{R_j^s|\mathbf{\Lambda}}(r_j^s|\mathbf{\Lambda}) = \sum_{t=1}^{\mathcal{L}}\sum_{\vartheta_1,\ldots,\vartheta_t}(-1)^{t+1}\sum_{c\in\mathcal{A}}\sum_{n=0}^{L-1}\tilde{\mathcal{N}}_{c,n}\mathcal{B}_t\exp\left\{-r_j^s\mathcal{B}_t\right\}\left(\frac{\left(r_j^s\mathcal{B}_t\frac{\tilde{\Lambda}_n^{(c)}}{\eta}+1+\frac{\tilde{\Lambda}_n^{(c)}}{\eta}\right)}{\left(r_j^s\mathcal{B}_t\frac{\tilde{\Lambda}_n^{(c)}}{\eta}+1\right)^2}\right) \quad , \tag{4.55}$$

where

$$\tilde{\mathcal{N}}_{c,n} = \prod_{\substack{i \in \mathcal{A} \\ (i,k) \neq (c,n)}} \prod_{k=0}^{L-1} \frac{\tilde{\Lambda}_n^{(c)}}{\tilde{\Lambda}_n^{(c)} - \tilde{\Lambda}_k^{(i)}} \quad , \tag{4.56}$$

$$\tilde{\Lambda}_n^{(c)} = \begin{cases} \sum_{\substack{i=1 \\ i \neq j}}^{K_0} \Lambda_0^{i(c)} & , \quad c = 0 \\ \sum_{i=1}^{K_c} \Lambda_n^{i(c)} & , \quad c \neq 0 \end{cases} \quad . \tag{4.57}$$

By using (4.55) and (4.18), (4.17) becomes

$$\begin{aligned} P_j^s(\mathbf{\Lambda}, \mathbf{K}_\ell) &= \frac{1}{2} \sum_{t=1}^{\mathcal{L}} \sum_{\vartheta_1, \ldots, \vartheta_t} (-1)^{t+1} \sum_{c \in \mathcal{A}} \sum_{n=0}^{L-1} \tilde{\mathcal{N}}_{c,n} \\ &\times \left\{ 1 - \frac{\eta}{\mathcal{B}_t \tilde{\Lambda}_n^{(c)}} \exp\left\{ \frac{\eta}{\mathcal{B}_t \tilde{\Lambda}_n^{(c)}} + \frac{\eta}{\tilde{\Lambda}_n^{(c)}} \right\} E_1\left( \frac{\eta}{\mathcal{B}_t \tilde{\Lambda}_n^{(c)}} + \frac{\eta}{\tilde{\Lambda}_n^{(c)}} \right) \right\} . \end{aligned} \tag{4.58}$$

The values of $\Lambda_n^{i(c)}$ in (4.58) are obtained from (4.54) and (4.6). Finally, Eqs. (4.19) and (4.20) give the area averaged bit error probability and the area averaged outage probability, respectively.

### 4.5.3 Numerical Results

Again, all numerical results assume a processing gain of $\eta = 1000$, and only the multiple access interference from the reference base-station and the first tier of interfering base-stations is included in the calculations. All numerical results were obtained by using the exact conditional PDF's for $\mathrm{f}_{R_j^s|\mathbf{\Lambda}}(r_j^s|\mathbf{\Lambda})$ and the associated error probabilities in (4.47) and (4.58).

Fig. 4.11 plots the bit error probability against the number of channel paths. Results are shown without power control and with intrasector power balancing. Again, a small amount of multipath diversity improves the performance significantly. However, downlink power control offers very little improvement in the area averaged bit error probability.

Fig. 4.12 plots the bit error probability as a function of the normalized distance from the base-station. From this diagram, it is apparent that downlink power control is quite effective for combating the corner effect, and its usefulness tends to be more apparent when diversity is used.

### 4.5.4 Estimate of Downlink Capacity

To estimate the downlink capacity, we follow the same procedure as for the uplink. Once again, the bit error probability is almost constant throughout the cell if intra-sector power balancing is used. As a result, the same analysis that was used for the uplink can be applied, except that (4.39) is slightly different. In particular, transmissions on the downlink can be made chip asynchronous by introducing a random chip delay into each of the waveforms. However, since one modulator is used, the transmissions from the same base-station will be phase synchronous. Moreover, the transmissions from other interfering base-stations will be phase synchronous with respect to each other, but asynchronous with respect to the desired signal. Therefore, like the uplink, the effective processing gain is still increased by approximately 3 [10]. Furthermore, comparison with the results in [35] shows that the adjacent cells will increase the level of multiple-access interference by a factor of 1.7. This is slightly higher than the factor of 1.5 for the uplink, and the difference can be attributed to the corner effect. Therefore, for the downlink

$$\bar{\gamma} = \frac{3\eta/2}{1.7(K/6-1)L} \quad . \tag{4.59}$$

The resulting downlink capacities are listed in Table 4.2.

Comparison of Tables 4.1 and 4.2 shows that the downlink capacity is less than the uplink capacity. Mobile antenna diversity is necessary to prevent an excessively high error probability for channels with a single faded path, as shown in Fig. 4.11. Similar to the uplink, CDMA yields a larger capacity than TDMA provided that a 2 or 3-tap RAKE receiver is used.

## 4.6 Concluding Remarks

This section has illustrated some of the typical properties and characteristics of a DS CDMA mobile radio system. For the uplink channel, a significant improvement in performance can be obtained by using macroscopic base-station diversity. Our results have also shown that average uplink power control will provide a nearly uniform bit error probability and outage probability throughout the system area. A significant

Downlink Capacity Estimates (Capacity CDMA/Capacity TDMA)

| Channel Paths $L$ | Antennas $n_A$ | RAKE Taps $\mathcal{L}$ | Selective Combining | | Maximal Ratio Combining | |
|---|---|---|---|---|---|---|
| | | | Coherent | Diff. Coherent | Coherent | Diff. Coherent |
| 1 | 1 | 3 | 0.27 | 0.15 | 0.27 | 0.15 |
| 2 | 1 | 3 | 2.82 | 1.02 | 2.34 | 1.16 |
| 3 | 1 | 3 | 2.48 | 1.62 | 4.42 | 2.11 |
| 1 | 2 | 1 | 3.31 | 2.01 | 4.65 | 2.30 |
| 2 | 2 | 1 | 2.82 | 1.02 | 2.34 | 1.16 |
| 3 | 2 | 1 | 1.12 | 0.69 | 1.57 | 0.79 |
| 4 | 2 | 1 | 0.85 | 0.53 | 1.18 | 0.60 |
| 2 | 2 | 2 | 5.52 | 3.74 | 11.77 | 5.41 |
| 3 | 2 | 2 | 3.69 | 2.50 | 7.86 | 3.62 |
| 4 | 2 | 2 | 2.78 | 1.88 | 5.90 | 2.72 |
| 3 | 2 | 3 | 5.57 | 3.91 | 15.44 | 6.63 |
| 4 | 2 | 3 | 4.18 | 2.94 | 11.59 | 4.98 |

Table 4.2: Downlink Capacity Estimates (Capacity CDMA/Capacity TDMA)

improvement can also be obtained from various microscopic diversity techniques and voice activity detection. For the downlink channel, downlink power control does not change the area averaged bit error probability. However, it is quite effective for combating the corner effect so as to provide a more uniform bit error probability and outage probability throughout the system area. The usefulness of downlink power control becomes more apparent when microscopic diversity is used. Finally, it was shown that CDMA can provide a larger capacity than TDMA provided that antenna diversity is used with at least a two-tap RAKE receiver on each antenna. If antenna diversity is not used, then CDMA will result in less capacity than TDMA if the channel exhibits a single faded link. It is to be noted that urban mobile radio channels typically exhibit less than 1 $\mu$ s delay spread 60% of the time [25]. Hence, a CDMA system with approximately a 1 Mchip/s clock rate will experience a single faded link 60% of the time in an urban environment.

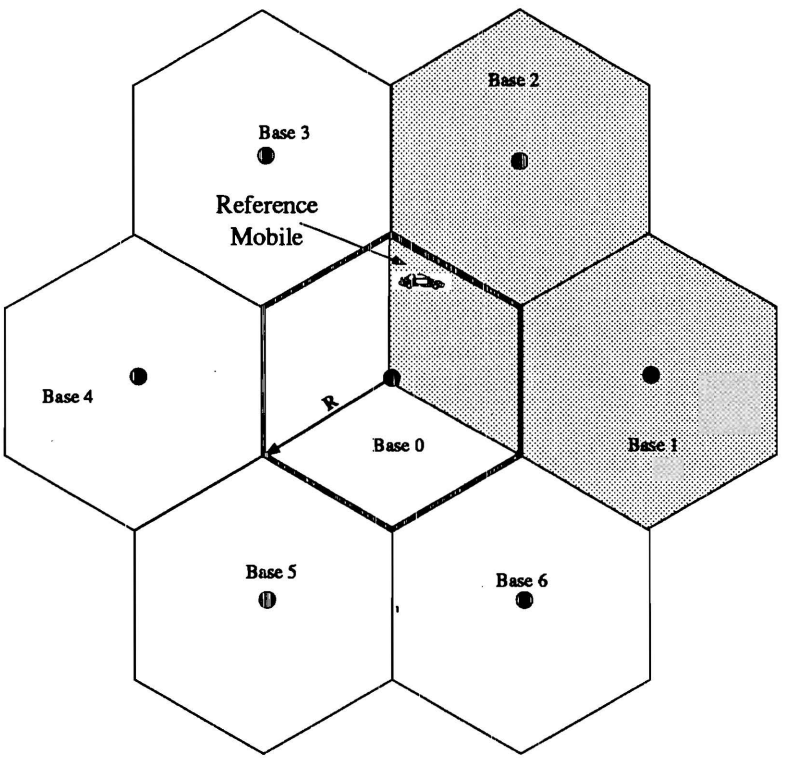


Figure 4.1: Uplink transmissions from mobiles located in the shaded area will cause multiple-access interference with the uplink transmission from the reference mobile.

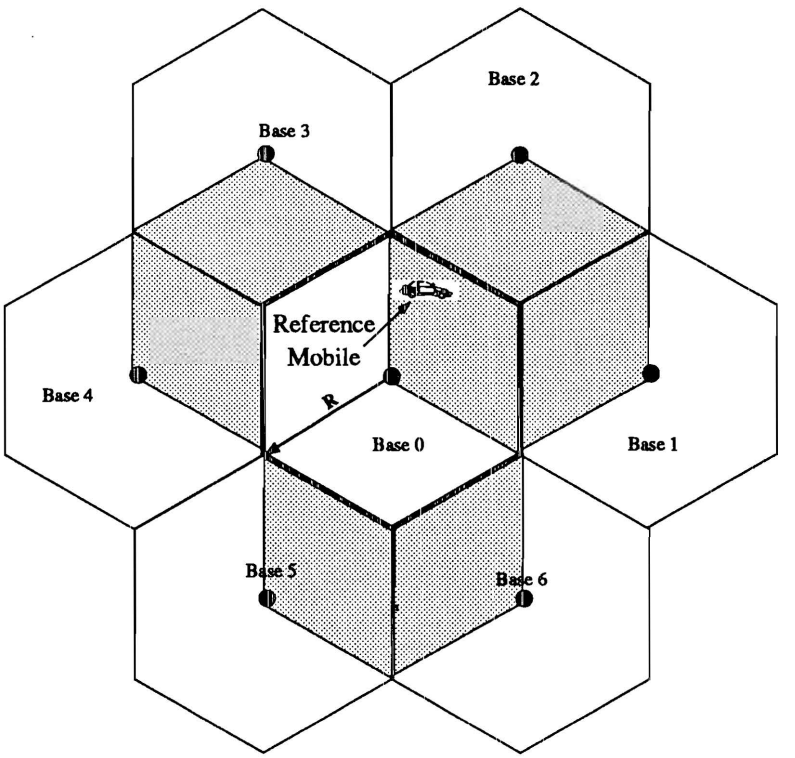


Figure 4.2: Downlink transmissions to mobiles located in the shaded areas will cause multiple-access interference with the downlink transmission to the reference mobile.

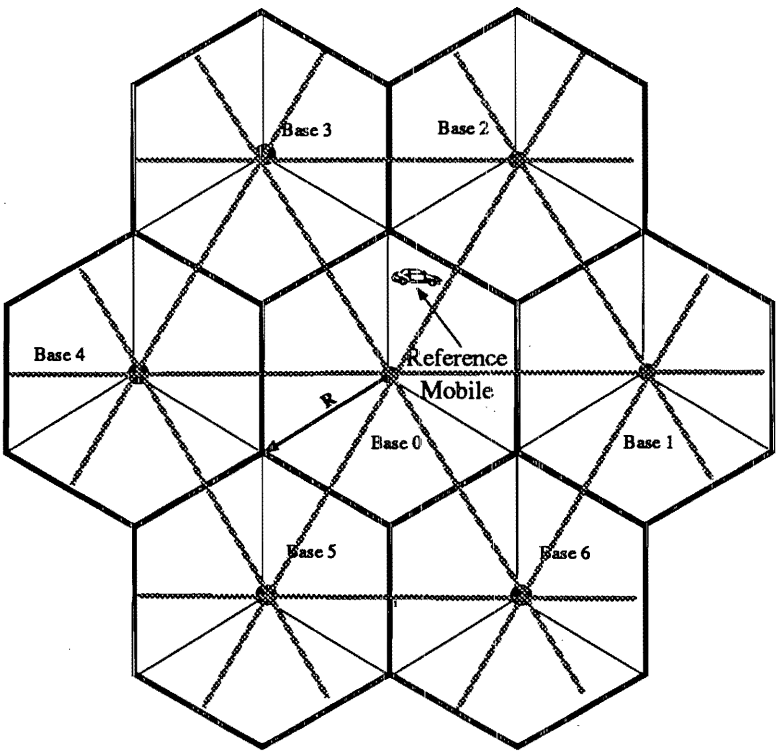


Figure 4.3: Triangular coverage areas will result when the three closest base-stations are used to provide macroscopic diversity for the uplink transmissions.

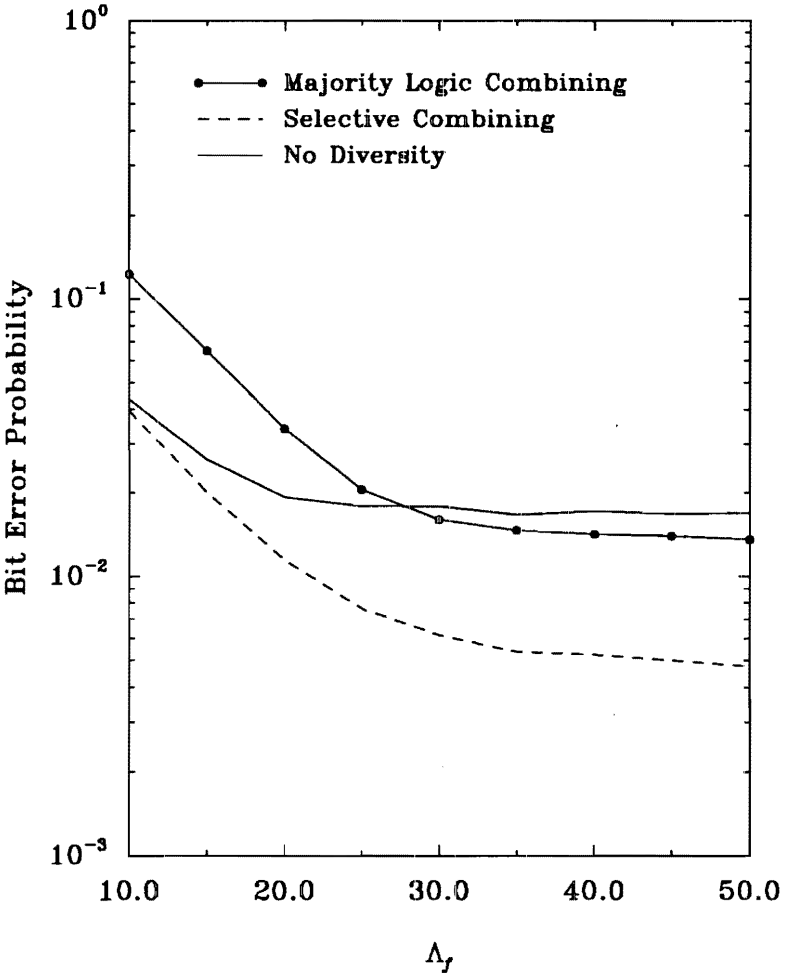


Figure 4.4: Uplink area averaged bit area probability against $\Lambda_f$. Macroscopic base-station diversity is used with a multipath rejection receiver. Uplink power control is not used; $K = 5$, $L = 2$, and $p = 1.0$.

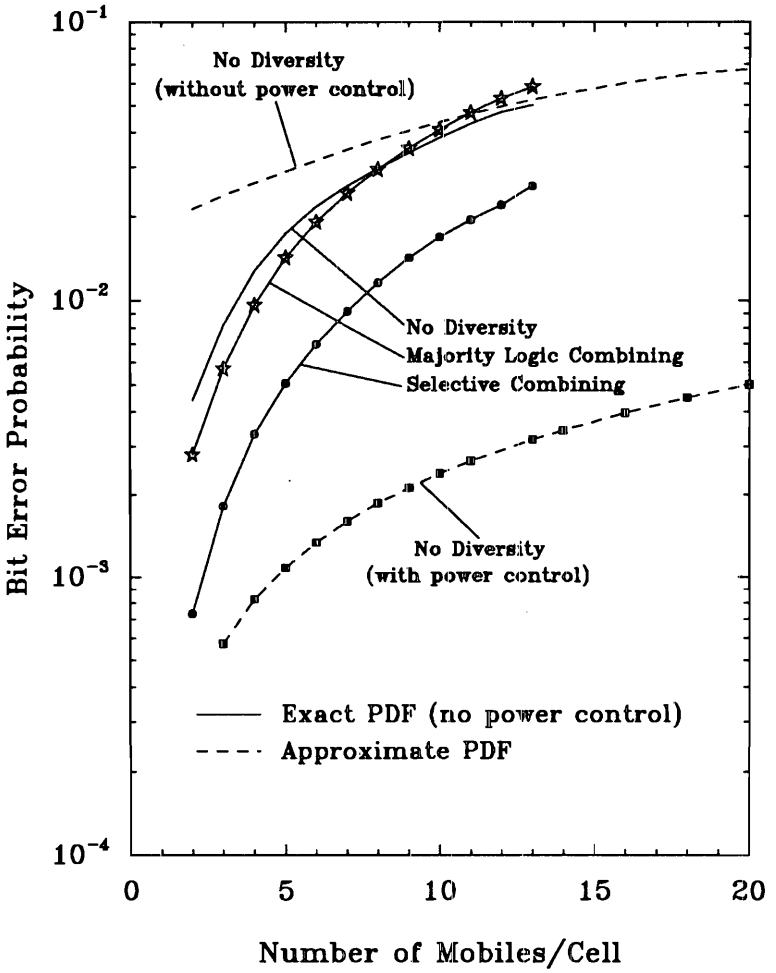


Figure 4.5: Uplink area averaged bit error probability against number of mobiles per cell. Macroscopic base-station diversity is used with a multipath rejection receiver, and a comparison is made between error probabilities given by (4.24) and (4.28) ; $L = 2$, and $p = 1.0$.

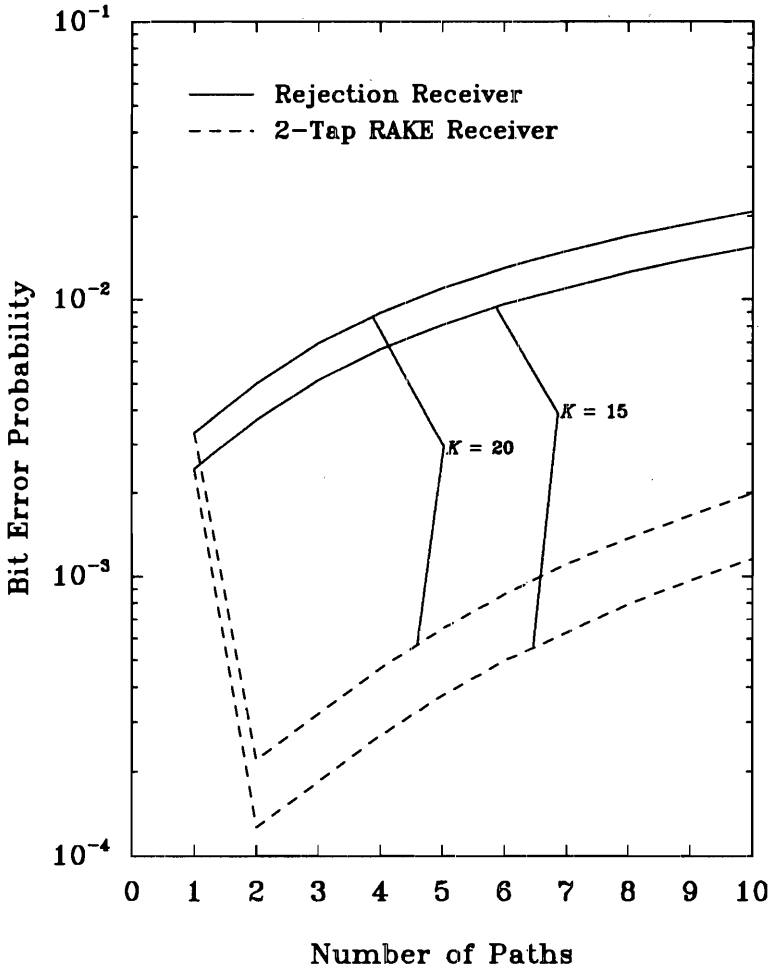


Figure 4.6: Uplink area averaged bit error probability against number of channel paths. Results are shown for a multipath rejection receiver and a 2-tap RAKE receiver with selective combining. Average uplink power control is used; $p = 1.0$.

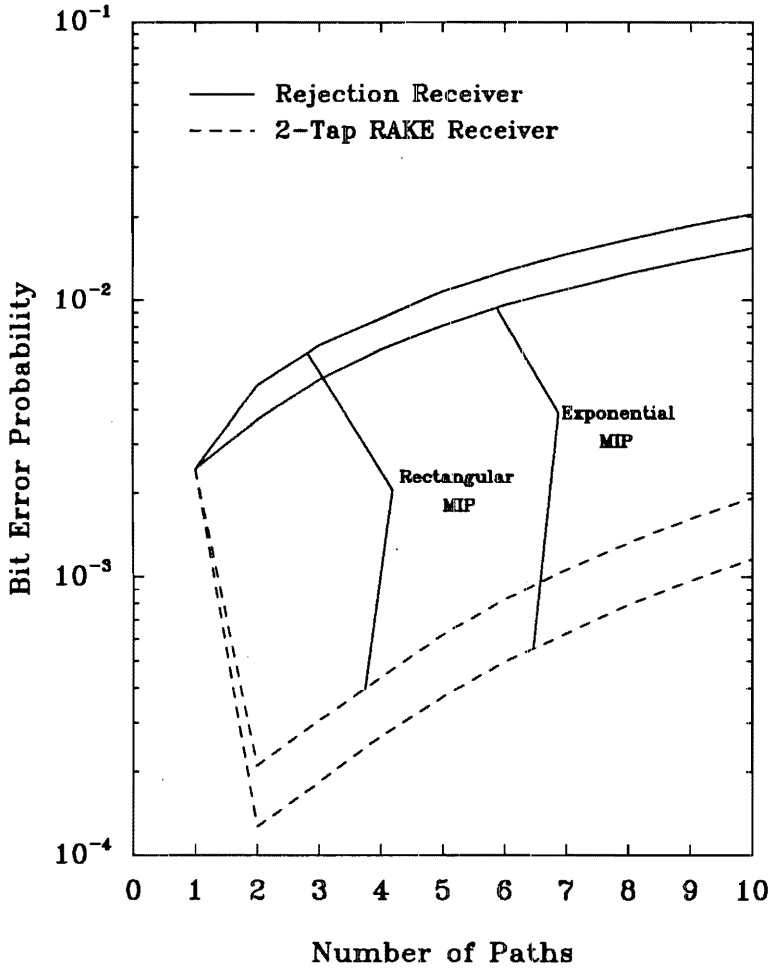


Figure 4.7: Uplink area averaged bit error probability against number of channel paths. Results are shown for exponential and rectangular power delay profiles. Average uplink power control is used; $K = 20$, $p = 1.0$.

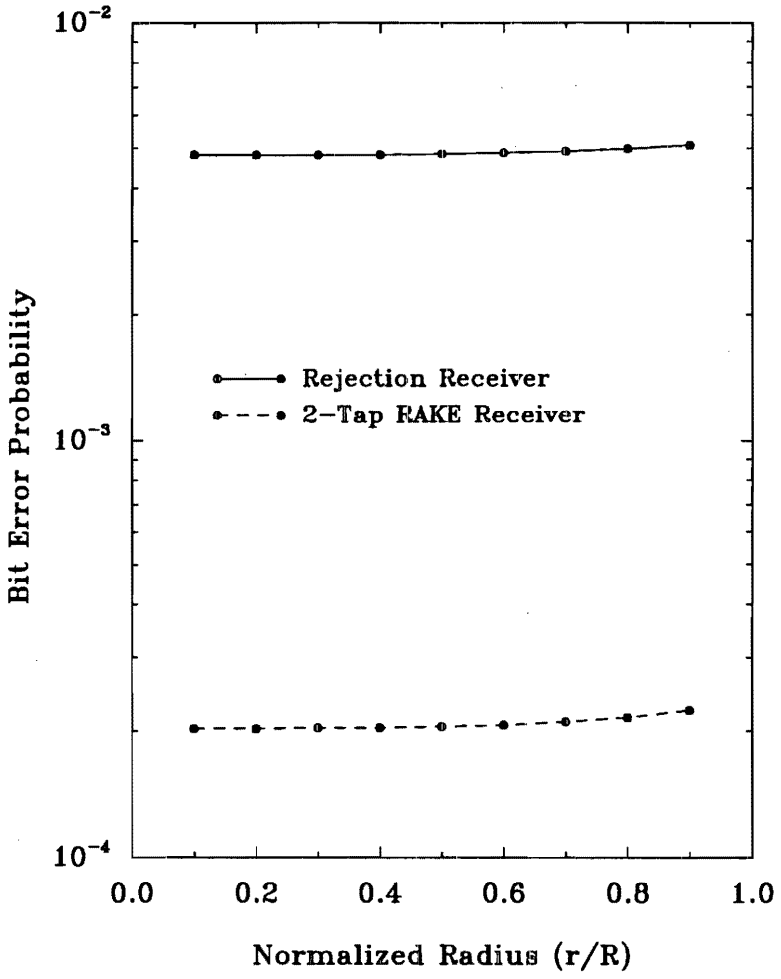


Figure 4.8: Uplink bit error probability as a function of the normalized distance from the base-station. Results are shown for a multipath rejection receiver and a 2-tap RAKE receiver with selective combining. Average uplink power control is used; $K = 20$, $p = 1.0$.

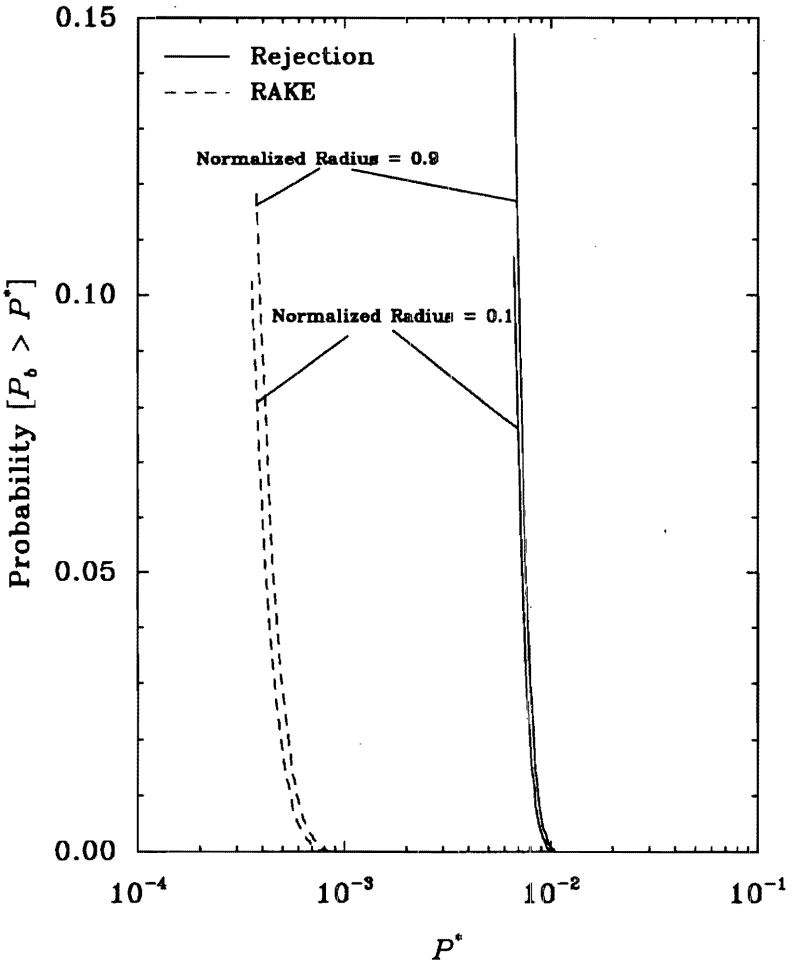


Figure 4.9: Uplink outage probability for various normalized distances from the base-station. Results are shown for a multipath rejection receiver and a 2-tap RAKE receiver with selective combining. Average uplink power control is used; $K = 20$, $p = 1.0$.

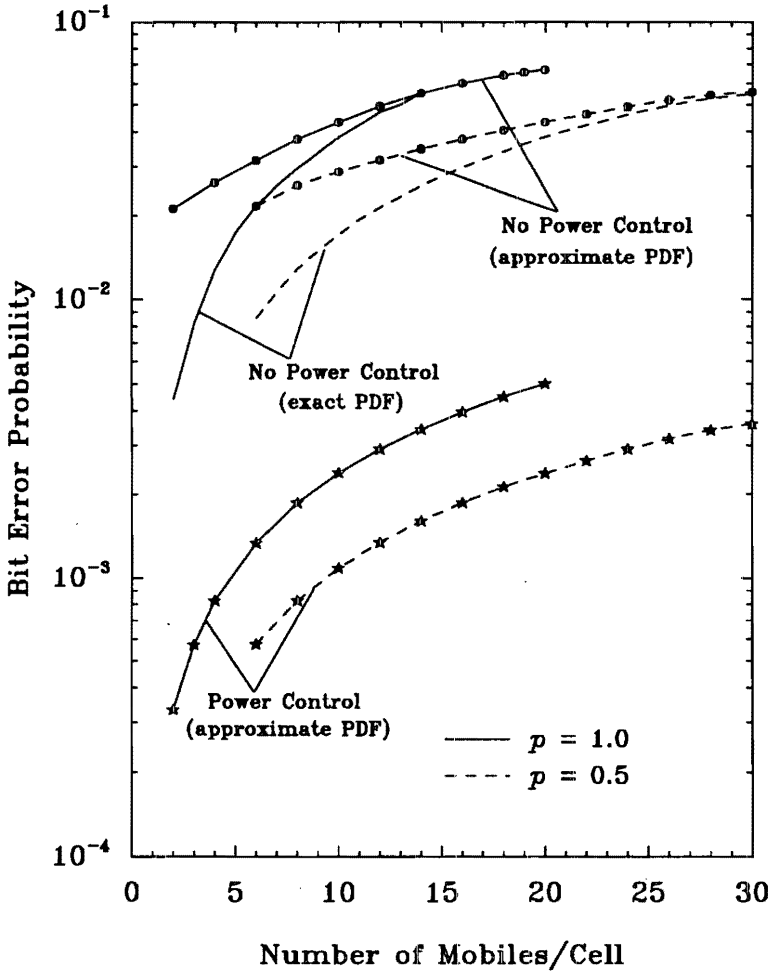


Figure 4.10: Uplink area averaged bit error probability against number of mobiles per cell, with voice activity detection. Results are shown for a multipath rejection receiver, and with and without average uplink power control; $L = 2$.

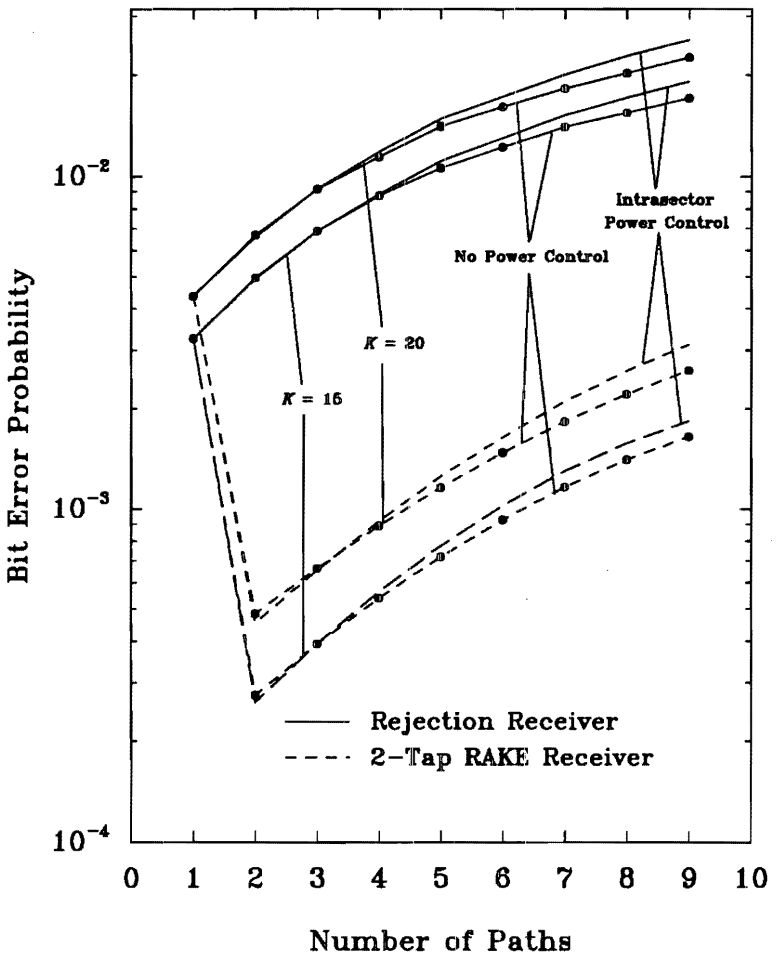


Figure 4.11: Downlink area averaged bit error probability against number of channel paths. Results are shown for a multipath rejection receiver and a 2-tap RAKE receiver with selective combining. The effect of using intrasector power balancing is also shown; $p = 1.0$.

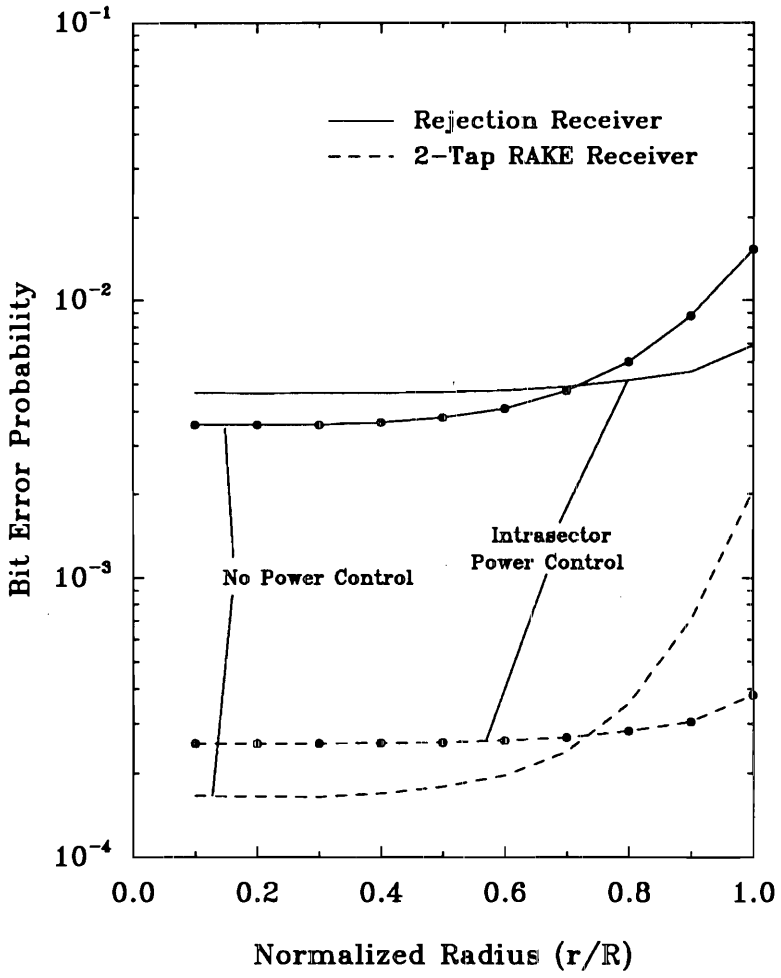


Figure 4.12: Downlink bit error probability as a function of the normalized distance from the base-station. Results are shown for a multipath rejection receiver and a 2-tap RAKE receiver with selective combining. The effect of using intrasector power balancing is also shown; $K = 15$, $p = 1.0$.

# 5 Non-Iterative Algorithm for Adaptive Channel Estimation[22]

## 5.1 Introduction

The most widely used channels for digital communications are the voice band telephone channels [23]. However, wireless channels are being used increasingly for digital communications. Second generation cellular mobile telephone systems based on digital technology are being developed for the North American, European, and Japanese markets. These cellular markets are experiencing exponential growth. Currently, there are about 4 million mobile telephone subscribers in North America. It is anticipated that this number will increase to 15-20 million by the mid 1990's [49].

Many impairments appear when using HF or UHF/VHF channels for digital communications, such as multipath spread, multipath-fading, Doppler spread, and frequency offset [23]. Multipath spread causes InterSymbol Interference (ISI) between consecutive symbols, multipath-fading causes a very low received signal-to-noise ratio when the channel exhibits a deep fade, and Doppler spread is indicative of rapid channel variations and necessitates an adaptive receiver with a fast convergent algorithm.

The optimum (maximum likelihood) method for detecting digital signals corrupted by ISI and additive noise is Maximum Likelihood Sequence Estimation (MLSE). One problem with MLSE is that the receiver complexity is proportional to $M^L$, where $M$ is the size of the signal constellation and $L+1$ is the length of the channel impulse response. This difficulty can be overcome by using reduced complexity receivers that retain most of the MLSE performance. Reduced-State Sequence Estimation (RSSE) [50], [51], and Delayed Decision Feedback Sequence Estimation (DDFSE) [52] are two such methods. It is well known that MLSE, RSSE, DDFSE, and other sequence estimation techniques can be efficiently implemented by using the Viterbi algorithm. Another approach is to use various forms of Sequential Sequence Estimation (SSE)

[22]The work in this section was performed with the assistance of Kahlid Hamied.

with the Fano algorithm or stack algorithm [55].

All sequence estimators require knowledge of the channel impulse response when computing the branch metrics, so that an adaptive channel estimator is necessary. Various channel estimators have been proposed in the literature [56], [57]. Usually, a transversal digital filter with the least mean squares (LMS) algorithm is used for this purpose, because of its computational efficiency and simplicity in implementation, [56], [58], [57]. It has been reported that the LMS algorithm performs almost as well as the Kalman algorithm for the purpose of channel estimation [57].

The usual procedure is to train the channel estimator with a known synchronization sequence, and during this time the channel estimator is in "training mode". After the channel estimator has been trained, a decision feedback mechanism is used to adapt the channel estimator during data transmission, and the channel estimator is in "data mode." In a conventional receiver, the LMS algorithm is used for both the training and data modes. However, the LMS algorithm converges very slowly when the channel impulse response changes rapidly during the training mode. Furthermore, the accuracy of the channel estimate during the data mode, is quite sensitive to the accuracy of the initial channel estimate that is obtained after the training mode. Hence, for rapidly time-variant channels, the performance of the LMS algorithm degrades. This problem can be remedied by using fast convergent recursive least squares algorithms, such as the Kalman algorithm, during the training mode. Unfortunately, these algorithms are quite complicated to implement, because require multiplications and divisions. In [59], a non-iterative algorithm was proposed for fast start-up equalization of baseband signaling on linear filter ISI (telephone) channels. This algorithm is extended in this section, so as to provide rapid equalizer training for adaptive equalization of quadrature modulation on multipath-fading ISI (mobile telephone) channels. A channel estimator that uses the proposed algorithm is very easy to implement in any DSP processor, because no multiplications nor divisions are needed. The algorithm only requires a specific training sequence. During the data mode, the adaptive channel estimator uses the LMS algorithm.

The remainder of this section is as follows. Subsection 5.2 describes the system

and multipath-fading ISI channel model that is used to evaluate the proposed algorithm. The algorithm is described in Subsection 5.3, and the statistical properties of the noisy estimate are given. Finally, Subsection 5.4 discusses the performance of the new adaptive channel estimator by using software simulation studies. In particular, the algorithm is applied to the North American AMPS D (IS-54) cellular standard.

## 5.2 System and Channel Model

The model chosen to represent the channel is the (L+1)-tap transversal filter with tap spacing equal to the symbol duration $T$. The model is shown in Fig. 5.1 for $D$ diversity branches, where $\eta_k^d$ is the noise in the $d^{th}$ diversity branch. The transmitted sequence is denoted by $x_0,\ x_1, \ldots$ and the sequence received over diversity branch $d$ is denoted by $y_0^d,\ y_1^d \ldots$. The sampled impulse response of diversity branch $d$ is

$$G^d \ = \ (g_0^d,\ g_1^d,\ \ldots,\ g_L^d)^T \tag{5.1}$$

All signals are written in baseband form and hence they are complex valued. The received sampled symbol at time $t = kT$ is given by

$$y_k^d \ = \ \sum_{i=0}^{L} g_i^d x_{k-i} + \eta_k \qquad k = S, S+1, \ldots \tag{5.2}$$

where $S$ is an arbitrary index and $\{\eta_k\}$ are zero-mean Gaussian random variables with variance $\frac{1}{2}\mathrm{E}[|\eta_k|^2] = N_o$.

The tap coefficients $\{g_i^d\}$ are assumed to be independent zero mean complex Gaussian random processes, so that the $\{|g_i^d|\}$ are Rayleigh distributed. It is important to note that in an actual channel, the tap coefficients may be correlated. Hence, our model is somewhat simplified, but it is widely used and accepted in the study of multipath-fading ISI channels [60], [61], [62], [1]. Regardless of the channel model, the adaptive channel estimator will work for any multipath-fading ISI channel. However, the exact performance will depend on the specific choice of channel model.

In the simulation studies, the coefficients $\{g_i^d\}$ are obtained by using the method suggested by Jakes [63], with appropriate corrections to ensure that the coefficients $\{g_i^d\}$ are independent complex Gaussian random processes.

## 5.3 The Non-Iterative Algorithm

First assume a noiseless environment, and choose $S = L$ in (5.2). In this case equation (5.2) can be written as

$$y_k^d = \sum_{i=0}^{L} g_i^d x_{k-i} \qquad k = L, L+1, \ldots \tag{5.3}$$

Equation (5.3) can be used to form consecutive $(L+1) \times (L+1)$ systems of linear equations. The starting index of the $n^{\text{th}}$ system (the subscript associated with $y^d$ is)

$$S_n = L + n(L+1) \qquad n = 0, 1, 2, \ldots \tag{5.4}$$

where $(L+1)$ is the number of unknown complex tap coefficients .

If the transmitted symbols are known to the receiver (which is the case during the training mode), then any linear system represented by (5.3) can be solved, assuming that the $(L+1)$ equations are linearly independent. The system of linear equations can be forced to be linearly independent by transmitting the following special training sequence

$$x_k = \begin{cases} -1 - j & k = 0, 1, \ldots, L-1 \\ (1+j)(-1)^{\lfloor k-L/L+1 \rfloor} & k = L, L+1, \ldots \\ & \ldots, L + N(L+1) - 1 \end{cases} \tag{5.5}$$

where $N$ is a positive integer, and $\lfloor x \rfloor$ is the largest integer contained in $x$.

If the above sequence is transmitted, then consecutive $(L+1) \times (L+1)$ linear systems of equations of the following form can be generated

$$Y_n^d = (-1)^n A G_n^d, \qquad n = 0, 1, 2, \ldots \tag{5.6}$$

where

$$A = \begin{bmatrix} 1+j & -1-j & -1-j & \ldots & -1-j \\ 1+j & 1+j & -1-j & \ldots & -1-j \\ 1+j & 1+j & 1+j & \ldots & -1-j \\ \vdots & \vdots & \vdots & & \vdots \\ 1+j & 1+j & 1+j & \ldots & 1+j \end{bmatrix}$$

$$Y_n^d = \begin{bmatrix} y_{S_n}^d \\ y_{S_n+1}^d \\ \vdots \\ y_{S_n+L}^d \end{bmatrix} \quad \text{and} \quad G_n^d = \begin{bmatrix} g_{0,n}^d \\ g_{1,n}^d \\ \vdots \\ g_{L,n}^d \end{bmatrix}$$

Any system of equations given by (5.6) is linearly independent. Assuming that the channel does not change during the formation of any system in Eq. (5.6), the solution of that system is given by

$$g_{0,n}^d = \frac{(-1)^n}{2(1+j)} \left[ y_{S_n}^d + y_{S_n+L}^d \right] \tag{5.7}$$

$$g_{i,n}^d = \frac{(-1)^n}{2(1+j)} \left[ y_{S_n+i}^d - y_{S_n+i-1}^d \right] \tag{5.8}$$

$$i = 1,\ 2,\ \ldots,\ L$$
$$n = 0,\ 1,\ \ldots$$

The division by $2(1+j)$ can be avoided by defining

$$\tilde{g}_{i,n}^d = 2(1+j) g_{i,n}^d \qquad i = 0,\ 1,\ \ldots,\ L \tag{5.9}$$

The $\{g_{i,n}\}$ can be found easily from $\{\tilde{g}_{i,n}\}$ as follows:

$$\Re(g_{i,n}^d) = \frac{1}{4} \left( \Re(\tilde{g}_{i,n}^d) + \Im(\tilde{g}_{i,n}^d) \right) \tag{5.10}$$

$$\Im(g_{i,n}^d) = \frac{1}{4} \left( \Im(\tilde{g}_{i,n}^d) - \Re(\tilde{g}_{i,n}^d) \right) \ ,$$

where $\Re(z)$ and $\Im(z)$ denote the real and imaginary part of $z$, respectively. The division by 4 in Eq. (5.10) is simply performed by two logical shifts.

Now assume that additive white Gaussian noise is present. Let $\{\hat{g}_{i,n}^d\}$ denote the noisy estimate of $g_i^d$ using the $n^{\text{th}}$ linear system $i = 0, 1, \ldots, L,\ n = 0, 1, \ldots$ The solution of the $n^{\text{th}}$ noisy estimate is given by (5.7) and (5.8), where $y_k^d$ is given by (5.2). The mean square error of the noisy estimate is

$$\frac{1}{2} E \left[ \left| \hat{g}_{i,n}^d - g_{i,n}^d \right|^2 \right] = \frac{N_o}{4} \qquad i = 0, 1, \ldots L \ . \tag{5.11}$$

If we assume that the channel does not vary during a time interval of length $(L+1)NT$, where $N$ is a positive integer, then we can use (5.7) and (5.8) for $n = 0, 1, 2, \ldots, N-1$ and obtain $N$ different solutions. Any difference in the solutions is due to noise, provided that the above assumption is valid. In this case, the mean square error of the estimate can be reduced by averaging the $N$ different solutions. Taking the average over $N$, and denoting the new estimate as $\hat{g}_i^d$, $i = 0, 1, \ldots, L$, and using (5.7) and (5.8) gives

$$\hat{g}_o^d = \frac{1}{2N(1+j)} \sum_{n=0}^{N-1} (-1)^n \left[ y_{S_n}^d + y_{S_n+L}^d \right] \tag{5.12}$$

$$\hat{g}_i^d = \frac{1}{2N(1+j)} \sum_{n=0}^{N-1} (-1)^n \left[ y_{S_n+i}^d - y_{S_n+i-1}^d \right] \tag{5.13}$$

$$i = 1,\ 2,\ \ldots,\ L$$

The mean square error of the estimate in this case is equal to

$$\frac{1}{2} E\left[ \left| \hat{g}_i^d - g_i^d \right|^2 \right] = \frac{N_o}{4N} \quad i = 0, 1, \ldots L \ . \tag{5.14}$$

For rapidly varying channels $N$ must be chosen very carefully. If it is chosen too large, then the accuracy of the channel estimate will degrade.

## 5.4 Simulation Results

In this subsection, the new adaptive channel estimator is applied to the North American IS-54 digital cellular standard. It can also be applied to other cellular standards, such as the Japanese digital cellular standard, and to a lesser extent the European GSM-System. The IS-54 standard uses $\pi/4$ QPSK and TDMA. Each frame is divided into six slots. Each slot consists of 162 symbols, of which 14 consecutive symbols are used for equalizer training and slot identification. It is assumed that the receiver is implemented using the MLSE structure shown in Fig. 5.2.

Suppose that the channel consists of two, equal strength, Rayleigh faded rays, i.e., $\mathrm{E}[|g_0|^2] = \mathrm{E}[|g_1|^2]$. For this channel condition, Figs. 5.3 and 5.4 show the performance of an MLSE receiver at 40 km/h and 100 km/h, respectively. In each plot,

three curves are shown. One corresponds to an ideal channel estimator where the branch metrics are formed by using an exact, but delayed version, of the channel impulse response. This delay corresponds to the decision delay of the Viterbi algorithm. For our purpose, we assume a decision delay of 8 symbols, although this can be varied.

Another curve in each of Figs. 5.3 and 5.4 shows the performance when the LMS algorithm is used in both the training mode and data mode. In this case, that the synchronization sequence is assumed to precede the data sequence. The stepsize of the LMS algorithm was chosed to be 0.3, which gives near optimal performance.

The final curve in each graph shows the performance when the new algorithm is used during the training mode, and the LMS algorithm is used during the data mode. Again, the stepsize of the LMS algorithm was chosen to be 0.3. For a channel impulse response of length 2, only 3 symbols are required to obtain a channel estimate with the new channel estimator. As a result, it is assumed that the frame structure is modified slightly when using the new algorithm. In particular, four 3-symbol training sequences are equally spaced throughout the frame. Each training sequence is followed by a 37-symbol data sequence. The remaining 2 symbols in each slot can be used for slot synchronization.

At both vehicle speeds, the new algorithm improves the bit error performance significantly. In fact, at 100 km/h the LMS training algorithm yields an unacceptably high error probability. At this same vehicle speed, the new algorithm keeps the error rate below $10^{-2}$, which is acceptable for a properly designed voice coder.

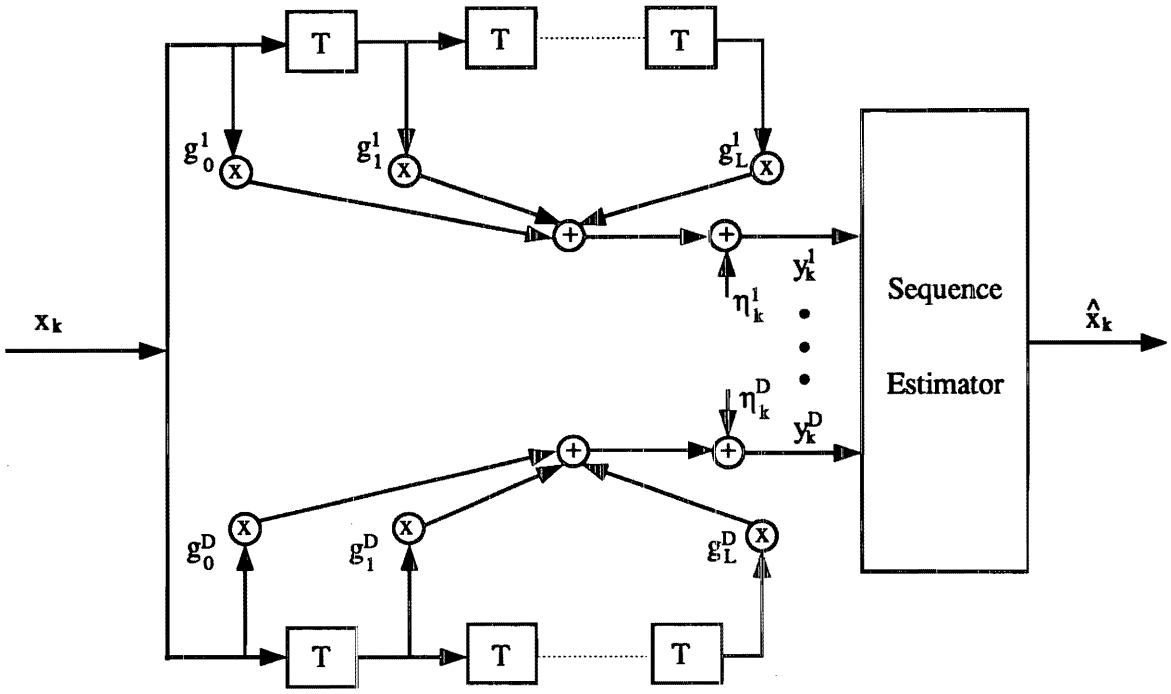


Figure 5.1: Uncoded System with an Equivalent Discrete-Time White Noise Channel Model, from [61]

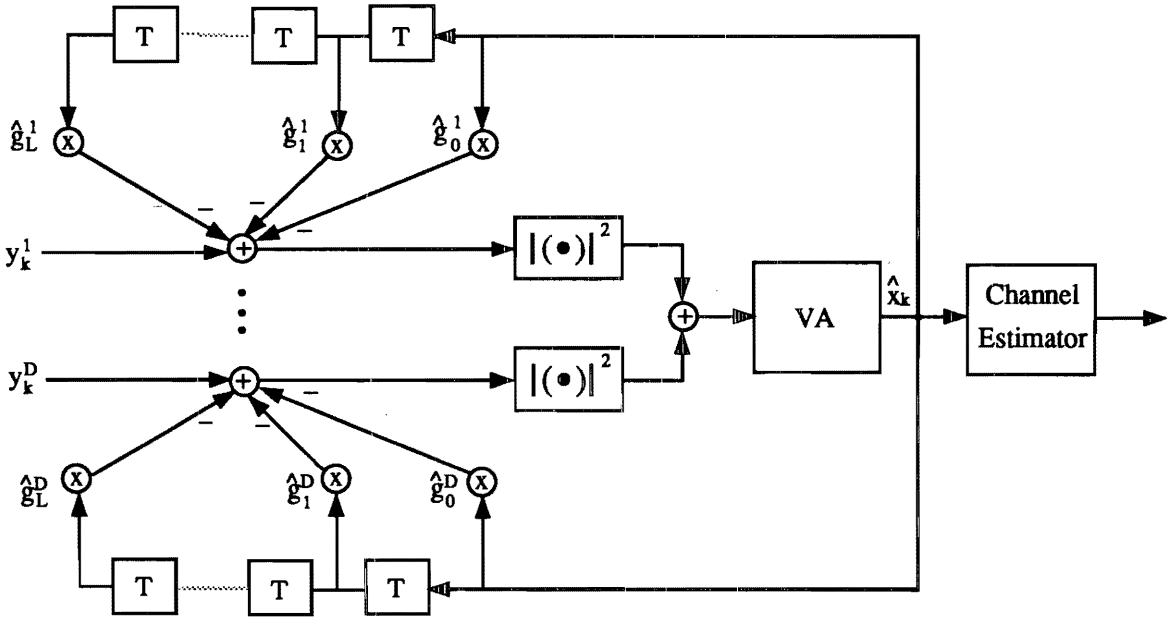


Figure 5.2: MLSE Receiver Structure, from [63]

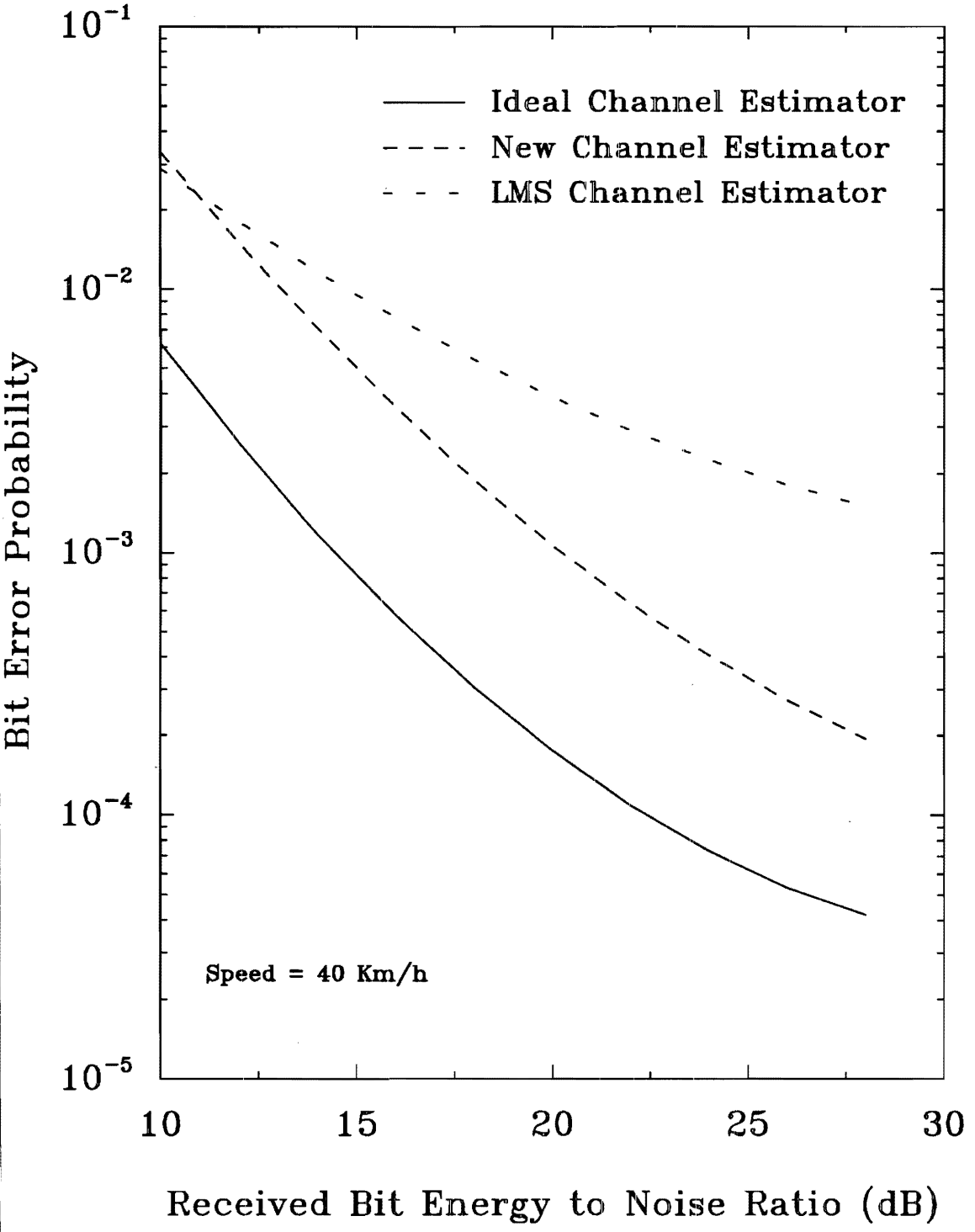


Figure 5.3: Performance of the New Channel Estimator at 40 km/h

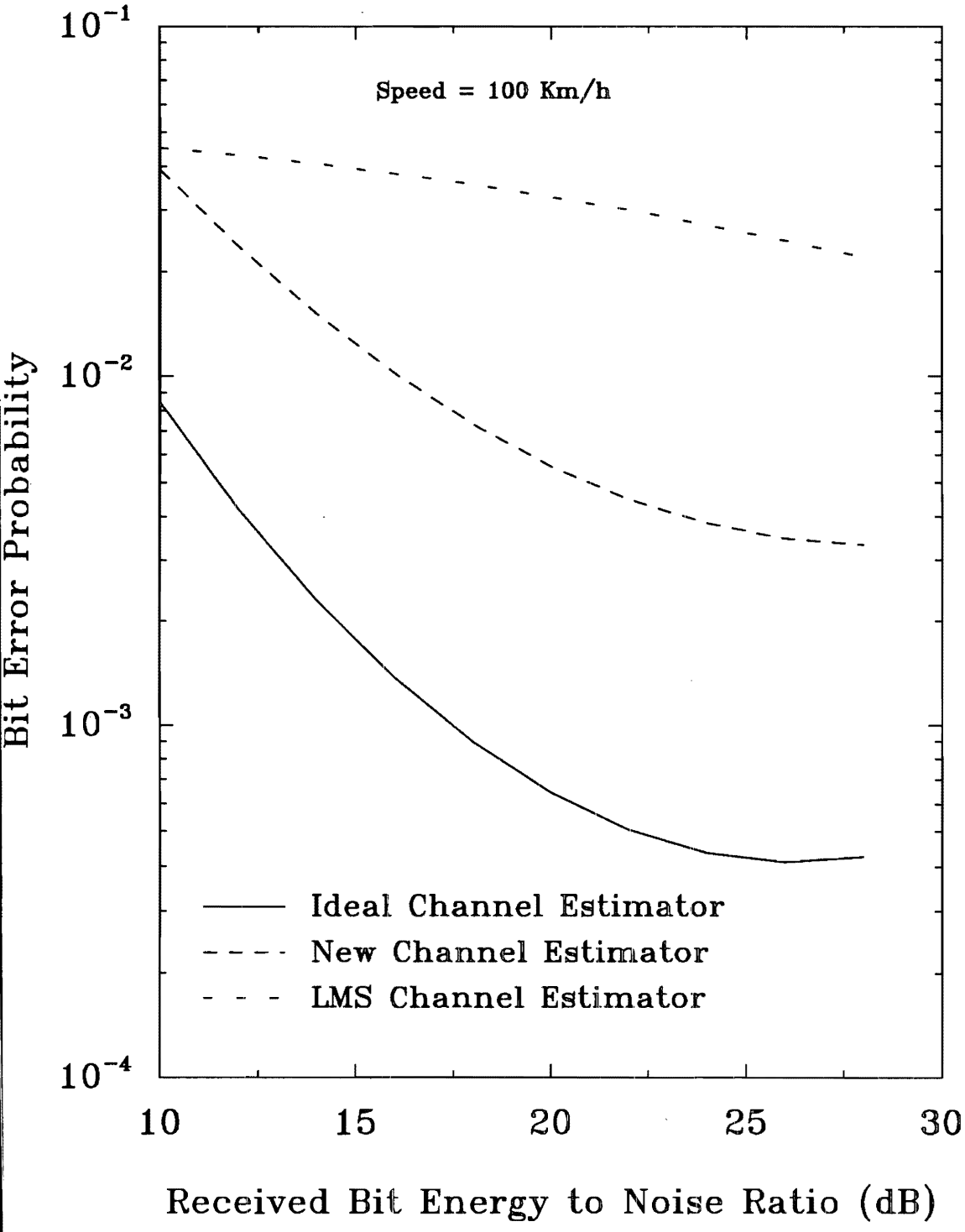


Figure 5.4: Performance of the New Channel Estimator at 100 km/h

# 6 Personal Communications and Microwave Radio[23]

## 6.1 Introduction

Recent proposals have been made by PCN America to use direct-sequence code division multiple-access DS CDMA as a channel access method for personal communication networks (PCN's). It is anticipated that these PCN's will share spectrum with existing private microwave radio systems in the 1850-1990 MHz band. In this study, we will determine the level of interference that a victim microwave receiver can tolerate from an overlaying PCN that uses DS CDMA. At this point, two victim receivers have been considered. The first is the Harris Farinon DM2-4A-12 Digital Microwave Radio System. The second is a generic analog FDM/FM system. The overlaying PCN is assumed to use DS/BPSK modulation with raised cosine pulse shaping and various pseudo-noise chip rates or bandwidths. PCN systems having the following two bandwidths have been considered:

- 1.25 MHz, corresponding to the DS CDMA system proposed by Qualcomm.
- 48 MHz, corresponding to the DS CDMA system proposed by PCN America.

The DS/BPSK transmitters and victim receivers have been constructed in software using the Block Oriented System Simulator (BOSS) from Comdisco Systems. BOSS is a system time domain simulation package. The transmitter and receiver models, and various test systems, have been carefully constructed so as to meet all the appropriate manufacturer specifications and CCIR recommendations. Therefore, the performance results that have been obtained will closely reflect those that will be obtained from hardware implementations.

The remainder of this section is organized as follows. Subsection 6.2 discusses the PCN transmitters, and Subsection 6.3 discusses the victim microwave receivers that have been implemented. Subsection 6.4 , describes the various experiments that were conducted to determine the level of interference that the microwave systems can tolerate from the PCN system.

[23]The work in this section was performed with the assistance of Lih-Bor Yiin and Ming-Ju Ho.

## 6.2 Transmitter Models

### 6.2.1 PCN Transmitters

An overview of the transmitter used for the various PCN systems is shown in Fig. 6.1. As shown, the PCN transmitter uses direct-sequence spread spectrum with binary phase shift keyed modulation (DS/BPSK).

The data sequence in the PCN transmitter is assumed to be random. In the particular system proposed by PCN America, the data sequence is a 32 kb/s delta modulated voice signal. The spreading sequence is also assumed to be a random binary sequence. In practice pseudo-noise (PN) spreading sequences, such as Gold sequences or Kasami sequences are used. Random spreading sequences have a power spectral density that is almost the same as deterministic PN sequences. Baseband filtering is used prior to modulation to control the shape of the transmitted spectrum. In particular, frequency domain raised cosine filtering is used with a roll-off factor of unity. Two different PN chip rates are included in this study; 0.625 Mchips/s and 24 Mchips/s, corresponding to modulated bandwidths of 1.25 MHz and 48 MHz, respectively. If a chip rate of 24 Mchips/s is used with 32 kb/s delta modulated voice, then the processing gain is 750.

### 6.2.2 Microwave Transmitter Models

*1) Harris Farinon DM2-4A-12 Transmitter:* Fig. 6.2 presents an overview of the Harris Farinon DM2-4A-12 microwave transmitter. The transmitter sends information using 16-QAM with a baud rate of $T_S = 3,223,750$ symbols/s. As shown in Fig. 6.2, data is generated by using four independent random binary data sources. In practice, the four data streams are generated by using a serial-to-parallel converter. Under the assumption that the data bits are uncorrelated they can be effectively generated by the four independent random binary data sources as shown in Fig. 6.2. The four data sources are then processed with four stages; (2-2) differential encoding, gray encoding, 16 QAM modulation, and square-root raised cosine filtering.

The (2-2) differential encoder is detailed in Fig. 6.3. Since 2 bits are inputed

into each encoder for each symbol, $T_S/2$ delay elements are used. The differential encoder performs the following operation

$$b_k = a_k \oplus b_{k-1} \quad , \tag{6.1}$$

where $a_k$ is the input sequence to each (2-2) differential encoder and $b_k$ is the encoded sequence. With the encoder structure shown in Fig. 6.3, the sequence of even bits $\{a_0, a_2, a_4, \cdots, a_{2k}, \cdots\}$ is applied to the upper branch, and the sequence of odd bits $\{a_1, a_3, a_5, \cdots, a_{2k+1}, \cdots\}$ is applied to the lower branch. The upper encoder output is the sequence $\{b_0, b_2, b_4, \cdots, b_{2k}, \cdots\}$, while the lower encoder output is the sequence $\{b_1, b_3, b_5, \cdots, b_{2k+1}, \cdots\}$.

The differentially encoded data bits are then applied to the Gray encoder that is illustrated in Fig. 6.4. The Gray encoded symbols are applied to the 16-QAM modulator. The resulting 16-QAM signal set is shown in Fig. 6.5. The use of Gray encoding ensures that the signal points closest in Euclidean distance differ by a single bit position.

Finally, a square-root raised cosine filter is used to control the transmitted spectrum. A square-root raised cosine filter is used so that the receiver can use a matched filter to obtain a raised cosine response. The roll-off factor of the raised cosine filter is chosen to be 0.0857. This rather small roll-off factor corresponds to a transmitted signal bandwidth of only 3.5 MHz. As a result of the small roll-off factor, the receiver is quite sensitive to timing phase jitter. In practice, the raised cosine filter must be placed before the 16-QAM modulator. However, the 16-QAM modulator provided in BOSS requires logical inputs. Therefore, we cannot filter the inputs before applying them to the BOSS 16-QAM modulator. To circumvent this problem, we have implemented the modulator in equivalent complex baseband form.
*2) Analog FDM/FM Transmitter:* An overview of the analog FDM/FM transmitter with 600 channels capacity is shown in Fig. 6.6. A white noise generator is used to produce a noise spectrum that simulates the spectrum that is produced by a multichannel multiplex system. The noise level is chosen, according to CCIR Rec. 399-3 [64], such that the ratio of the peak value to the rms value is about 12 dB at the

transmitter output. The noise source is then passed through a bandpass filter with high-pass cut-off frequency and low-pass cut-off frequency of 60 kHz and 2600 kHz, respectively. The bandpass filter has been implemented by using an Elliptic highpass and an Elliptic lowpass filter. Both filters are of sixth order and have 0.05 dB p-p ripple. The frequency response of the lowpass filter is shown in Fig. 6.7 and the frequency response of the highpass filter is shown in Fig.6.8. The output of the bandpass filter represents a system of 600 voice channels operating at full traffic load. This signal is then processed by two different branches: the upper branch has a blocking (bandstop) filter while the lower branch does not.

The function of the blocking filter is to remove the signals in a certain voice channel, whose center frequency in our system is 2438 kHz. The roll-off characteristic, based on CCIR Rec. 399-3 [64], is shown in Fig. 6.9. The blocking filter has been implemented by using an elliptic eighth order filter with passband edges of 2438 $\pm$60 kHz, stopband edges of 2438$\pm$1.5 kHz, and 0.05 dB p-p ripple. On the lower branch, a two-sample delay is introduced to offset the delay caused by the blocking filter.

The pre-emphasis characteristic, as recommended by CCIR Rec. 275-3 [65], is given by the following expression:

$$\text{Relative deviation (dB)} = 5 - 10\log\left[1 + \frac{6.90}{1 + \frac{5.25}{\left(\frac{f_r}{f} - \frac{f}{f_r}\right)^2}}\right] , \qquad (6.2)$$

where $f_r$ is the resonant frequency of the pre-emphasis circuit and is equal to 3325 kHz. The variation of deviation with frequency is shown in Fig. 6.10. The pre-emphasis filter has been implemented by using a second order pole-zero filter.

The pre-emphasized signals are then frequency modulated. The peak frequency deviation, $\Delta f$, is given by

$$\Delta f = 4.47\, d \log^{-1}\left(\frac{-15 + 10\log N}{20}\right) , \qquad (6.3)$$

where $d$ = 140 kHz is the rms frequency deviation per channel, and $N$ = 600 is the number of voice channels. The deviation constant is the ratio of $\Delta f$ to the peak

value of the pre-emphasized signal. In our case, the deviation constant is set to 4.1172371 MHz/v. Similar to the digital microwave case, the system is implemented in the equivalent complex baseband form. Therefore, the carrier frequency of the FM modulator is 0 Hz.

## 6.3 Receiver Models

This subsection describes the receivers models that have been implemented for the various victim microwave receivers.

### 6.3.1 Harris Farinon DM2-4A-12 Receiver

Fig. 6.11 shows an overview of the DM2-4A-12 receiver. The receiver consists of a square-root raised cosine filter, timing circuits, and a 16-QAM demodulator. As shown in Fig. 6.11, ideal timing circuits have been assumed. Therefore, the effects of timing jitter are not included in the subsequent simulations.

The purpose of the square-root raised cosine filter is to provide matched filtering and to reject out-of-band noise and interference.

The 16-QAM demodulator simply selects the signal points that are closest in Euclidean distance to the sample values at the output of the matched filter. The Gray decoder, shown in Fig. 6.12, on the inphase and quadrature branches maps the received signal point onto the corresponding data bits. The data bits on the inphase and quadrature streams are then processed by a differential decoder. As shown in Fig. 6.13, the differential decoder generates an estimate of the information sequence, $\{\hat{a}_k\}$, by the following operation

$$\hat{a}_k = c_k \oplus c_{k-1} \quad , \tag{6.4}$$

where $\{c_k\}$ is the sequence at the output of the Gray decoder.

### 6.3.2 Analog FDM/FM Receiver

The analog FDM/FM receiver is shown in Fig. 6.14. The upper and lower branches have exactly the same function. The receiver filter is designed to reject out-of-band

noise and interference. For this purpose, a $4^{th}$ order Butterworth lowpass filter with a passband edge 6 MHz and a passband attenuation of 1 dB has been used. The frequency response of this filter is shown in Fig. 6.15.

A balanced discriminator detector is used to implement the FM demodulator. The demodulated signal is then fed into the de-emphasis filter, whose transfer function is the inverse of that of the pre-emphasis filter. The roll-off characteristic of the de-emphasis filter is shown in Fig. 6.16. Finally, a bandpass filter with center frequency 2438 kHz is applied to extract the signal power in that voice channel. The bandpass filter is matched to the bandstop filter in the transmitter. It has been implemented by using an elliptic eighth order filter with passband edges of 2438± 1.5 kHz, stopband edges of 2438±60 KHz, and 0.009 dB p-p ripple. The frequency repsonse of this filter is shown in Fig. 6.17.

## 6.4 Interference Tests

### 6.4.1 Harris Farinon DM2-4A-12 Digital Microwave System

The co-channel interference objective for a digital system is the threshold-to-interference ($T/I$) ratio. As described in EIA-10E [66, pp.21], it is defined as the ratio of the desired signal power to the interfering signal power that degrades the bit error rate performance from $10^{-6}$ to $10^{-5}$. The carrier-to-interference ($C/I$) ratio is then determined by

$$C/I = T/I + \text{Fade Margin (dB)} \quad , \tag{6.5}$$

where the fade margin is 35 dB in the 1.9 GHz frequency band.

*1) Test procedure:* The test set up is illustrated in Fig. 6.18. White noise is applied to the DM2-4A-12 receiver so that the bit error rate is $10^{-6}$. The spread-spectrum CDMA signals are then injected to the system until a bit error rate of $10^{-5}$ is obtained. The relative level of desired signal power and interfering signal power is the desired $T/I$ ratio.

*2) Test Results:* The simulation result of the bit error probability for the DM2-4A-12

system, along with the theoretical bit error probability performance for 16 QAM, is shown in Fig. 6.19. When $\gamma_b$ (bit energy-to-noise ratio) equals 15 dB or, equivalently, the symbol energy-to-noise ratio is 21 dB, the bit error probability is actually $10^{-6}$. We also notice that a one dB degradation in bit energy-to-noise ratio increases the bit error probability from $10^{-6}$ to $10^{-5}$. It can be argued that the wideband 48 MHz CDMA signals appear as additive white Gaussian noise. If this is indeed the case, the interference produced by the CDMA signals must be such that they cause no more than 1 dB degradation in the received carrier-to-(noise plus interference) ratio of the microwave receiver. Therefore, the interference power must be roughly 6 dB below the thermal noise power. Hence, the bit energy-to-interference ratio should be approximately 27 dB.

The simulation results from four different cases of CDMA interference are shown in Table 6.1 where we have assumed a fade margin of 35 dB. The first case is a 48 MHz CDMA signal where the carrier frequencies are exactly coincident. The second case is a 1.25 MHz CDMA signal with a relative carrier offset of 0 Hz, 1 MHz, and 2 MHz. From Table 6.1, we observe that the simulation results are within 1 or 2 dB of the expected 27 dB.

| Bandwidth | Frequency Offset | $T/I$ | $C/I$ |
|---|---|---|---|
| 48 MHz | 0 Hz | 29 | 64 |
| 1.25 MHz | 0 Hz | 26 | 61 |
| 1.25 MHz | 1 MHz | 26 | 61 |
| 1.25 MHz | 2 MHz | 27 | 62 |

Table 6.1: Interference Objectives for Harris Farinon DM2-4A-12 System

### 6.4.2 Analog FDM/FM Microwave Radio System

For analog FDM/FM system, the threshold is defined as the RF carrier level that produces a flat signal-to-noise[24] ratio (S/N) of 30 dB in the worst voice channel (2438 kHz in our case). Therefore, the carrier-to-interference ratios obtained from the

[24]The noise here stands for intermodulation noise.

simulations are actually the threshold-to-interference ($T/I$) ratios. Like the digital microwave system, the real CIR should be

$$C/I = T/I + \text{Fade Margin (dB)} \ . \tag{6.6}$$

The co-channel interference criterion is that the interfering signals introduce 1 dB degradation in S/N, i.e., from 31 dB to 30 dB. The $S/N$ can be converted to another measure, the noise power ratio (NPR), by the following relation,

$$88 - \text{S/N} = 71.6 - \text{NPR} \ . \tag{6.7}$$

Thus, the co-channel interference criterion is that the interfering signals cause the NPR of the FDM/FM system to decrease from 14.6 dB to 13.6 dB.

*1) Test Procedure–NPR Test:* The test set-up for the analog FDM/FM system is shown in Figs. 6.20 and 6.21. NPR is the ratio of the noise level in a measuring channel with the baseband fully loaded to the noise level in that channel with the baseband fully loaded except for the measuring channel. The channel is first adjusted so that the NPR is 14.6 dB, by adjusting the level of additive white Gaussian noise. Then the CDMA interference is applied to decrease the NPR to 13.6 dB.

*2) Test Results:* The variation of NPR value with time, with no interference, is shown in Figs. 6.22 and 6.23. At 0.5 s, the 5,000,000 samples have been processed. The NPR value clearly converges to 14.6 dB.

Figs. 6.24 and 6.25 show the simulation results of NPR for 48 MHz CDMA interference case. Two curves are drawn, which correspond to carrier-to-interference ratios of 25 dB and 28 dB, respectively. With CIR of 25 dB, the NPR converges to around 13.2 dB; while for a CIR of 28 dB the, NPR converges to 13.75 dB. We conclude that the actual CIR that drives the NPR to 13.6 dB is about 27 dB.

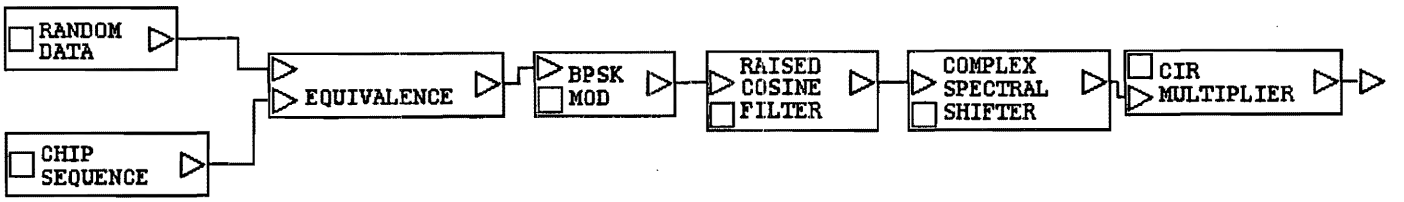


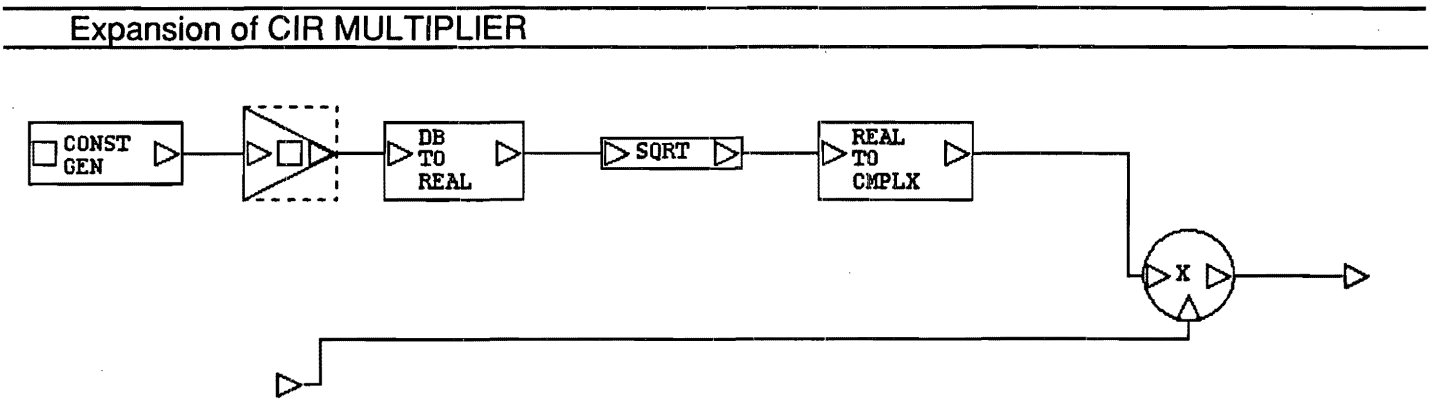


Figure 6.1: DS/BPSK Transmitter for PCN's.

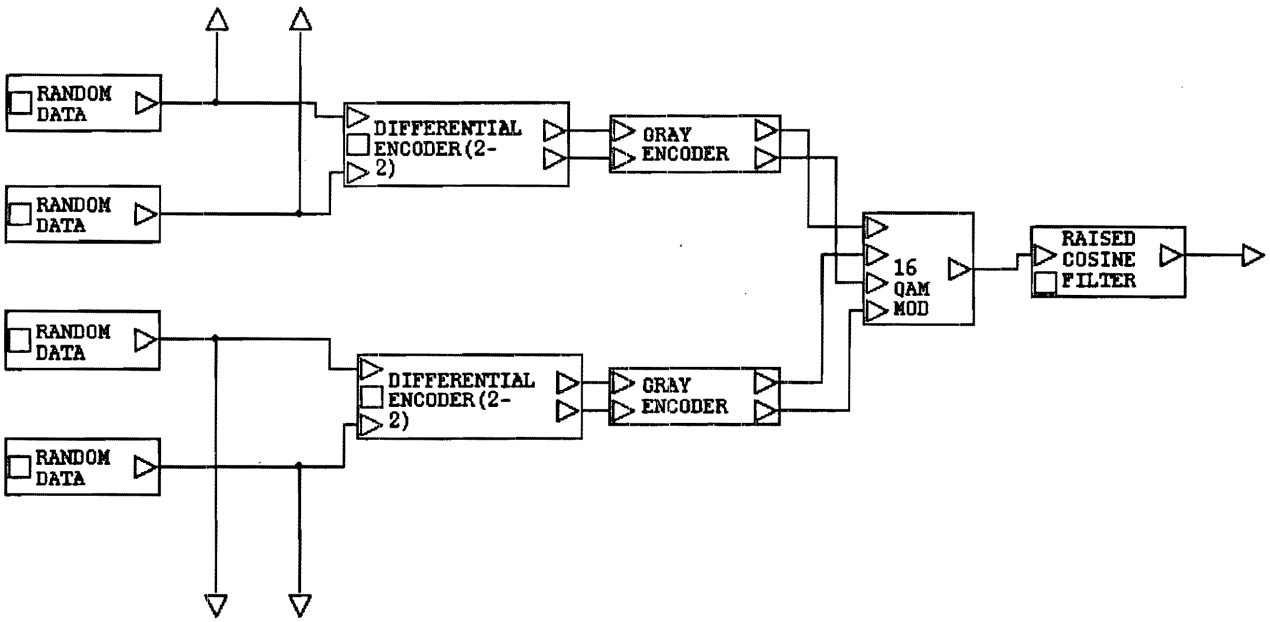


Figure 6.2: Harris Farinon DM2-4A-12 Transmitter.

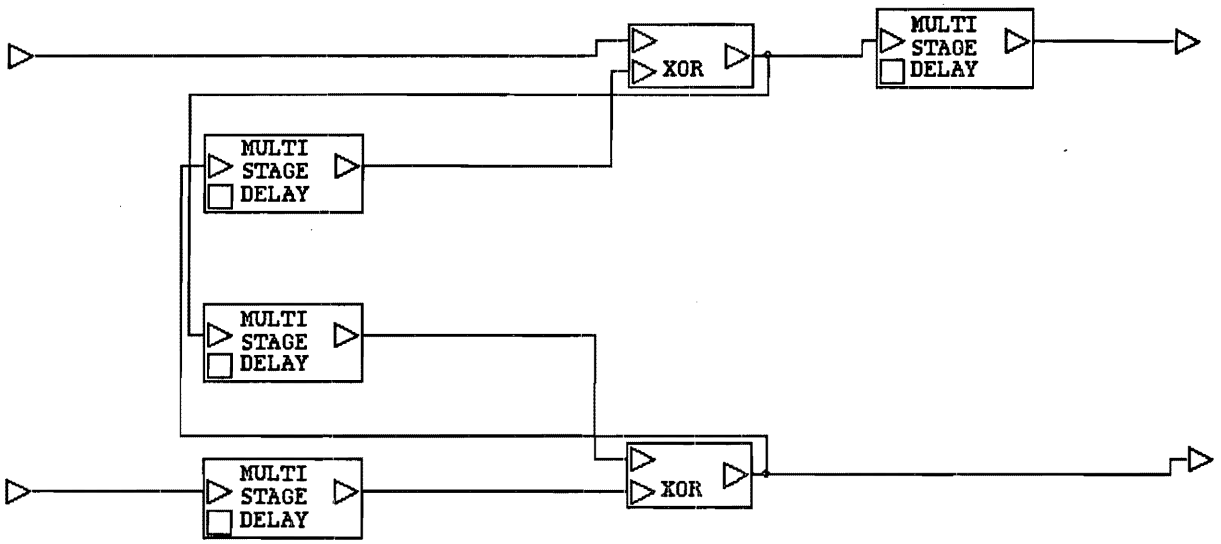


Figure 6.3: (2-2) Differential Encoder.

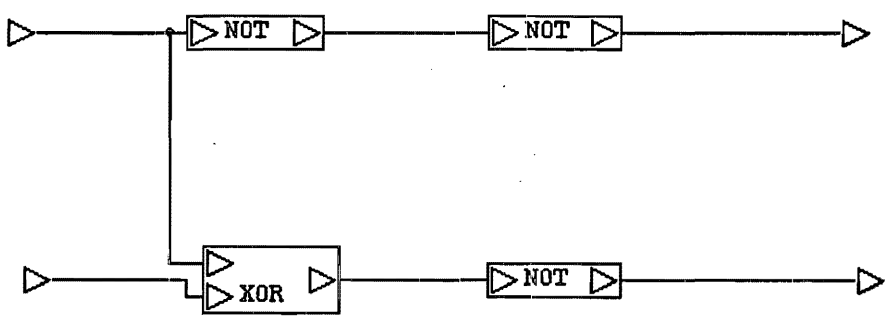


Figure 6.4: Gray Encoder

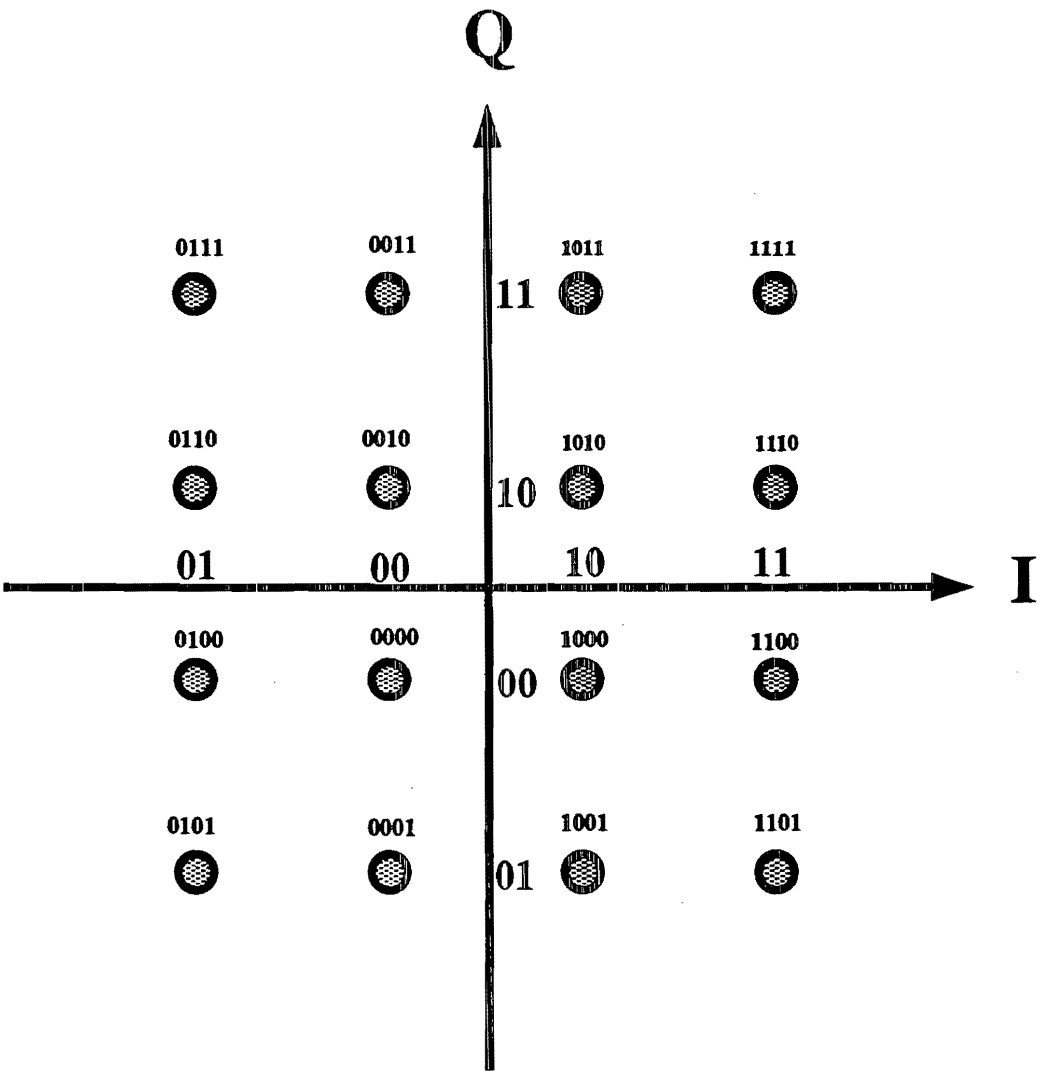


Figure 6.5: 16-QAM Signal Set.

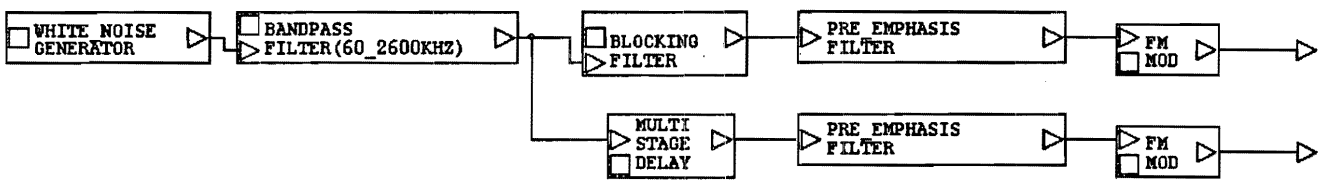


Figure 6.6: Overview of Analog FDM/FM Transmitter.

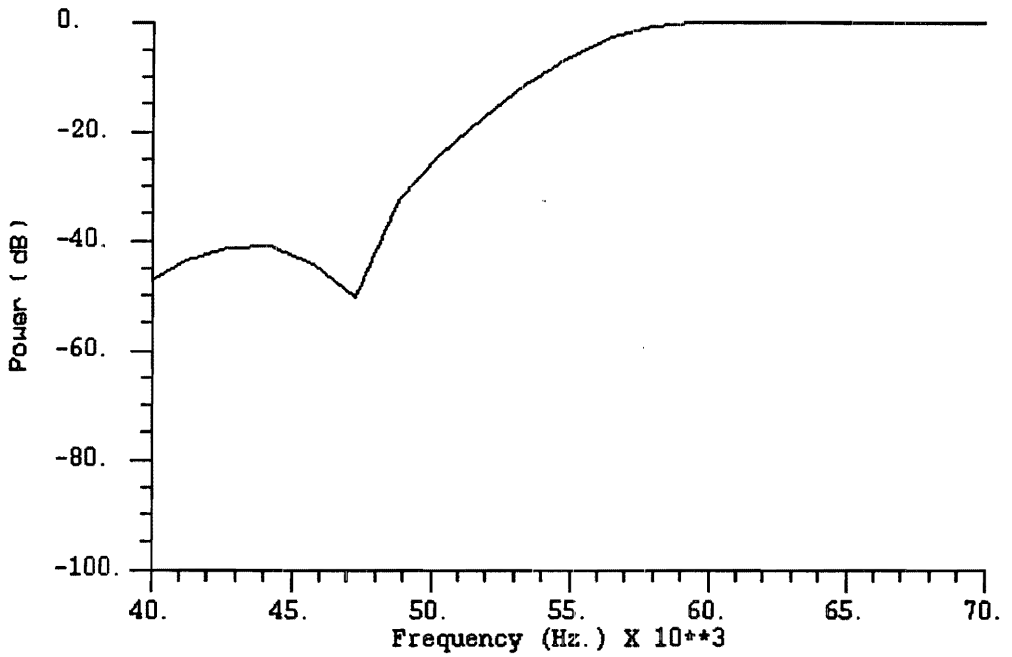


Figure 6.7: Frequency Response of Elliptic Lowpass Filter.

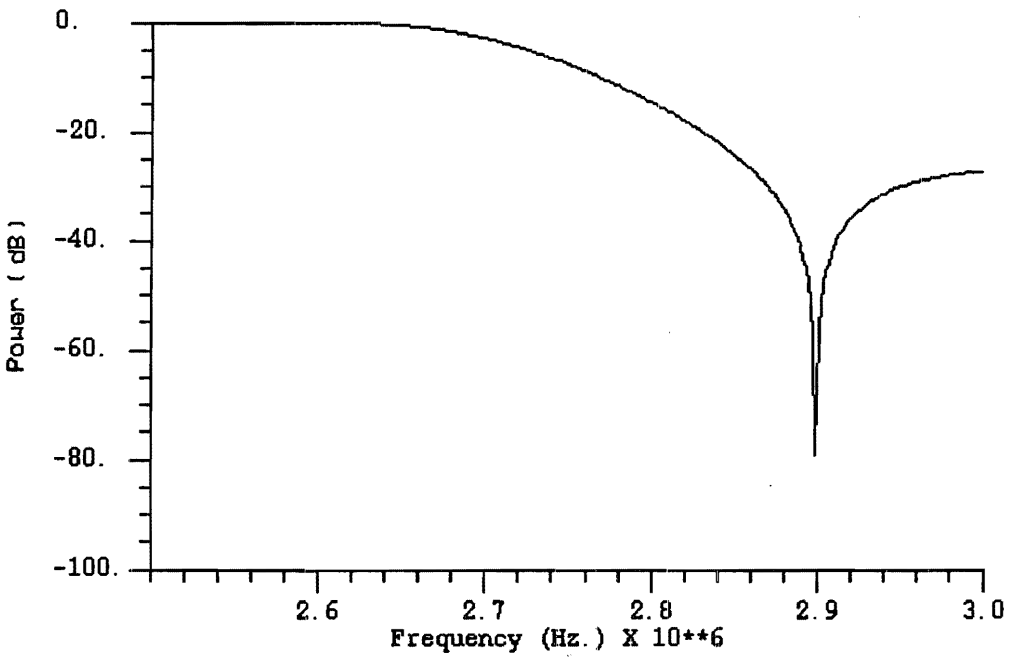


Figure 6.8: Frequency Response of Elliptic Highpass Filter.

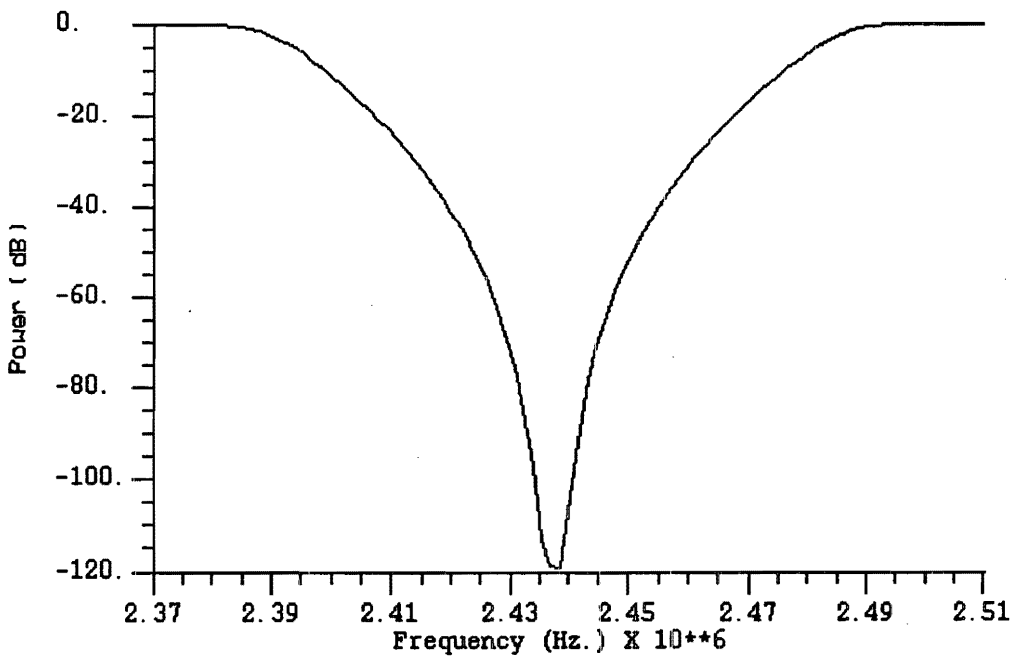


Figure 6.9: Frequency Response of Blocking Filter.

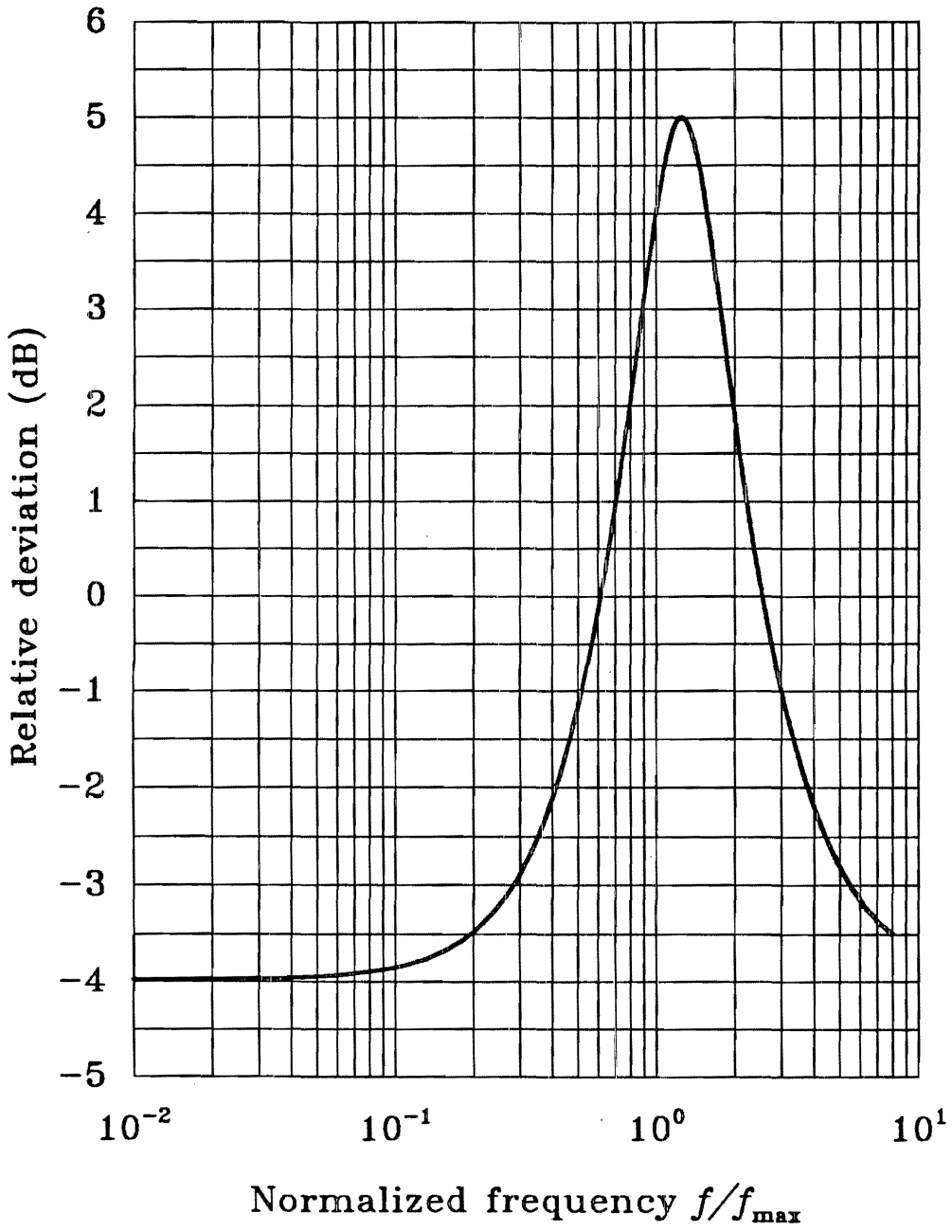


Figure 6.10: Deviation Characteristic of Pre-empahsis Filter.

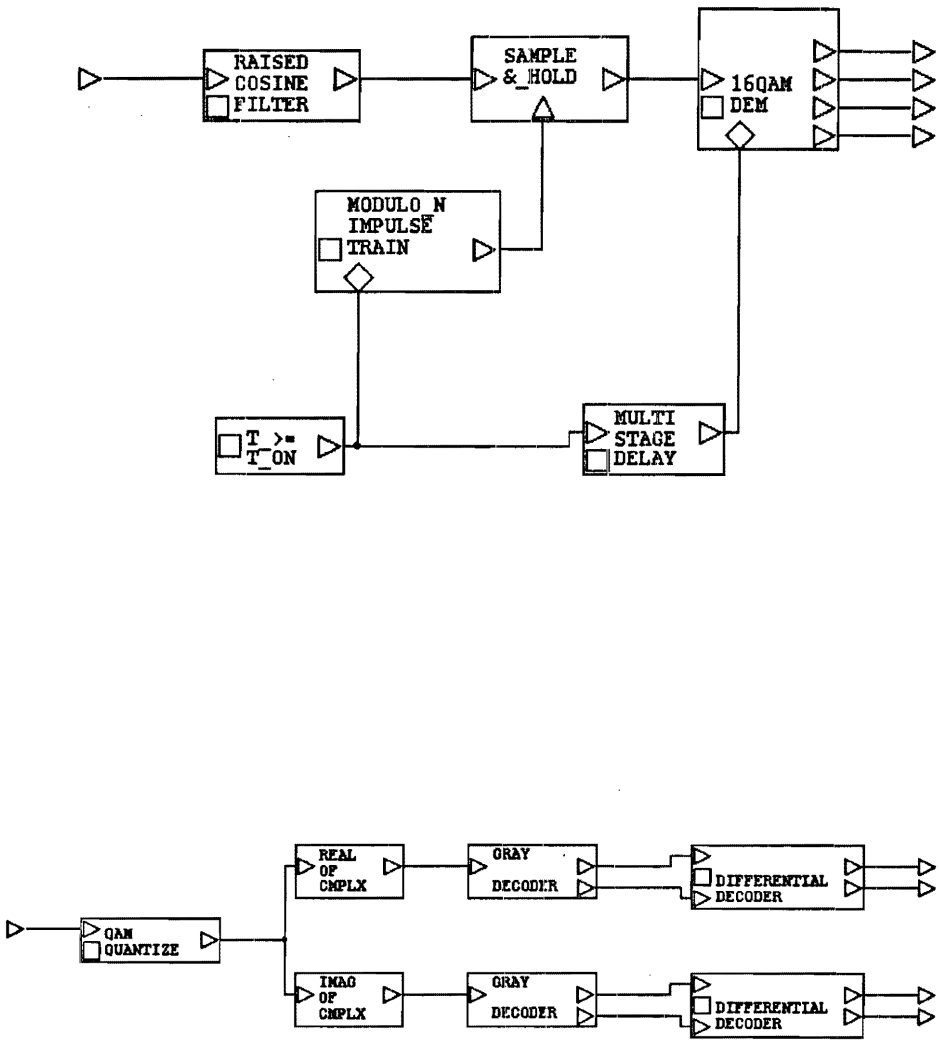


Figure 6.11: Harris Farinon DM2-4A-12 Receiver.

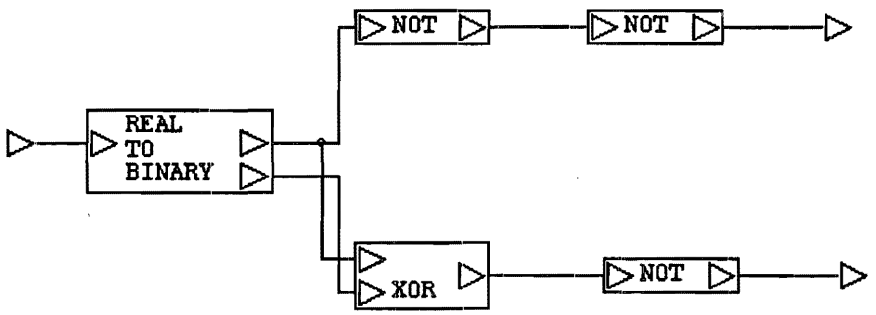


Figure 6.12: Gray Decoder.

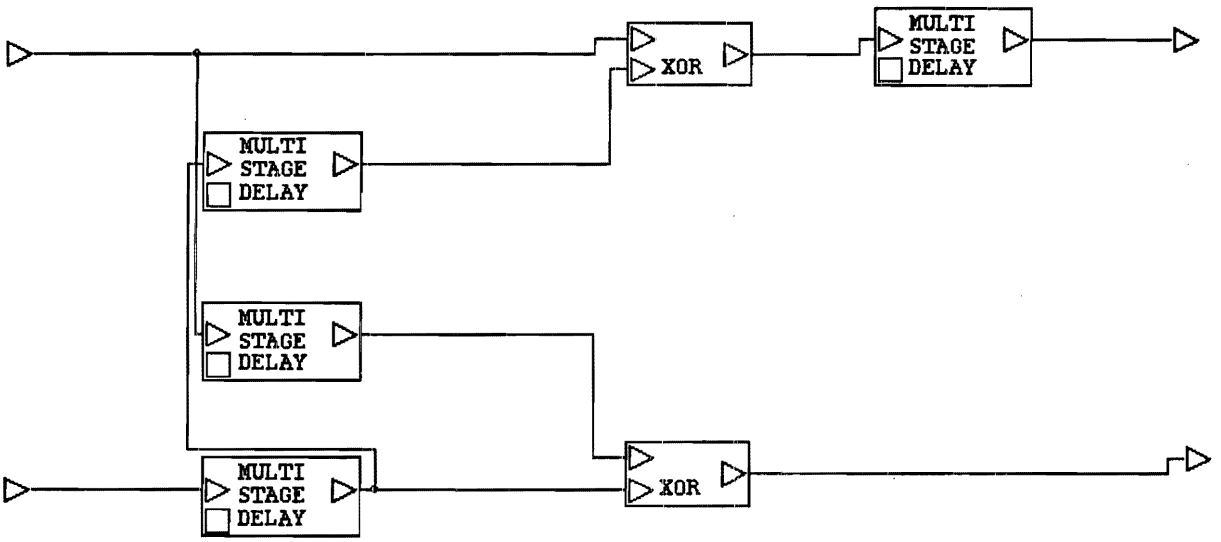


Figure 6.13: Differential Decoder.

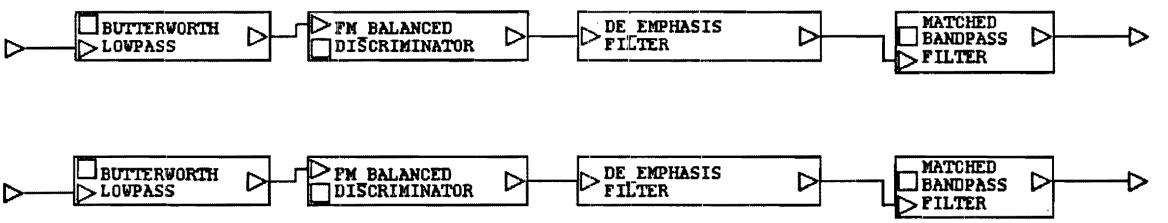


Figure 6.14: Analog FDM/FM Receiver.

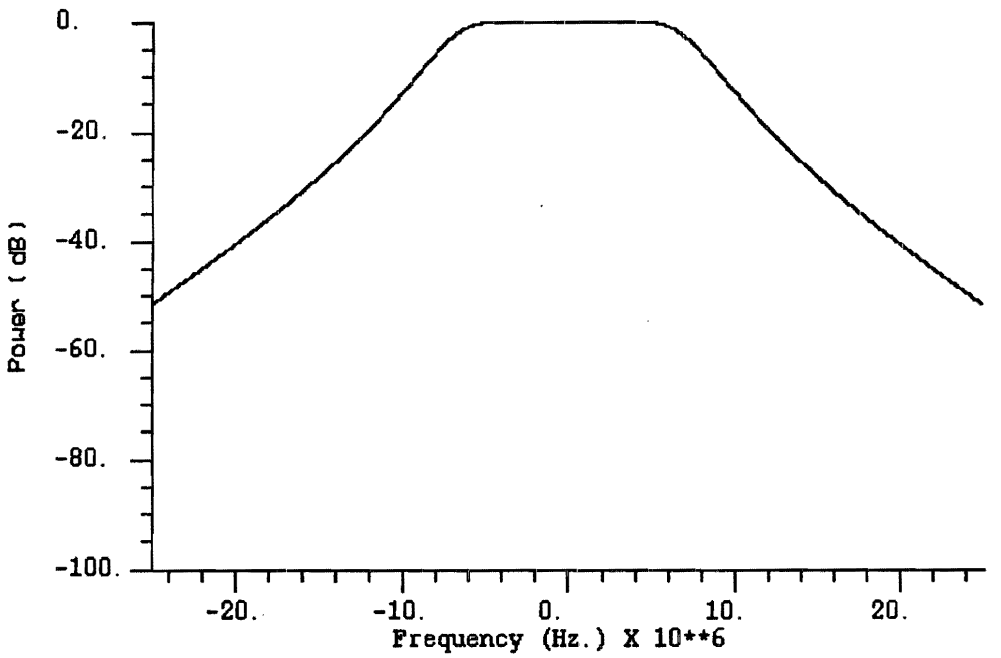


Figure 6.15: Receiver Filter.

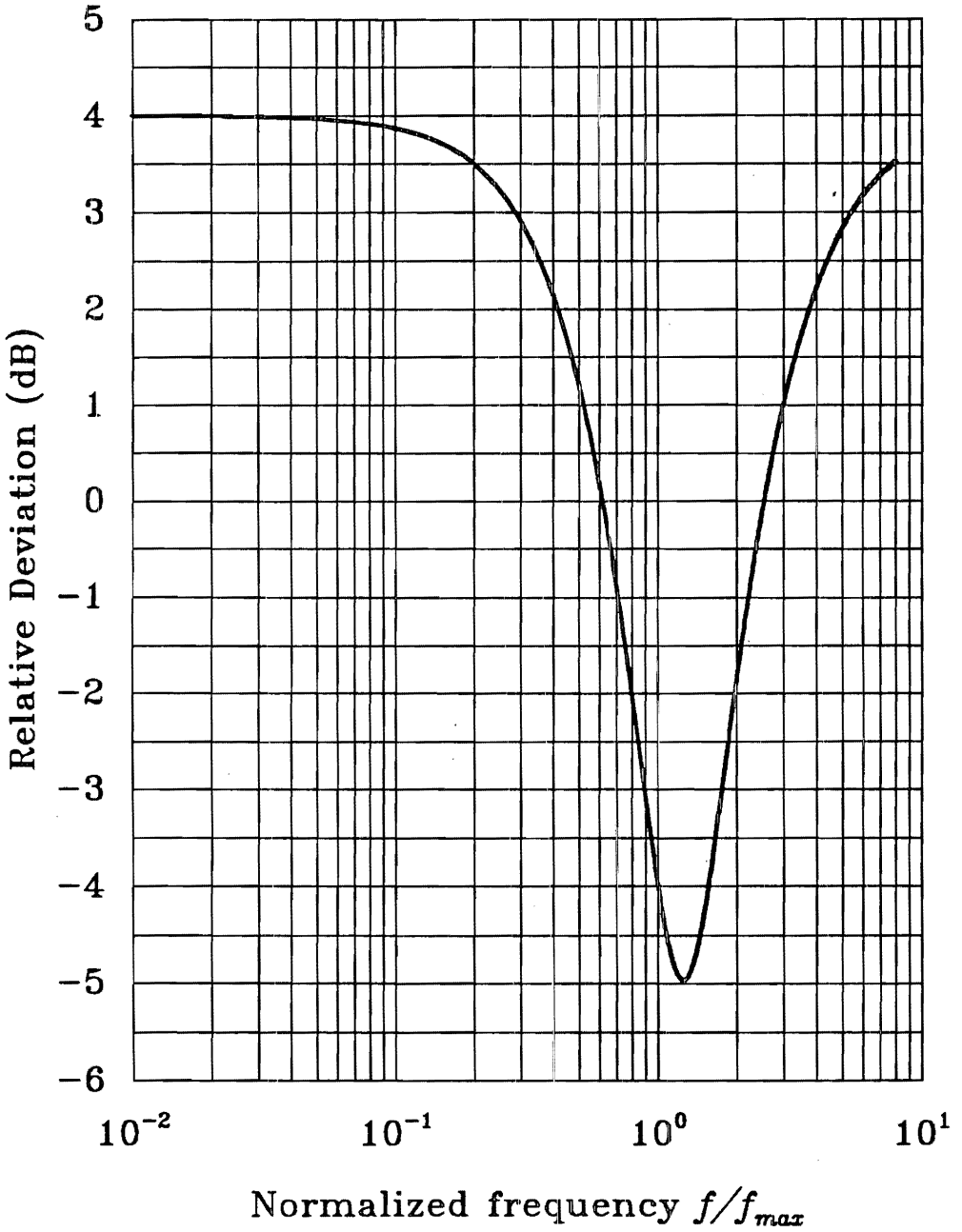


Figure 6.16: Deviation Characteristic of De-emphasis Filter.

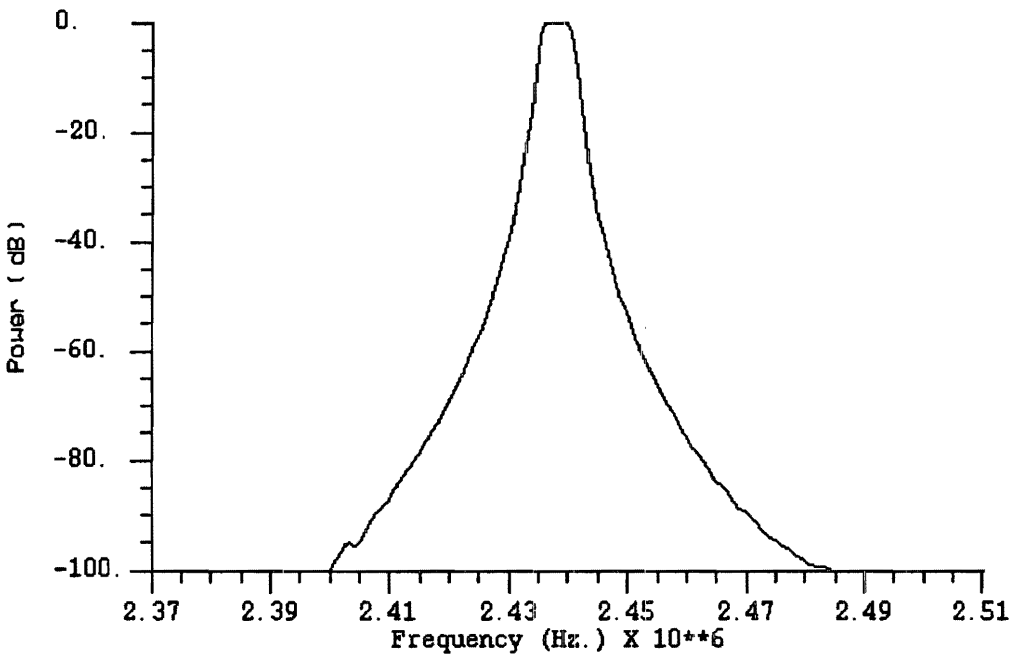


Figure 6.17: Bandpass Filter.

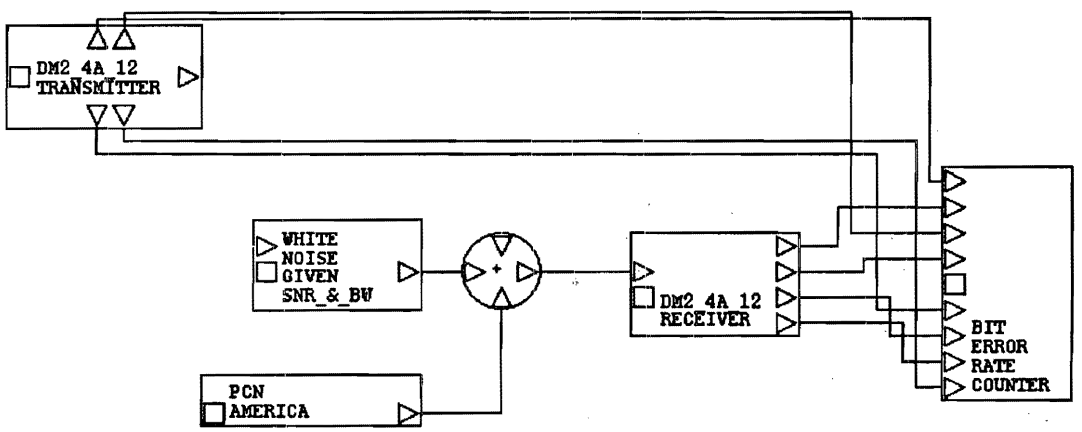


Figure 6.18: Test Set-up for Harris Farinon DM2-4A-12 System.

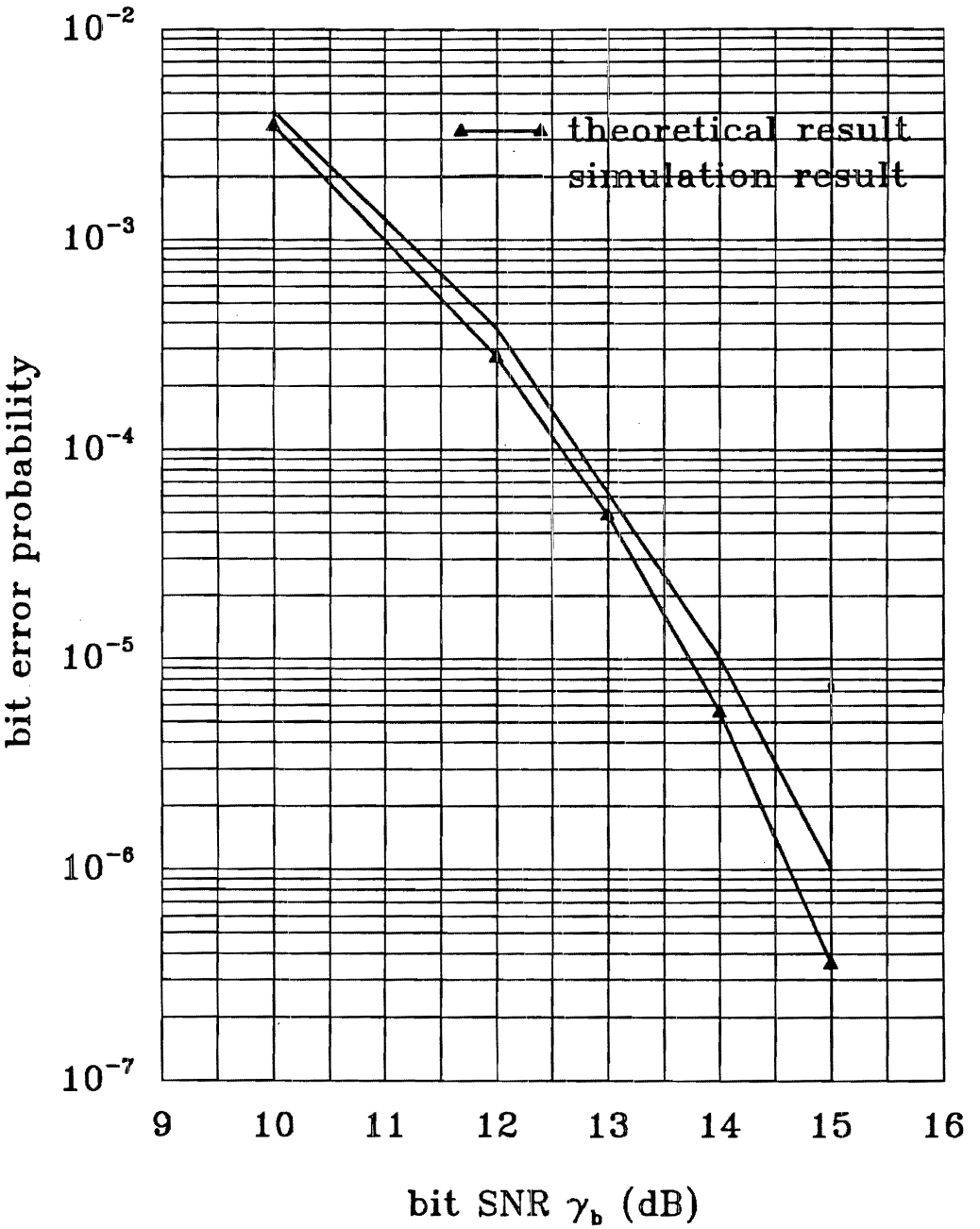


Figure 6.19: Bit Error Probability Performance for Harris Farinon DM2-4A-12 System.

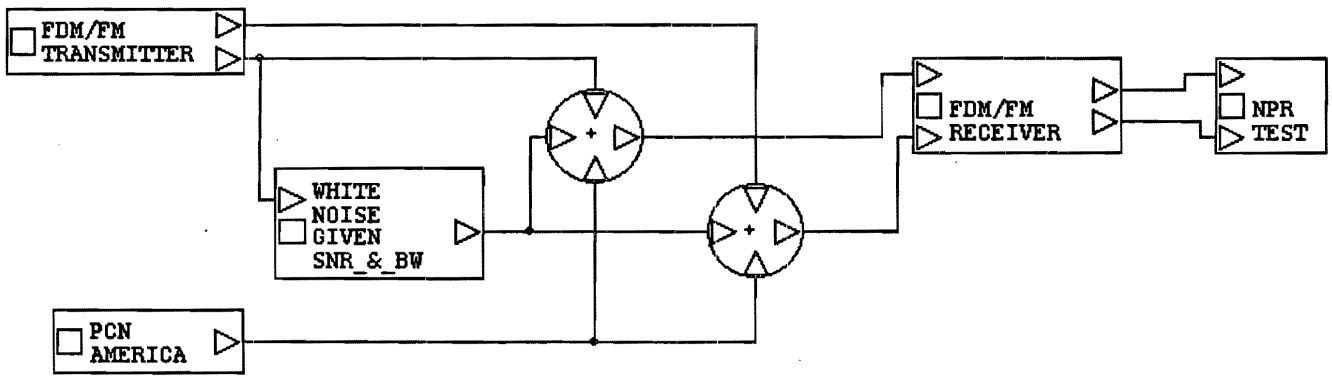


Figure 6.20: Test Set-up for Analog FDM/FM System.

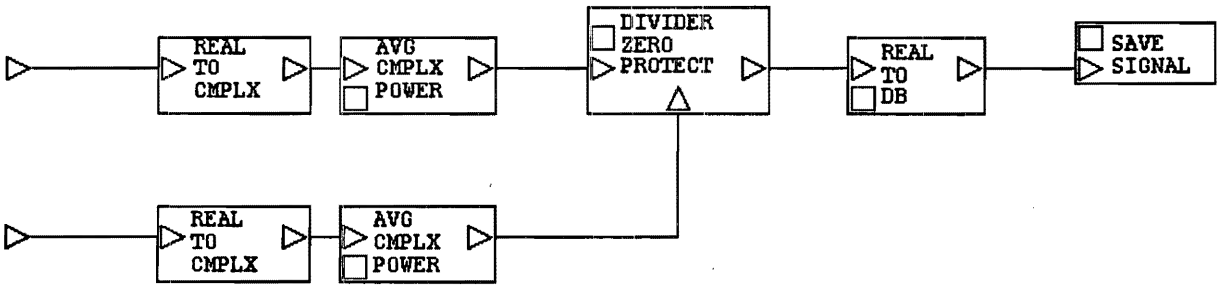


Figure 6.21: Test Set-up for NPR Measurement in Analog FDM/FM System.

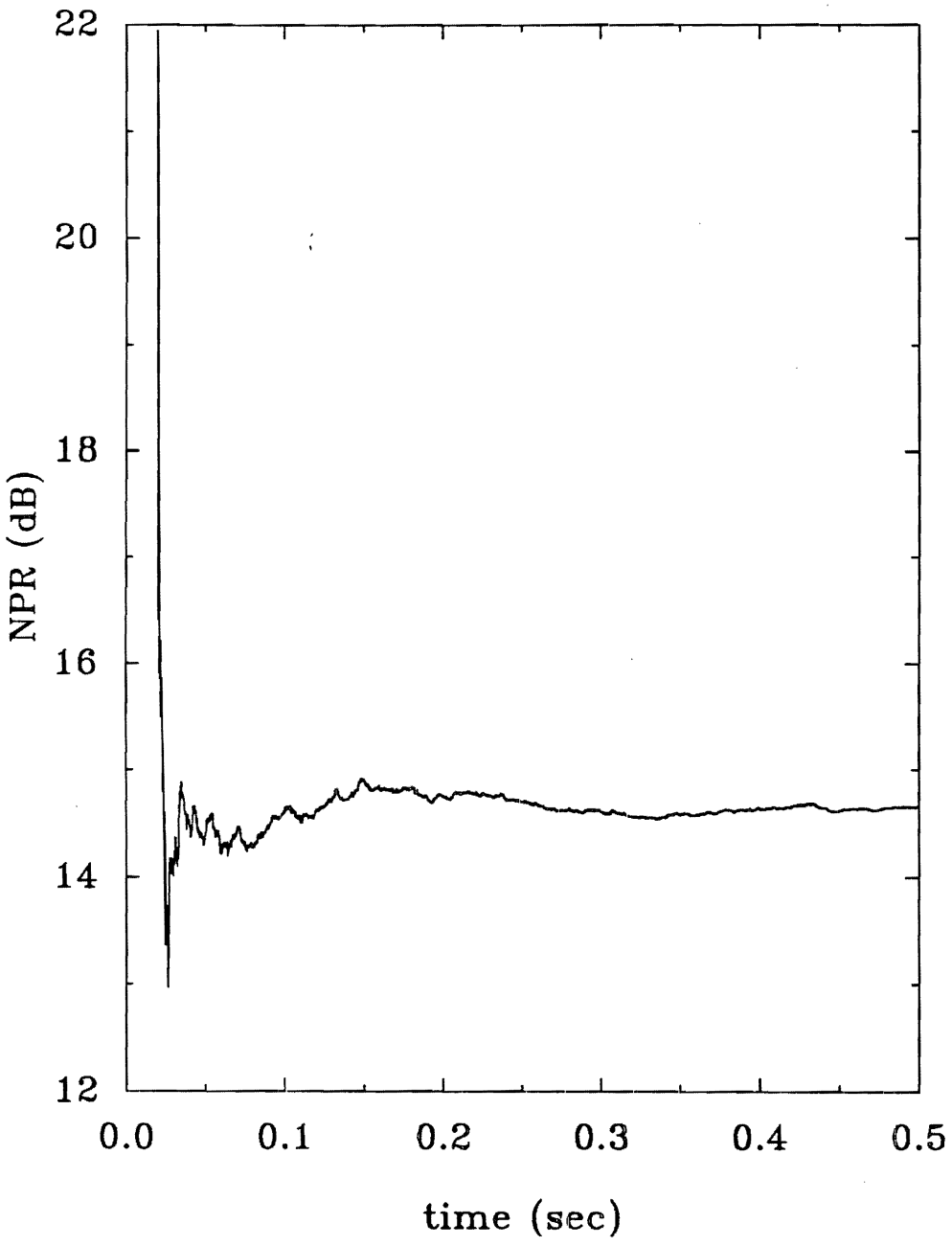


Figure 6.22: Variation of NPR with Time in Analog FDM/FM System.

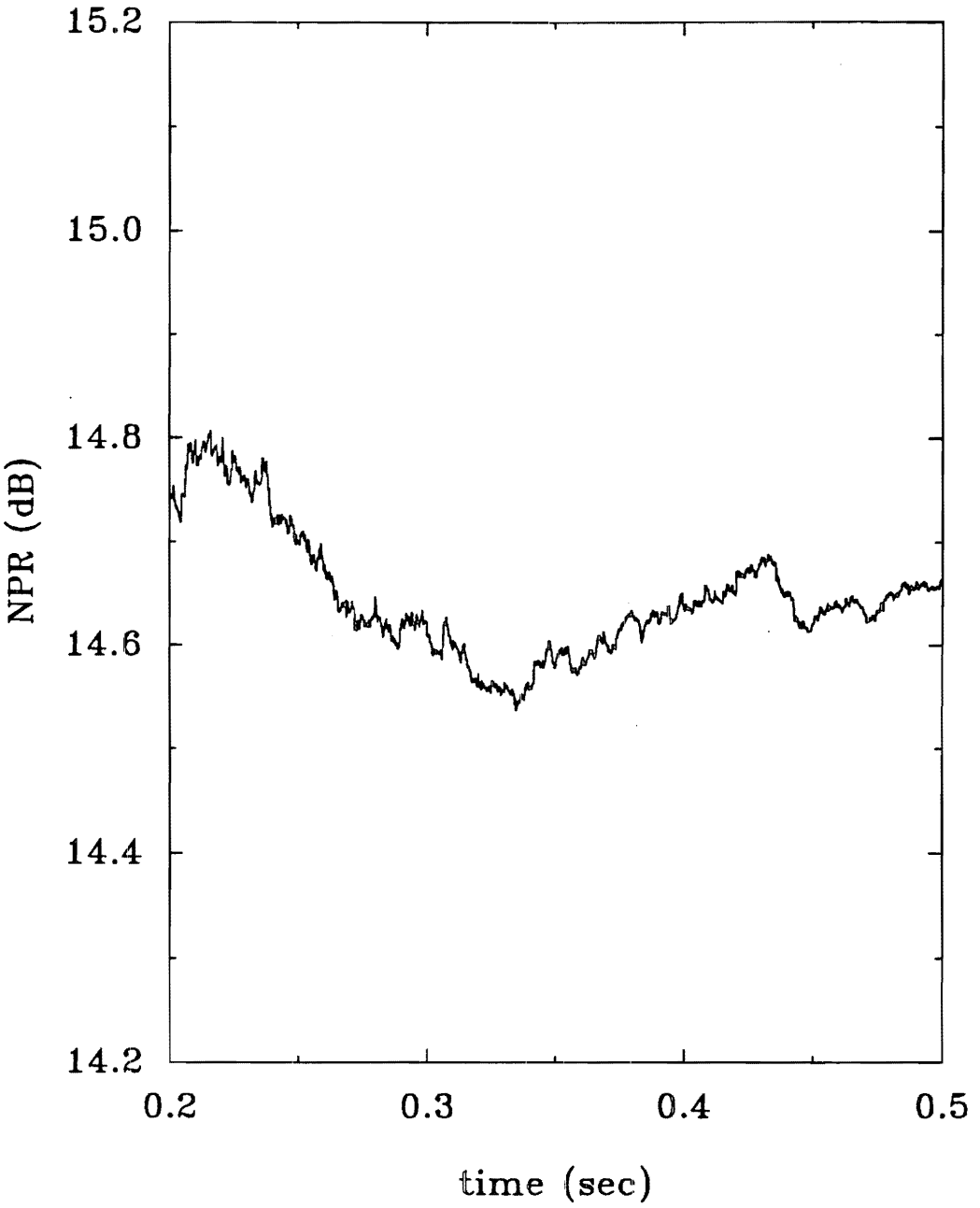


Figure 6.23: Variation of NPR with Time in Analog FDM/FM System.

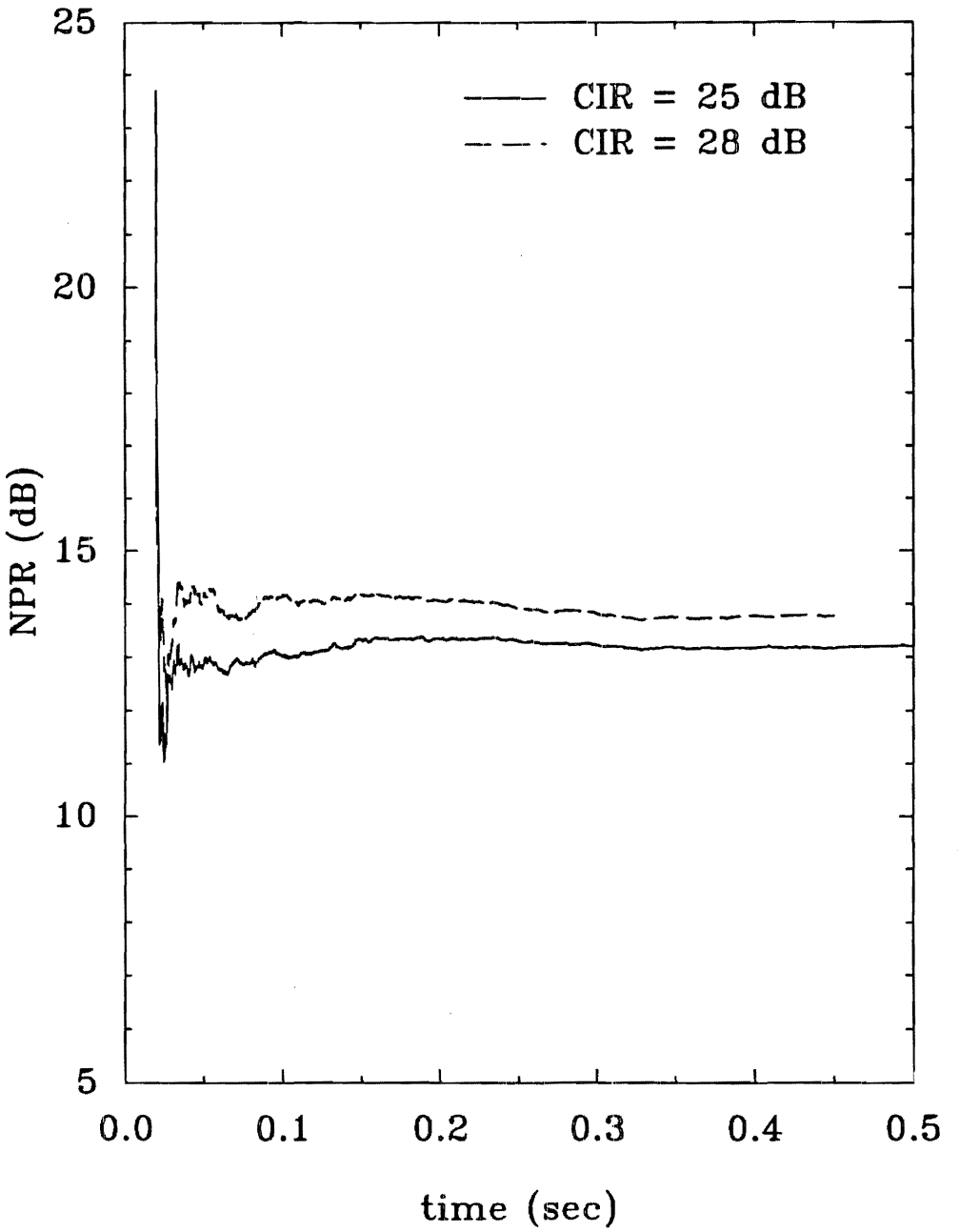


Figure 6.24: NPR with in Analog FDM/FM System with 48 MHz CDMA Overlay.

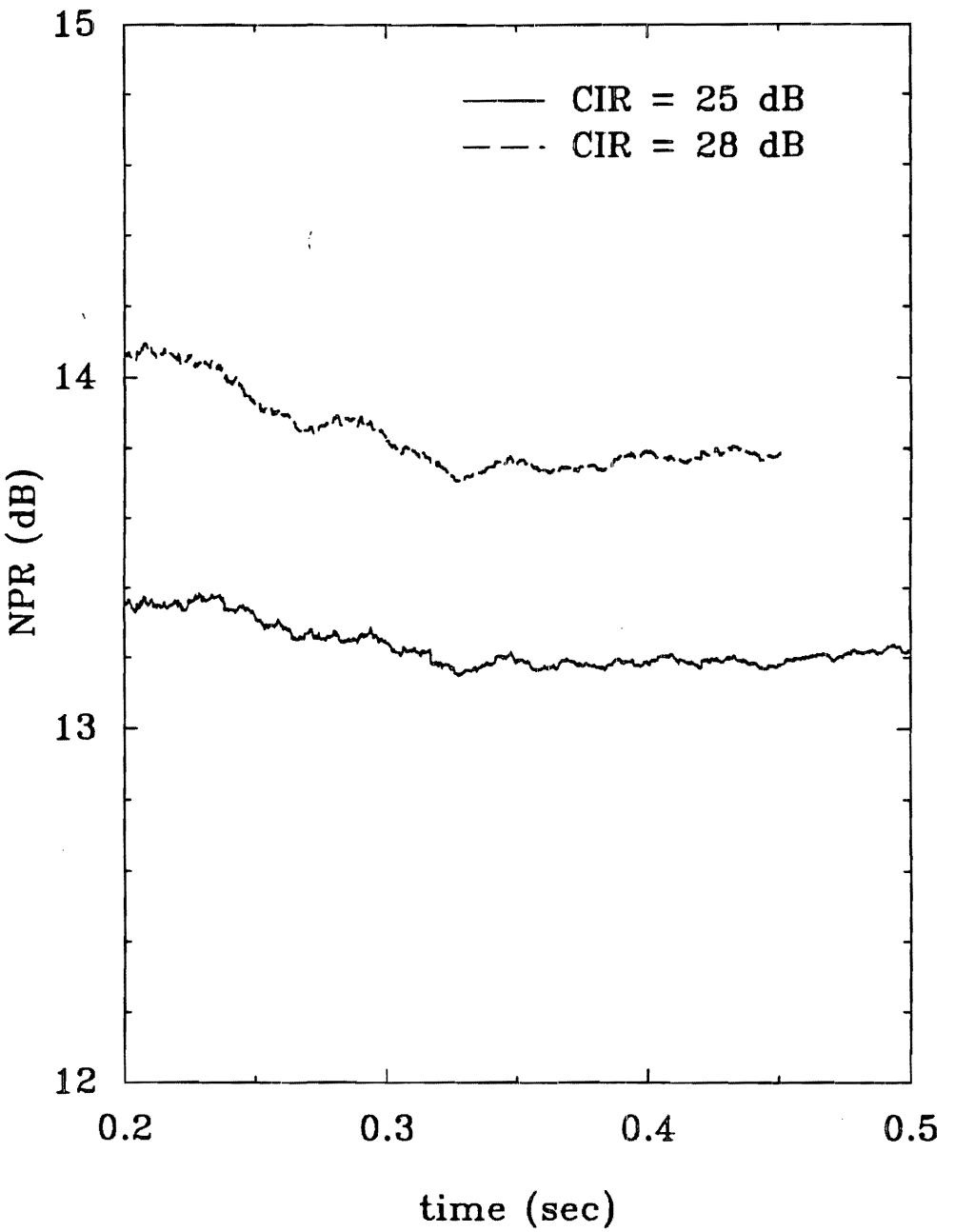


Figure 6.25: NPR with in Analog FDM/FM System with 48 MHz CDMA Overlay.

# References


[1] F. M. Gardner, ed., *Phaselock Techniques, second ed.* John Wiley & Sons, Inc., 1979.

[2] W. C. Jakes, Jr., *Microwave Mobile Communications.* Wiley, 1975.

[3] G. L. Stüber and L. Yiin, "Downlink outage predictions for cellular radio systems," Aug. 1991.

[4] D. L. Schilling, R. Pickholtz, and L. Milstein, "Spread spectrum goes commercial," *IEEE Spectrum*, pp. 40–45, August 1990.

[5] G. R. Cooper and R. W. Nettleton, "A spread-spectrum technique for high-capacity mobile communications," *IEEE Trans. on Vehicular Tech.*, Vol. VT-27, pp. 264 – 275, Nov. 1978.

[6] M. B. Pursley, D. V. Sarwate, and W. E. Stark, "Error probability for direct-sequence spread-spectrum multiple-access communications - part I: Upper and lower bounds," *IEEE Trans. on Commun.*, Vol. COM-30, pp. 975–984, May 1982.

[7] E. A. Geraniotis and M. B. Pursley, "Error probability for direct-sequence spread-spectrum multiple-access communications - part II: Approximations," *IEEE Trans. on Commun.*, Vol. COM-30, pp. 985–995, May 1982.

[8] J. S. Lehnert and M. B. Pursley, "Error probability for binary direct-sequence spread-spectrum communications with random signature sequences," *IEEE Trans. on Commun.*, Vol. COM-35, pp. 87–98, Jan. 1987.

[9] J. S. Lehnert, "An efficient technique for evaluating direct-sequence spread-spectrum multiple-access communications," *IEEE Trans. on Commun.*, Vol. 37, pp. 851–858, Aug. 1989.

[10] R. K. Morrow, Jr. and J. S. Lehnert, "Bit-to-bit error dependence in slotted DS/CDMA packet systems with random signature sequences," *IEEE Trans. on Commun.*, Vol. 37, pp. 1052–1061, Oct. 1989.

[11] E. A. Geraniotis and M. B. Pursley, "Performance of coherent direct-sequence spread-spectrum communications over specular multipath fading channels," *IEEE Trans. on Commun.*, Vol. COM-33, pp. 502–508, June 1985.

[12] E. A. Geraniotis and M. B. Pursley, "Performance of noncoherent direct-sequence spread-spectrum communications over specular multipath fading channels," *IEEE Trans. on Commun.*, Vol. COM-34, pp. 219–226, March 1986.

[13] E. A. Geraniotis, "Direct-sequence spread-spectrum multiple-access communications over nonselective and frequency-selective rician fading channels," *IEEE Trans. on Commun.*, Vol. COM-34, pp. 756–764, Aug. 1986.

[14] J. S. Lehnert and M. B. Pursley, "Multipath diversity reception of spread-spectrum multiple-access communications," in *Proc. Conf. Inform. Sci. Syst.*, (Johns Hopkins Univ., Baltimore, MD), March 1983.

[15] J. S. Lehnert and M. B. Pursley, "Multipath diversity reception of spread-spectrum multiple-access communications," *IEEE Trans. on Commun.*, Vol. COM-35, pp. 1189–1198, Nov. 1987.

[16] W. H. Lam and R. Steele, "Spread-spectrum communications using diversity in an urban mobile radio environment," in *IEEE Colloquium on Methods of Combating Multipath Effect in Wide Band Digital Cellular Mobile Systems*, (London, England), pp. 6/1–6/11, Oct. 1987.

[17] H. Hashemi, *Simulation of the Urban Mobile Radio Propagation Channel.* PhD thesis, Dept. Elect. Eng. Comp. Sci., University of California, Berkley, Aug. 1977.

[18] G. L. Turin, "The effects of multipath and fading on the performance of direct-sequence spread-spectrum CDMA systems," *IEEE Journal on Selected Areas in Commun.*, Vol. SAC-2, pp. 597–603, July 1984.

[19] H. Xiang, "Binary code-division multiple-access systems operating in multipath fading, noisy channels," *IEEE Trans. on Commun.*, Vol. COM-33, pp. 775–784, Aug. 1985.

[20] C. S. Gardner and J. A. Orr, "Fading effects on the performance of a spread spectrum multiple-access communication system," *IEEE Trans. on Commun.*, Vol. COM-27, pp. 143–149, Jan. 1979.

[21] T. Rappaport and L. Milstein, "Effects of path loss and fringe user distribution on CDMA cellular frequency reuse efficiency," in *GLOBCOM '90*, (San Diego, CA), pp. 404.6.1–404.6.7, 1990.

[22] T. Rappaport and L. Milstein, "Effects of radio propagation path loss on CDMA cellular frequency reuse efficiency for the reverse channel," Submitted to IEEE Trans. on Vehicular Tech.

[23] J. G. Proakis, *Digital Communications, second ed.* McGraw-Hill Book Company, 1989.

[24] W. C. Y. Lee, *Mobile Communications Design Fundamentals.* Howard W. Sams & Co., 1986.

[25] C. . T.-R. . (WG1):, "Proposal on channel transfer functions to be used in gsm tests late 1986," Sep. 1986. Paris.

[26] A. A. Giordano and F. M. Hsu, *Least Square Estimation with Applications to Digital Signal Processing.* Wiley, 1985.

[27] F. Ling and J. G. Proakis, "Adaptive lattice decision-feedback equalizers – their performance and application to time-variant multipath channels," *IEEE Trans. on Commun.*, Vol. COM-33, pp. 348–356, Apr. 1985.

[28] E. Eleftheriou and D. D. Falconer, "Adaptive equalization techniques for hf channels," *IEEE Journal on Selected Areas in Commun.*, Vol. SAC-5, pp. 238–247, Feb. 1987.

[29] H. Ochsner, "Direct-sequence spread-spectrum receiver for communication on frequency-selective fading channels," *IEEE Journal on Selected Areas in Commun.*, Vol. SAC-5, pp. 188–193, Feb. 1987.

[30] E. A. Geraniotis, "Performance of noncoherent direct-sequence spread-spectrum multiple-access communications," *IEEE Journal on Selected Areas in Commun.*, Vol. SAC-3, pp. 687–694, Sep. 1985.

[31] K. Feher, *Advanced Digital Communications.* Prentice-Hall, 1987.

[32] W. C. Y. Lee, *Mobile Cellular Telecommunications Systems.* New York, N. Y.: McGraw-Hill Book Company, 1989.

[33] R. Muammar and S. C. Gupta, "Cochannel interference in high-capacity mobile radio systems," *IEEE Trans. on Commun.*, Vol. COM-30, pp. 1973–1978, Aug. 1982.

[34] R. C. French, "The effect of fading and shadowing on channel reuse in mobile radio," *IEEE Trans. on Vehicular Tech.*, Vol. VT-28, pp. 171–181, Aug. 1979.

[35] C. Kchao and G. L. Stüber, "Analysis of a direct-sequence spread-spectrum cellular radio system," *to appear in IEEE Transactions on Communications.*

[36] K. S. Gilhousen, I. M. Jacobs, R. Padovani, L. A. Weaver, Jr., and C. W. III, "On the capacity of a cellular CDMA system," *IEEE Trans. on Vehicular Tech.*, Vol. VT-40, pp. 303–312, May 1991.

[37] W. C. Y. Lee, "Overview of cellular CDMA," *IEEE Trans. on Vehicular Tech.*, Vol. VT-40, pp. 291–302, May 1991.

[38] R. L. Pickholtz, L. B. Milstein, and D. L. Schilling, "Spread spectrum for mobile communications," *IEEE Trans. on Vehicular Tech.*, Vol. VT-40, pp. 313–322, May 1991.

[39] B. R. Vojčić, R. L. Pickholtz, and I. S. Stojanović, "Comparision of TDMA and CDMA in microcellular radio systems," in *ICC'91*, (Denver, CO), pp. 28.1.1–28.1.5, 1991.

[40] F. Simpson and J. Holtzman, "CDMA power control, interleaving, and coding," in 41$^{st}$ *IEEE Vehicular Technology Conf.*, (Saint Louis, Misssouri), pp. 362–367, 1991.

[41] S. Ariyavisitakul and L. F. Chang, "Signal and interference statistics of a simulated CMDA system with fast adaptive power control," submitted to IEEE Trans. on Commun.

[42] L. F. Chang and J. Chuang, "Diversity selection using coding in a portable radio communications channel with frequency-selective fading," *IEEE Journal on Selected Areas in Commun.*, Vol. SAC-7, pp. 89–98, Jan. 1989.

[43] R. W. Nettleton and H. Alavi, "Power control for a spread-spectrum cellular mobile radio system," in *IEEE Vehicular Technology Conference*, (Toronto, Ontario, Canada), pp. 242–246, May 1983.

[44] H. Alavi and R. W. Netteton, "Downstream power control for a spread-spectrum cellular mobile radio network," in *Globcom'82*, (Miami, Florida), pp. A.3.5.1–A.3.5.5, Nov. 1982.

[45] K. S. Gilhousen, I. M. Jacobs, R. Padovani, and L. A. Weaver, Jr., "Increased capacity using CDMA for mobile satellite communications," *IEEE Journal on Selected Areas in Commun.*, Vol. SAC-8, pp. 503–514, May 1990.

[46] C. L. Weber, G. K. Huth, and B. H. Batson, "Performance considerations of code division multiple-access systems," *IEEE Trans. on Vehicular Tech.*, Vol. VT-30, pp. 3–9, Feb. 1981.

[47] C. Kchao, *Direct Sequence Spread Spectrum Cellular Radio.* PhD thesis, Georgia Institute of Technology, 1991.

[48] G. L. Stüber and C. Kchao, *Spread Spectrum Cellular Radio.* Georgia Institute of Technology, OCA Project No. E21-662 for Bell South Enterprises, December, 1990.

[49] K. Feher, "Modems for digital cellular and emerging digital mobile radio systems," in *ICC'91*, (Denver, CO), pp. 19.1.1–19.1.7, 1991.

[50] V. M. Eyuboğlu and S. U. Qureshi, "Reduced-state sequence estimation with set partitioning and decision feedback," *IEEE Trans. on Commun.*, Vol. COM-36, pp. 401–409, April 1988.

[51] V. M. Eyuboğlu and S. U. Qureshi, "Reduced-state sequence estimation for coded modulation on intersymbol interference channels," *IEEE Journal on Selected Areas in Commun.*, Vol. SAC-7, pp. 989–995, August 1989.

[52] A. Duel-Hallen and C. Heegard, "Delayed decision feedback sequence estimation," *IEEE Trans. on Commun.*, Vol. COM-37, pp. 428–436, May 1989.

[53] E. M. Long and A. M. Bush, "Decision-aided sequential sequence estimation for intersymbol interference channels," in *ICC'89*, (Boston, MA), pp. 26.1.1–26.1.5, 1989.

[54] A. P. Clark and R. Harun, "Assessment of kalman-filter channel estimator for an hf radio link," *Proc. IEE*, Vol. 133, pp. 513–521, October 1986.

[55] F. Magee and J. Proakis, "Adaptive maximum-likelihood sequence estimation for digital signaling in the presence of intersymbol interference," *IEEE Trans. Information Theory*, Vol. IT-19, pp. 120–124, January 1973.

[56] S. Haykin, ed., *Adaptive Filter Theory.* New Jersey: Prentice-Hall, 1986.

[57] K. Hamied, M. Rahman, and M. El-Hennancy, "A new channel estimator for fast start-up equalization," *IEEE Trans. on Commun.*, Vol. COM-39, pp. 177–181, February 1991.

[58] E. Eleftheriou and D. D. Falconer, "Adaptive equalization techniques for hf channels," *IEEE Journal on Selected Areas in Commun.*, Vol. SAC-5, pp. 238–247, February 1987.

[59] A. A. Giordano and F. M. Hsu, eds., *Least Square Estimation with Applications to Digital Signal Processing.* John Wiley & Sons, Inc., 1985.

[60] F. Ling and J. Proakis, "A generalized multichannel least-squares lattice algorithm based on sequential processing stages," *IEEE Trans. ASSP*, Vol. ASSP-32, pp. 381–389, April 1984.

[61] W. H. Sheen and G. L. Stüber, "Mlse equalization and decoding for multipath-fading channels," *IEEE Trans. on Commun.*, Vol. COM-39, pp. 1455–1464, October 1991.

[62] W. Jakes, ed., *Microwave Mobile Communications.* New York: Wiley, 1974.

[63] W. H. Sheen, *Performance Analysis of Sequence Estimation Techniques for Intersymbol Interference Channels.* PhD thesis, Georgia Institute of Technology, 1991.

[64] International Telecommunication Union, *Measurement of Noise Using a Continuous Uniform Spectrum Signal on Frequency-Division Multiplex Telephony Radio-Relay Systems.* 1982.

[65] International Telecommunication Union, *Pre-emphasis Characteristic for Frequency Modulation Radio-Relay Systems for Telephony Using Frequency-Division Multiplex.* 1982.

[66] Electronics Industry Association, *Interference Criteria for Microwave Systems in the Private Radio Services.* November 1990.